Downward Propagation of Planetary Wave Packets from the Stratosphere to the Troposphere

松山, 裕矢

Downward Propagation of Planetary Wave Packets from the Stratosphere to the Troposphere

MATSUYAMA Yuya

Department of Earth and Planetary Sciences

Kyushu University

February 2023

Contents

Abstract

In this study, the statistical characteristics of the downward propagation of planetary wave packets are examined by using the Japanese reanalysis data (JRA-55) and a large ensemble dataset (d4PDF). We use Eliassen-Palm flux (EPF; Andrews et al., 1987) and Plumb (1985)'s wave activity flux (WAF) to investigate the propagation of waves.

Firstly, the statistical characteristics of downward propagation events ("DP events") are investigated by the use of JRA-55. DP events are extracted on the basis of EPF. It is found that most of the events occur in the Western Hemisphere in the Northern Hemisphere, while several events occur in the Eastern Hemisphere. These events are classified on the basis of the longitudinal distribution of the events along with the results of EOF analyses for vertical components of WAF (WAFz) at 30 hPa on the event day, and after that composite analyses to the classified groups are conducted. In the events in the Western Hemisphere, there are roughly proportional relationships between the intensity of downward propagation of wave packets in the Western Hemisphere and several indices, i.e., the intensity of the quasi-barotropic developed Aleutian high, the intensity of penetrated cyclonic anomalies to the troposphere there, and the magnitude of the cold anomalies below the DP region in the troposphere. For the events in the Eastern Hemisphere, their characteristics are qualitatively similar to those in the Western Hemisphere, although the occurrence longitudes are different.

On the other hand, in d4PDF dataset, we obtain a similar longitudinal distribution of the events to that in the reanalysis data; in addition, there are two large separated peaks in the

longitudinal distribution in the Western Hemisphere. Similarly, the events are classified on the basis of their distribution, and composite analyses are conducted. These two peaks are considered to be generated by the differences in longitudes of upward propagation prior to the event day along with the ridge of zonal wavenumber 1 components of geopotential heights around the event day.

Next, the statistical characteristics of the locally downward propagation events ("LDP events") are investigated on the basis of WAFz. Note that the LDP events do not necessarily show downward propagation in EPF, because wave packets propagate downward only locally. Such events are extracted under a specified criterion for the WAFz at 30 hPa. The longitudinal distribution of the LDP events is similar to that in the DP events in d4PDF; there are two large peaks in the Western Hemisphere and a weak peak in the Eastern Hemisphere. The histogram of the longitudinal width of downward propagation of the LDP events also has two large peaks. The events are classified on the basis of these features, and composite analyses are conducted. The events with wide LDP in the Western Hemisphere are associated with cold anomalies in the troposphere below the LDP region. However, it is difficult to conduct statistical analysis for the events with narrow LDP, because their event numbers are small.

In d4PDF dataset, we can obtain a similar distribution of occurrence longitudes and longitudinal width of the LDP events. Furthermore, it make possible to obtain more statistically significant results. In particular, features of temperature anomalies in the troposphere associated with the events are clarified, including events with narrow LDP.

1. Introduction

1.1 Stratosphere and Planetary waves

The atmosphere of the earth is generally divided into four layers on the basis of the vertical profile of temperature. Figure 1-1-1 is sited from Andrews (2010) and shows the vertical structure of atmospheric temperature. The bottom layer is the troposphere, which covers the layer form the ground to the tropopause located around 12 km altitude. The temperature in this layer decreases with height due to absorption of solar visible and infrared radiation by the ground, along with the so-called greenhouse effect. The layer above the troposphere is the stratosphere, which covers the layer from the tropopause to the stratopause located around 50 km altitude. The temperature in this layer increases with height due to absorption of solar ultraviolet radiation by the ozone layer in the stratosphere. The mesosphere and thermosphere are located above the stratosphere, in which the temperatures decreases and increases, respectively. In the current study, we focus on the stratosphere and the interaction between the stratosphere and the troposphere.

In the stratosphere, there exist various phenomena which cannot be seen in the troposphere. Among them Sudden Stratospheric Warming (SSW) has been attracted many researchers due to their spectacular features. During a SSW event, the polar temperature in the stratosphere suddenly rises more than 30 K in several days and the meridional temperature gradient reverses correspondingly. The polar night westerly jet is drastically decelerated and changes to easterly.

In the atmosphere, there exist various kinds of waves supported by the corresponding restoring forces. Planetary waves are one of the atmospheric waves having a planetary horizontal scale and cause the inherent phenomena in the stratosphere, including SSW events. In the climatological circulation in the Northern Hemisphere (NH) stratosphere, the polar vortex, a large-scale cyclone, is developed near the winter pole in the stratospheric, along with the Aleutian high, a relatively small anticyclone over the Aleutian Islands. Figure 1-1-2 is the temperature in the Northern Hemisphere at a level near 24 km altitude, during a period when the stratosphere was disturbed by a stratospheric warming. The cold (warm) region roughly corresponds to the cyclone (anticyclone) region. Therefore, the stratospheric winter has large scale anomalous components along a latitudinal circle, i.e., predominant zonal wavenumber (WN) 1 and subsidiary WN 2 and 3 components, which are called planetary waves. Thus, in the NH winter, stationary or quasi-stationary planetary waves are developed due to large-scale topography and/or land-sea heat contrast (e.g., Holton and Hakim, 2012), while in the Southern Hemisphere, such planetary wave activity is relatively weak.

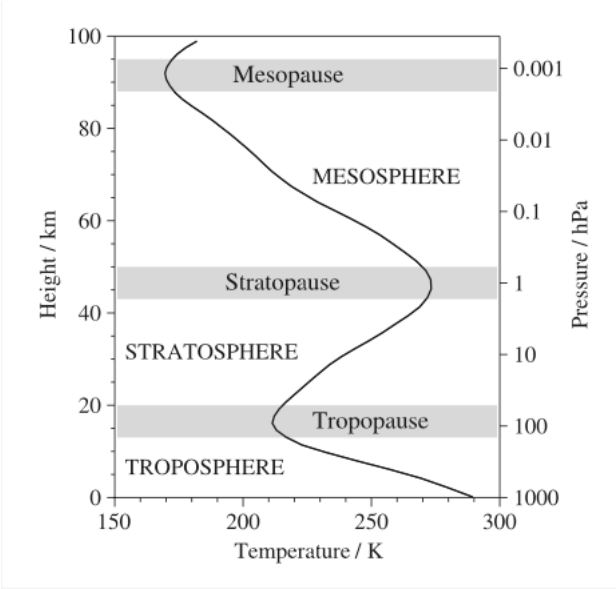

Figure 1-1-1: Typical vertical structure of atmospheric temperature (K) in the lowest 100 km of the atmosphere. From Andrews (2010).

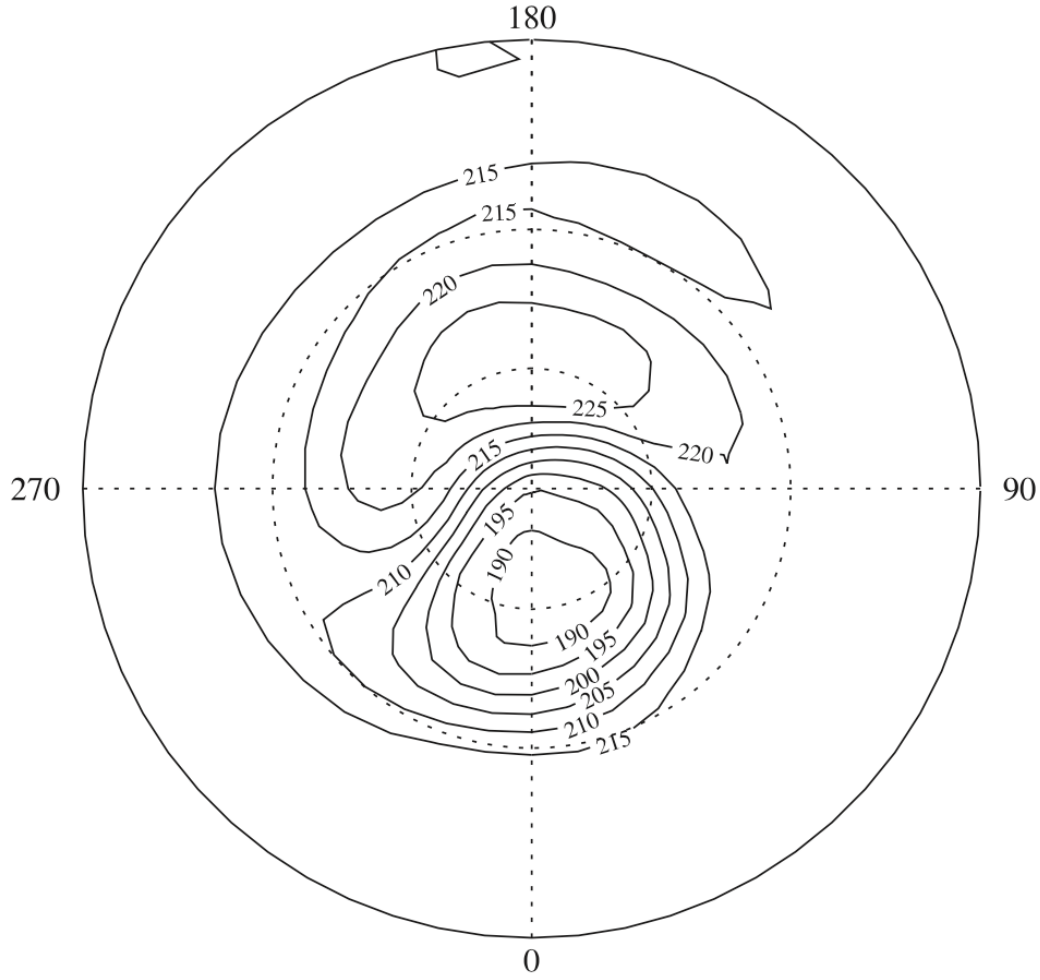

Figure 1-1-2: Polar stereographic map of atmospheric temperature (K) near 24 km altitude in the Northern Hemisphere stratosphere on 9 January 1992, as measured by the Improved Stratospheric and Mesospheric Sounder (ISAMS) on the Upper Atmospheric Research Satellite (UARS). The North Pole is at the centre, the 60◦ N and 30◦ N latitude circles are shown and the equator is the outer circle; four longitudes are also shown. From Andrews (2010).

1.2 Downward Propagation of Planetary Waves

As described above, quasi-stationary planetary waves are forced in the troposphere by large-scale topography and/or land-sea heat contrast. They propagate upward from the troposphere to the stratosphere, causing various phenomena inherent to the stratosphere, such as SSWs. However, their waves are sometimes observed to propagate downward or to be reflected from the stratosphere to the troposphere (e.g., Perlwitz and Harnik, 2003, 2004; Kodera et al., 2008, 2013; Shaw and Perlwitz, 2013; Kodera and Mukougawa, 2017).

In order to investigate the propagation of planetary waves, wave activity flux is a useful tool. Wave activity flux is defined as a vector quantity, the group velocity of the waves multiplied by the wave activity; hence, we can investigate waves propagation by using this kind of flux. We use two-dimensional Eliassen-Palm flux (Andrews et al., 1987) and three-dimensional Plumb (1985)'s flux. We discuss these fluxes in Section 2.

Traditionally, propagation of waves has been discussed using Eliassen-Palm flux (EPF). In addition, zonal asymmetry of downward propagation of wave packets has attracted large interests by using Plumb's wave activity flux (WAF). When waves propagate downward on the basis of EPF, wave packets propagate downward over North America, accompanied by prior upward propagation of wave packets over Eurasia on the basis of WAF (e.g., Kodera et al., 2008, 2013; Jadin, 2011).

Here, we introduce the results in Kodera et al. (2008). They investigated wave and wave packets propagation during a SSW of March 2007. Figure 1-2-1 is cited from Figure 1 in

Kodera et al. (2008). This figure shows the variation of the north polar temperature at 30 hPa during January-March 2007 and latitude-height sections of the zonal-mean zonal winds and EPF during March 2 to 5, 2007. Waves propagated upward strongly on March 2 and 3. Easterly winds were established by the upward propagation, and waves started to propagate downward on March 4. This wind structure is favorable condition for the occurrence of downward propagation (Petlwitz and Harnik, 2003), discussed in Section 2.3. On March 5, downward propagation develops. Figure 1-2-2 is also cited from Figure 2 in Kodera et al. (2008). This figure shows WAF at 100 hPa for March 2 and 4. Upward and downward propagation of wave packets occurred in different sectors; wave packets propagate upward over Siberia and downward over North America. Figure 1-2-3 shows the 850 hPa temperature change over the American-Atlantic sector from March 4 to 6. Cold weather cover North American continent at the same period as the downward propagation in the stratosphere.

As described above, wave packet is confirmed to propagate over North America. On the other hand, wave packets propagated downward over Central Eurasia in January 2008 (Nath et al., 2014). Their longitude distribution has not been statistically clarified. Different characteristics and time variations of events are expected depending on the longitude of downward propagation.

On the other hand, Mukougawa et al. (2017) dealt with the same event as that in Kodera et al. (2008), which was the case after the occurrence of a SSW in March 2007. They made a linear stability analysis using a nondivergent barotropic vorticity equation on a sphere.

They found that upward propagating planetary waves before the event caused a barotropically unstable polar vortex which generated anomalous components to change the vertical phase structure to determine whether the incoming planetary waves are eventually absorbed or emitted downward in the stratosphere. Thus, there are several suggestions for causes of downward propagation; however, we have not yet attained a thorough understanding of this issue.

Waves propagate downward also in the SH (e.g., Harnik and Linden, 2001). Downward propagation occurs from September to December there (Harnik et al., 2011). One of the multiple events investigated in Kodera et al. (2013) was related to a blocking event in the SH; they concluded that characteristics of downward propagation in this case were similar to those of the NH events. Anyhow, fewer analyses have been done on downward propagation in the SH than those in the NH, so their features of the events are also unclear.

Downward propagation events receive much interest also from the viewpoint of their influences on the tropospheric circulation. On the other hand, numerous studies have been based on zonal mean fields such as EPF. Although studies using Plumb (1985) 's flux to focus on wave packets have been increasing in recent years, such statistical analyses are still limited and longitudinal structure and distribution of events are unknown. Hence, the current study aims to seek the longitude distribution of downward propagation events and to reveal statistical features in the stratosphere and troposphere of each event group classified by occurrence longitudes of downward propagation.

In the first part of this thesis, we investigate the statistical features of events of the downward propagation of planetary waves.

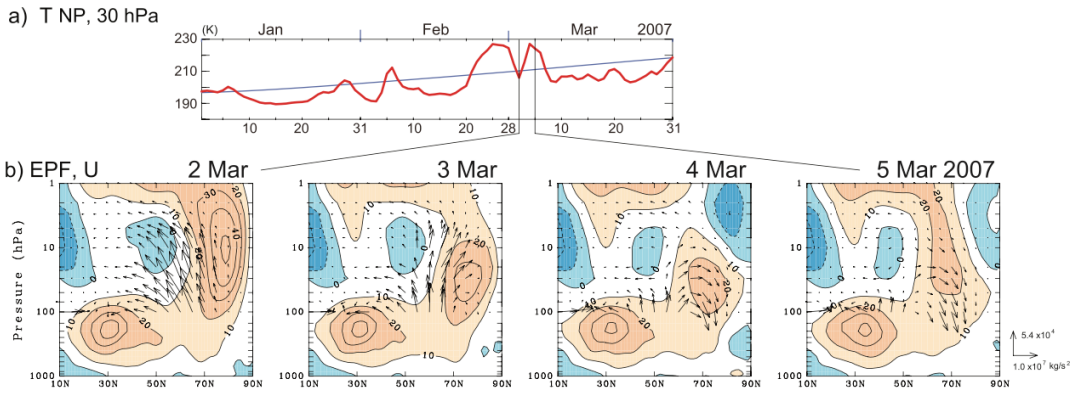

Figure 1-2-1: (a) Time series of the north polar temperature at 30 hPa from January 1 to March 31, 2007 (red line). Climatology is represented by a blue line. (b) Meridional sections of the daily averaged zonal-mean zonal wind (contours) and the total E-P flux (arrows) from March 2 to 5, 2007 (indicated by vertical lines in Figure 1a). Contour interval is 10 m s^{-1}. Positive (negative) values are indicated by reddish (bluish) colors. Arrows at the right bottom indicate the scale of vertical and meridional components of the EPF. From Kodera et al. (2008).

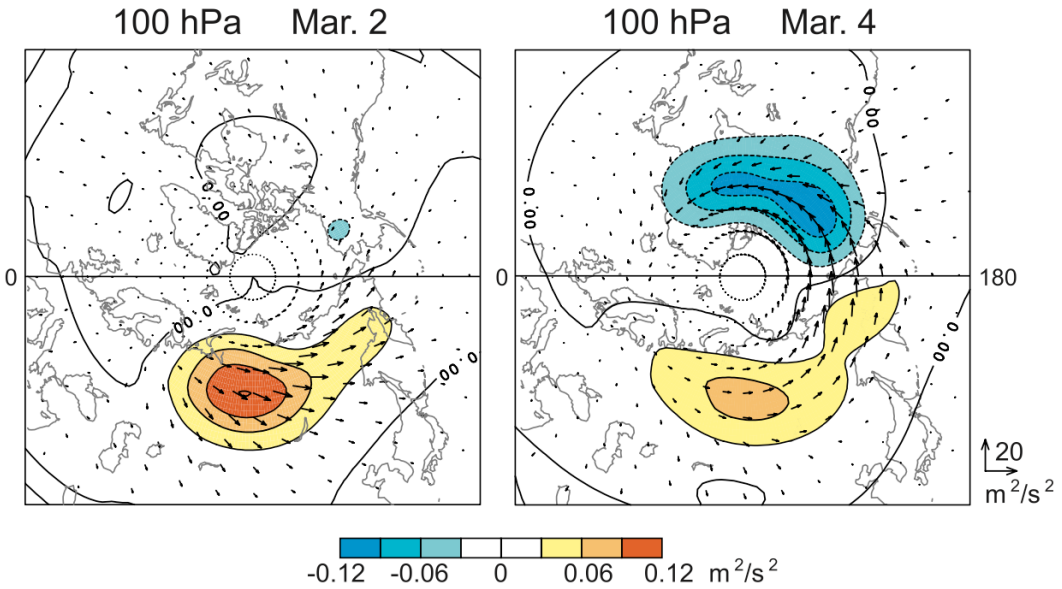

Figure 1-2-2: The 3-D Plumb flux for zonal-wave 1 to 3 at 100 hPa on (left) March 2 and (right) March 4, 2007. Vertical and horizontal component are indicated by contours and arrows, respectively. Counter interval is 0.03 m^2 s^{-2}, and arrows at the right bottom correspond to horizontal component of 20 m^2 s^{-2}. From Kodera et al. (2008).

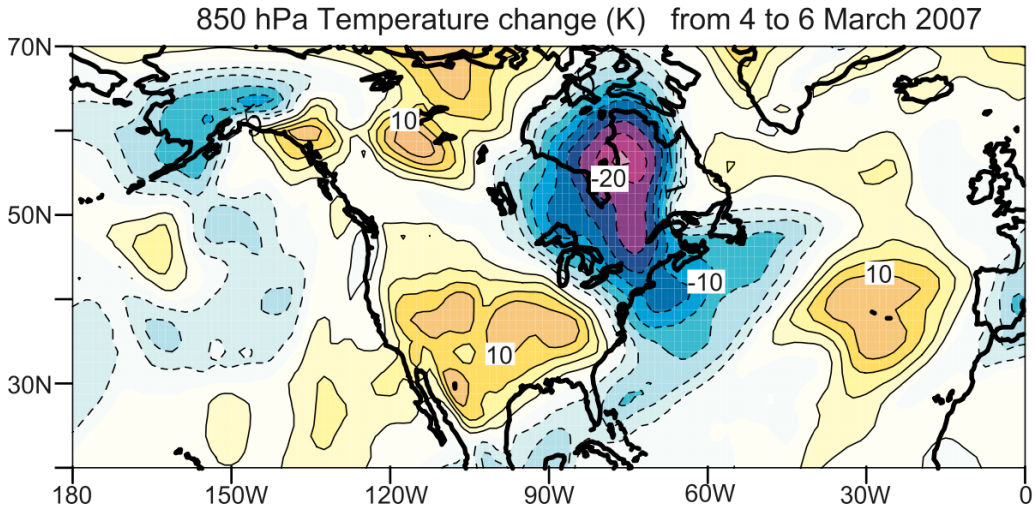

Figure 1-2-3: Air temperature change at 850 hPa (contour interval: 2.5 K) from 4 to 6 March 2007 illustrating a domain of 20°N to 70°N and 180°W to 0°E and zero contour lines are omitted. From Kodera et al. (2008).

1.3 Downward Propagation of Planetary Wave packets

More recently, the idea of "partial reflection" (PR; Nath et al., 2014) has been becoming widespread, which might develop the above studies. This idea does not indicate downward propagation captured by the EPF, but rather localized events that cannot be captured by it. Nath et al. (2014) reported that PR sometimes occurred in East Asia, bringing a cold wave. In doing so, they discuss the PR occurrence using an index proposed by Perlwitz and Harnik (2003) without zonal and winter averaging. On the other hand, Matthias and Kretschmer (2020) suggested a useful index for detecting PR based on the subtraction of the heat flux averaged over Canada and that averaged over Siberia. They investigated the events detected by using this index, showing the stratospheric pressure distribution during the events and the occurrences of cold temperature anomalies over North America after the events.

Here, we introduce the results in Matthias and Kretschmer (2020). They investigated the several cold spells over North America and Eurasia in the winter of 2017/18, and indicated the cold spells over North America were related to blocking events and downward propagation. Blocking events cause advection of cold Arctic air downstream, and downward propagation enhance the blocking events. However, the index based on zonal averages for downward propagation missed their downward propagation. Thus, they made a useful index for detection of such events. It is defined as the difference between the standardized meridional eddy heat flux over Siberia and Canada averaged between 45˚ and 75˚N at 100 hPa. A wave reflection event is defined when this index exceeds 1.5. Resultantly, they detected 41 events. Figure 1-3-1

shows the composite results of geopotential height and WAF for the 41 events in longitude-height section and polar stereographical map. Wave packets propagate downward over North America and propagate upward over North Pacific simultaneously because these 41 events are PR events. Moreover, they investigated the cold spells during the 41 events. Figure 1-3-2 shows the evolution of the index, surface temperature, and the blocking index. A several days after the PR, temperature drop, and the blocking events occur.

Although Matthias and Kretschmer (2020) 's index described above is helpful, it has two problems: One is that the longitude scales of PR are prescribed because the heat fluxes are averaged longitudinally. The other is that the longitude occurrence region of PR is limited to Canada (or North America). This longitude scale and area were defined by features of WAF in the downward propagation events captured by EPF. However, the PR events may have different characteristics from those events extracted by EPF because their detection ways are different, so that the PR events should be extracted on the basis of their characteristics. To conduct such an examination, it is necessary to detect PR events considering various longitude distributions and scales, but such a task is complex and has not been done. Thus, PR events have not been fully understood statistically, because it is difficult to detect PR events on the basis of their inherent features.

The source of downward propagation is not necessarily limited to the reflection; some downward propagation events might be caused by wave generation in the stratosphere (Mukougawa et al., 2017). Since we conduct analysis without categorizing by occurrence

sources, usage of the word "reflection" is considered to be inappropriate. Hence, we name the detected events "Localized Downward Propagation (LDP) events" instead of PR events.

In addition, plausible impacts on the tropospheric circulation and weather system due to downward propagation of planetary waves from the stratosphere are also important issues for our social activity. Downward propagation triggers positive North Atlantic Oscillation events (Shaw and Perlwitz, 2013; Shaw et al., 2014; Lubis et al., 2016) and contributes to the occurrence of cold spells (Kodera et al., 2008; Kretschmer et al., 2018; Matthias and Kretschmer, 2020).

The locations of cold spells with downward propagation are different among events, with two main types noted. One is a cold spell in approximately the same region where waves propagate downward in the stratosphere. Specifically, downward propagation and cold spells occur over North America (e.g., Matthias and Kretschmer, 2020). The other has different regions of downward propagation and cold spells. For example, downward propagation over North America in the stratosphere caused a cold spell in Central and Western Eurasian regions (Kodera and Mukougawa, 2017). This positional relationship between downward propagation and cold spells should be examined as the statistical relationship is. In addition, statistical analysis should also discuss the characteristics of downward propagation events that contribute significantly to tropospheric influences such as cold spell development.

In the second part of this thesis, we make the statistical analysis for the events of the downward propagation of planetary wave packets.

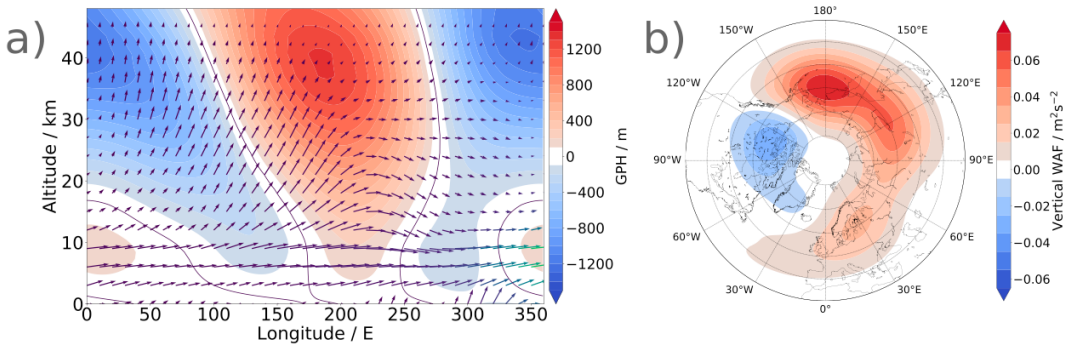

Figure 1-3-1: (a) Composite of the height–longitude cross sections of eddy geopotential heights (shading) and of wave activity fluxes (arrows), averaged over 60˚N–70˚N during the 41 reflection events. (b) As in (a), but for the vertical component of the wave activity flux at 100 hPa. From Matthias and Kretschmer (2020).

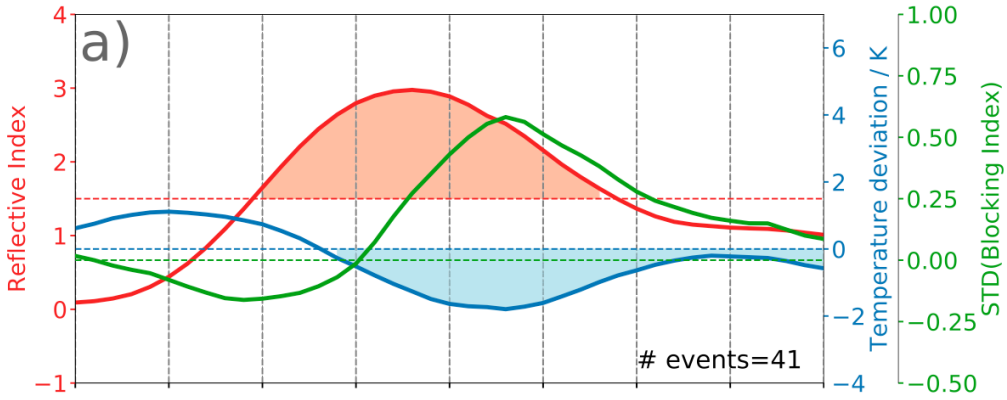

Figure 1-3-2: Evolution of the regional reflective index (in red), surface temperature anomalies over northeastern North America (40˚–60˚N, 260˚–290˚E, in blue), and the North Pacific blocking index (calculated over 150˚–230˚E, in green) averaged the 41 events. From Matthias and Kretschmer (2020).

2. Theoretical Background

2.1 The TEM Equations and Eliassen-Palm Flux

We briefly review the Transformed Eulerian Mean (TEM) equations (Andrews and McIntyre, 1976; Andrews et al., 1987). For large-scale atmospheric phenomena, hydrostatic balance can be applied to a good approximation:

$$\frac{\partial p}{\partial z^*} = -\rho g, \tag{1}$$

where p, z^*, ρ, g are pressure, geometric height, density, and acceleration of gravity. Under hydrostatic balance, we can use the pressure coordinate as the vertical coordinate; however, when the order of the pressure changes greatly with height, it is convenient to use the log-pressure coordinate defined by

$$z = -H \ln \frac{p}{p_s}, \tag{2}$$

where H is a mean scale height and, p_s is a standard reference pressure. In the stratosphere, it is common to let H = 7 km.

There are two kinds of basic equations to describe large-scale atmospheric phenomena, i.e., primitive equations and quasi-geostrophic equations. The former is usually based on spherical coordinates and able to give more precise results. However, it is difficult to use because the equations are complex. The latter is an approximate version based on Cartesian coordinates on the tangent plane at one latitude and longitude. In addition, the β-plane approximation and quasi-geostrophic approximation are applied, so that the quasi-geostrophic equations are easy to use, but they cannot describe equatorial phenomena. Because the current

study deals with planetary waves in middle-high latitudes, the quasi-geostrophic equations are mainly used.

In the quasi-geostrophic equations, we introduce Cartesian coordinates (x, y, z) in the longitudinal, latitudinal, and vertical directions, respectively. The equations are as follows:

$$\frac{D_g u_g}{Dt} - f_0 v_a - \beta y v_g = X, \tag{3.1}$$

$$\frac{D_g v_g}{Dt} - f_0 u_a - \beta y u_g = Y, \tag{3.2}$$

$$\frac{\partial u_a}{\partial x} + \frac{\partial v_a}{\partial y} + \frac{1}{\rho_0}\frac{\partial(\rho_0 w_a)}{\partial z} = 0, \tag{3.3}$$

$$\frac{D_g \theta_e}{Dt} + w_a \frac{d\theta_0}{dz} = \frac{J}{c_p}\, e^{\kappa z/H}, \tag{3.4}$$

where $u, v, w, \theta, f_0, \beta, c_p, \kappa, J, and\ \rho_0$ are zonal winds, meridional winds, vertical winds, potential temperature, Coriolis parameter, the latitudinal derivative of Coriolis parameter, specific heat at constant pressure, a ratio of gas constant and c_p, diabatic heating, and standard density. Subscripts g and a denote the geostrophic and ageostrophic components. X and Y are unresolved horizontal components of friction or other non-conservative dynamical forcings.

We separate each variable in equation (3) into zonal-mean parts denoted by an overbar, and disturbance parts denoted by a prime: for example,

$$\bar{u}(y,z,t) = \frac{1}{a_0}\int_0^{a_0} u(x,y,z,t)dx\,, \tag{4}$$

$$u' = u - \bar{u}\,. \tag{5}$$

We can obtain the quasi-geostrophic Eulerian-mean equations by substituting the above equations into equations (3) and taking the zonal average:

$$\frac{\partial \bar{u}_g}{\partial t} - f_0 \bar{v}_a - \bar{X} = -\frac{\partial \left(\overline{v_g' u_g'}\right)}{\partial y} , \tag{6.1}$$

$$f_0 \bar{u}_a + \beta y \bar{u}_g - \bar{Y} = -\frac{\partial \left(\overline{v_g'^2}\right)}{\partial y} , \tag{6.2}$$

$$\frac{\partial \bar{\theta}_e}{\partial t} + \bar{w}_a \frac{d\theta_0}{dz} - \frac{\bar{J}}{c_p} e^{\kappa z/H} = -\frac{\partial \left(\overline{v_g' \theta_e'}\right)}{\partial y} , \tag{6.3}$$

$$\frac{\partial \bar{v}_a}{\partial y} + \frac{1}{\rho_0} \frac{\partial (\rho_0 \bar{w}_a)}{\partial z} = 0 , \tag{6.4}$$

$$f \frac{\partial \bar{u}_g}{\partial z} - \frac{R}{H} \frac{\partial \bar{\theta}_e}{\partial y} e^{-\frac{\kappa z}{H}} = 0 . \tag{6.5}$$

It is found to be difficult to examine interaction between wave activities and zonal mean (Eulerian-mean) fields by using the above equations; hence, these equations are transformed into an alternative form. The first approach is to define a residual mean meridional circulation by

$$\bar{v}^* = \bar{v}_a - \frac{1}{\rho_0} \frac{\partial}{\partial z} \left(\rho_0 \overline{v_g' \theta_e'} \,/\, \frac{d\theta_0}{dz} \right), \tag{7.1}$$

$$\bar{w}^* = \bar{w}_a + \frac{\partial}{\partial y} \left(\overline{v_g' \theta_e'} \,/\, \frac{d\theta_0}{dz} \right). \tag{7.2}$$

On substituting these equations in Eqs. (6), the following transformed Eulerian-mean (TEM) equations are obtained:

$$\frac{\partial \bar{u}_g}{\partial t} - f_0 \bar{v}^* - \bar{X} = \frac{1}{\rho_0} \nabla \cdot \mathbf{F} \equiv DF , \tag{7.1}$$

$$\frac{\partial \bar{\theta}_e}{\partial t} + \bar{w}^* \frac{d\theta_0}{dz} - \frac{\bar{J}}{c_p} e^{\frac{\kappa z}{H}} = 0 , \tag{7.2}$$

$$\frac{\partial \bar{v}^*}{\partial y} + \frac{1}{\rho_0} \frac{\partial (\rho_0 \bar{w}_a)}{\partial z} = 0 , \tag{7.3}$$

$$f_0 \frac{\partial \bar{u}_g}{\partial z} - \frac{R}{H} \frac{\partial \bar{\theta}_e}{\partial y} e^{-\frac{\kappa z}{H}} = 0 . \tag{7.4}$$

The vector **F** is known as the Eliassen-Palm flux (EPF), defined by

$$\mathbf{F} \equiv (0,\, F^{(y)},\, F^{(z)}) = (0, -\rho_0 \overline{v_g' u_g'}, \rho_0 f_0 \overline{v_g' \theta_e'} \,/\, \frac{d\theta_0}{dz}) , \tag{8}$$

$$\nabla \cdot \mathbf{F} \equiv \frac{\partial F^{(y)}}{\partial y} + \frac{\partial F^{(z)}}{\partial z}. \tag{9}$$

For EPF, it can be shown that the following equations hold,

$$\mathbf{F} = \mathbf{c_g} A\,, \tag{10}$$

where $\mathbf{c_g}$ is the group velocity in the meridional plane, and A is the wave activity density. The direction of EPF is the same as that of the group velocity, because A is usually positive for planetary waves, and the magnitude of EPF is proportional to wave activity. Because of this relationship, we can examine propagation of planetary waves by using EPF in the meridional plane.

We conduct the Fourie expansion and calculate EPF from components of WN 1 through 3 to investigate the behavior of planetary waves in the meridional plane.

2.2 Plumb's Wave Activity Flux

We introduce three-dimensional fluxes to discuss the geographical features of waves propagation. In the current study, we use Plumb (1985) 's flux (WAF) for the purpose, defined as follows:

$$\mathbf{F_s} = \frac{\rho_0}{2}\begin{pmatrix} \left(\frac{\partial \psi'}{\partial x}\right)^2 - \psi' \frac{\partial^2 \psi'}{\partial x^2} \\ \frac{\partial \psi'}{\partial x}\frac{\partial \psi'}{\partial y} - \psi' \frac{\partial^2 \psi'}{\partial x \partial y} \\ \frac{f_0^2}{N_0^2}\left(\frac{\partial \psi'}{\partial x}\frac{\partial \psi'}{\partial z} - \psi' \frac{\partial^2 \psi'}{\partial x \partial z}\right) \end{pmatrix}, \tag{11}$$

where ψ is a geostrophic stream function. Eq. (10) also holds for WAF, and zonally averaged WAF equals EPF.

We conduct the Fourie expansion and calculate WAF from components of WN 1 through 3 to investigate behavior of planetary waves in the three-dimensional plane.

2.3 Vertical Shear of Zonal Winds

The refractive index (Dickinson, 1968; Matsuno, 1970) is the traditional one for examining wave propagation and reflection in the meridional plane. A negative refractive index in the upper stratosphere changes the direction of upward propagating waves, causing them to turn downward because waves propagate to avoid regions where this index is negative. Perlwitz and Harnik (2003) made statistical analyses of waves reflection in two-dimensional dynamical fields of latitude-height sections, focusing on reflection events when planetary waves of WN 1 were dominant. They introduced a convenient and simple index characterizing features of zonal-mean zonal winds when reflection was likely to occur, i.e., the difference in zonal mean zonal-wind between 2 and 10 hPa averaged over 58˚N through 74˚N and over multi months. This wind structure is favorable condition for occurrence of downward propagation and imply the formation of the vertical reflective layer in the upper stratosphere (Perlwitz and Harnik, 2003; Matthias and Kretschmer, 2020).

Recently, the index introduced in Perlwitz and Harnik (2003) has been calculated and used for zonal mean zonal wind on each day rather than those averaged over multi-month. The occurrence of downward propagation has been discussed in association with its negative index. Waves propagate downward during or shortly after periods when this index is negative (Harnik, 2009; Nath et al., 2016). Nath et al. (2014) extended this indicator to the one without zonal

averaging and discussed zonal asymmetry of downward propagation of wave packets. A negative index region was found to be formed west of the area where waves propagated downward before the downward propagation.

We calculate the vertical shear between 2 hPa and 10 hPa for zonal winds averaged over middle-high latitude (50˚N through 80˚ N or 50˚S through 80˚S), without zonal averaging, and denote it U(2-10) to discuss the occurrence of downward propagation.

3. Data and Analysis Methods

3.1 Long-term reanalysis data

We use the Japanese 55-year Reanalysis (JRA-55) data (Kobayashi et al., 2015) made by the Japan Meteorological Agency (JMA). Their horizontal resolution is 1.25˚×1.25˚ longitude-latitude grid spacing, and 37 layers in the vertical direction cover the region from 1000 hPa to 1 hPa. For the statistical analysis of the NH, the analysis period is December through March from 1980 to 2021. For example, when we refer to "the 2015 winter," we mean the winter December 2014 through March 2015. For the case in the SH, the analysis period is August through November from 1980 to 2021. The period before 1980 is not included in the analysis because of the data quality due to the lack of satellite data in the analysis model.

3.2 A Large Ensemble Dataset

In order to obtain statistical significance for the region where JRA-55 cannot give the sufficient significance, the database for Policy Decision making for Future climate change (d4PDF; Mizuta et al., 2017) is used to analyze the downward propagation of planetary waves. This data is produced by the global atmospheric model MRI-AGCM3.2H (Mizuta et al., 2012). We use the historical simulations in d4PDF, which cover the period 1951 through 2011 and have 100 ensemble members simulated under observations of SST, sea ices from COBE-SST2 (Hirahara et al., 2014) and greenhouse gas concentrations. Their horizontal resolution is 2.5˚ × 2.5˚, and 24 layers in the vertical direction cover the region from 1000 hPa to 0.5 hPa.

3.3 Others

We make time-lagged composite analyses for events of downward propagation with the key day of the mature date of each downward propagation event (“event day”). In particular, the event days are the days with the negative peak of the vertical components of EPF or WAF. Welch's t-test is made to investigate statistically significance with a 95% confidence level for JRA-55 and 99.9% confidence level for d4PDF.

Variables are averaged over middle-high latitude from 50 ˚N to 80 ˚N in the NH or from 50 ˚S to 80 ˚S in the SH.

We investigate the downward propagation events of planetary waves (“DP events”) in Section 4. Their events are detected on the basis of EPF. We next investigate the events of downward propagation of planetary waves packets in Section 5. In this case, the events are detected on the basis of WAF. As described in Introduction, we name the detected events the LDP events instead of PR events. For details of the analysis method will be described in each section.

4. Downward Propagation of planetary waves in the Northern and Southern Hemispheres

In this section, we focus on downward propagation events of planetary waves, not wave packets. This section is composed by two parts: The first part is about the results of downward propagation in the reanalysis data. By doing this, we clarify the statistical features of longitudinal distribution of events, their causation mechanisms, and impacts to the tropospheric circulation in the observational data. In the second part, we investigate the events more detail by using a large ensemble dataset on the basis of the results from the reanalysis data.

4.1 Events in the Reanalysis Data

4.1.1 Analysis Methods

We extract strong DP events because the characteristics of such events are highlighted. The criterion value for extracting significant downward propagation events is defined as follows. We calculate the vertical components of EPF (EPFz) averaged over 50°N through 80°N at 30 hPa on each day in the analysis period. This altitude is set to capture downward propagation events in the stratosphere.

Next, we extract days when the averaged values are negative and calculate mean and standard deviation values of them during the NH winters (December through March) in the analysis period; the resultant mean is -1.73×10^4 kg^2 s^{-2}, and the standard deviation is -1.86×10^4 kg^2 s^{-2}. We set a criterion value from the mean minus the standard deviation to -3.6×10^4 kg^2 s^{-2}.

By setting this criterion value, we can get about top 20 percentages of the downward propagation events in the NH and enough event number for statistical analyses. We use this criterion value for both hemispheres because we should compare the event number in the NH and SH. This criterion value is larger than that made in the same way for the SH, -2.5×10^4 kg^2 s^{-2}. Therefore, this criterion value is a somewhat stricter one for the events in the SH.

We extract successive days during which EPFz averaged over middle-high latitude (50˚N through 80˚N or 50˚S through 80˚S) at 30 hPa are more negative than the criterion value and seek dates of maximum negative EPFz values. To avoid double counting, we regard the successive days occurring within ten days to be included in the same events. Even for the events with relatively close event days, for example, those in the same month, upward wave propagation is observed between the event days, so that they can be judged independent events. The longitude distribution of the events is defined as a longitude where the vertical component of WAF (WAFz) at 30 hPa, averaged over middle-high latitude, has a maximum negative value on the event day.

To classify events based on the longitudinal structure of wave packets on the event days, we make an Empirical Orthogonal Function (EOF) analysis for WAFz averaged over middle-high latitude at 30 hPa for the event days extracted as described above. In particular, we classify the extracted events (in the NH, the events excepted three events in the Eastern Hemisphere) into three groups on the basis of their first principal component, i.e., groups consisting of events with leading principal component scores greater than half the standard

deviation, those with leading principal component scores greater than negative half one, and other events in between the two.

4.1.2 Events in the Northern Hemisphere

Figure 4-1-1 shows a bar graph of extracted event numbers in the NH at each longitude. In this graph, the event numbers are counted at 22.5˚ intervals, although the JRA-55 longitudinal grid spacing is 1.25˚. Resultantly, we obtain 25 events in the NH. Most of the events occurred in the Western Hemisphere, creating a large peak around 70˚W in event number. There are events also in the Eastern Hemisphere, and they are isolated from the large peak in the Western Hemisphere, although the number is much smaller than that in the Western Hemisphere. The bar colors in Fig. 4-1-1 denote the month of occurrence. No events are detected in December, while the events occur most frequently in February, followed by January.

Next, we make an EOF analysis to classify the detected events. The classification method is described in Section 3. As described earlier, since the peak of the event in the Eastern Hemisphere are isolated. So, an EOF analysis is made for the events occurring mainly in the Western Hemisphere, except for those three events over 0˚ through 90˚E (only one event is in the Eastern Hemisphere).

Figure 4-1-2 illustrates the results of the EOF analysis. The upper left panel is a scatter plot of each event's first and second principal component scores, color labeled according to the classification on the basis of their first principal component scores, explained in Analysis

Methods. The bottom left panel shows the contribution rate of each principal component up to the fifth, which indicates that the rate of the first principal component is approximately 60%. This contribution rate suggests that classification based on the first principal component is appropriate. The upper right panel depicts the longitude distribution of WAFz at 30 hPa regressed on the first principal component, corresponding to the colors in the upper left panel. These regression lines are calculated by the mean of all events (a blue line) plus or minus EOF1 (a broken red line). The type 2 events (an orange line) indicates strong downward propagation in the Western Hemisphere, while type 3 (a green line) is an event of weak downward propagation and occurs ubiquitously.

We also look at the second principal component (a lower right panel), although the NH events are classified on the basis of the first principal component. The blue line in Fig. 4-1-2c is equal to the solid line in Fig. 4-1-2d, and other lines in Fig. 4-1-2d are calculated in the same way as in Fig. 4-1-2c. EOF2 (a broken red line in Fig. 4-1-2d) does not capture intensities of downward propagation in the Western Hemisphere as in EOF1 but detailed longitudinal peaks of downward propagation. For example, a broken line (Fig. 4-1-2d) shows a downward propagation peak slightly to the west, and a dotted line represents a downward propagation peak slightly to the east compared to the average.

Hereafter, we classify the NH events into four groups: 'type 1 through 3' events based on the EOF analysis and 'east' event occurring over 0˚ through 90˚E. As described earlier, the type 1 events (the blue scatter plots in Fig. 4-1-2a and the blue line in Fig. 4-1-2c) has the

average longitudinal distribution of wave packets, the type 2 (the orange scatter plots in Fig. 4-1-2a and the orange line in Fig. 4-1-2c) event has strong downward propagation of wave packets in the Western Hemisphere, and the type 3 events (the green scatter plots in Fig. 4-1-2a and the green line in Fig. 4-1-2c) has weak downward propagation in the Western Hemisphere or but nearly ubiquitous occurrence along the latitudinal circle. The event numbers are 12, 5, and 5, respectively, and the east events are 3. Before making a composite analysis based on these classifications, we compare the strength of downward propagation in EPF and WAF in scatter plots to observe the expression of downward propagation intensity.

Figure 4-1-3 shows scatter plots of EPFz versus WAFz averaged over middle-high latitude at 30 hPa, occurrence longitude versus EPFz, and occurrence longitude versus WAFz on the event day, from left to right. The colors denote the event classification mentioned above, i.e., the type 1, 2, 3, and east events. The occurrence longitude denotes a longitudinal grid point of the strongest downward propagation, and the WAFz value in the scatter plots is a value at that longitude. The strong downward propagation events in EPFz occur over North America (Fig. 4-1-3b). The colors of the scatter plots well illustrate WAFz strength in the Western Hemisphere (Fig. 4-1-3c); this result indicates the event classification based on EOF1 (representing strength of downward propagation in the Western Hemisphere) is valid. As seen in Fig. 4-1-3a, the EPFz and WAFz intensities do not strongly correlate, so in Fig. 4-1-3b, the scatter plots are not neatly separated by color.

From here, we describe composite results for each event group to clarify their characteristics and differences. Figures 4-1-4 through 4-1-7 show the composite results for type 1, 2, 3, and east events, respectively. The composition of the panels is as follows: The variables in all panels except latitude-height sections are averaged over middle-high latitude. The upper two panels focus on the zonal mean fields. Time-height cross sections (left-upper panels) illustrate the zonal mean zonal winds (contours) and WAFz (color shading). Note that the zonal mean WAFz corresponds to EPFz. In the latitude-height sections (right-upper panels of figures), zonal mean zonal winds (contours) and their anomalies from the climatology (color contours and shadings) are drawn for three days before the event day. As discussed later, in days three days before the event day, westerly winds deaccelerate the most. The shadings are drawn only in the statistically significant parts.

On the other hand, lower panels of Figs. 4-1-4 through 4-1-7 focus on the longitudinal extent. Left-lower panels are longitude-time sections about U(2-10) (contours) and WAFz at 30 hPa (shading), and middle-lower panels are the same sections about the anomalies from the climatology of geopotential height (black and green contours) and those of temperature at 500 hPa (color contours and shadings). Each figure has three panels longitude-height sections on the right side. These panels show anomalies from zonal mean of geopotential height (contours) and WAF (vectors) on eight and four days before the event day, and on the event day. The green contours and colored vectors are statistically significant regions. The colors in WAFz shadings and that in the vertical components of WAF vectors are common to all panels, and their color

bar is shown on the far right. Using these multiple panels, we look at the composite results for each event group and compare them.

Figure 4-1-4 illustrates the composite results of the type 1 events. This event group features average downward propagation events in the Western Hemisphere. First, we focus on wave propagation features. In the zonal mean fields, waves propagate upward from the troposphere to the stratosphere before the event day and downward in the lower to the middle stratosphere around the event day (Fig. 4-1-4a). In the longitudinal distribution, wave packets propagate upward over the entire Eastern Hemisphere, followed by downward propagation over the entire Western Hemisphere (Fig. 4-1-4c). In the altitude direction, wave packets propagate upward or downward throughout the stratosphere (Fig. 4-1-4d and 4-1-4f).

We focus on the zonal winds of the type 1 events. In the zonal mean fields, wind speeds are about 30 m s^{-1} in the stratosphere ten days before the event day. After that, zonal winds decelerate mainly in the upper stratosphere, reaching a peak of deceleration four or three days before the event day, and then recovering (Fig. 4-1-4a). In the latitude-height cross section of zonal winds, three days before the event day, zonal winds decelerate weaker than the climatology in the upper stratosphere, forming a negative vertical shear of zonal winds (Fig. 4-1-4b), which is the characteristic of the occurrence of downward propagation (e.g., Perlwitz and Harnik, 2003). In addition, statistically significant easterly winds exist in the equatorial region at upper stratosphere, which correspond to the easterly phase appearing in solstice periods of the semiannual oscillation (SAO; e.g., Andrews et al., 1987). The SAO easterlies could be

considered to deflect waves from the equatorial region to middle and high latitudes, leading to downward propagation. Furthermore, the negative peak of U(2-10) appears roughly around 180˚ (Fig. 4-1-4c), and its temporal variation is consistent with the variation of zonal-mean zonal winds (Fig. 4-1-4a).

Finally, we focus on the geopotential height (GPH) and temperature. In the stratosphere, the Aleutian high around 180˚ is significantly developed quasi-barotropically (Fig. 4-1-4f). Wave packets propagate downward at the east edge of this high (Fig. 4-1-4e). The development of the Aleutian high seems to bring about the development of anticyclonic anomalies in the troposphere around 180˚ on the event day (Fig. 4-1-4d and 4.1.4e). In particular, the high-temperature anomalies are statistically significant on the event day (Fig. 4-1-4d). The penetration of cyclonic anomalies from the stratosphere into the troposphere strengthens as approaching the event day in the NH (Fig. 4-1-4e through 4.1.4g). In the troposphere, cyclonic and low-temperature anomalies are developed over the Western Hemisphere around the event day (Fig. 4-1-4d), but they are not statistically significant.

The overall features of wave packets, zonal winds, and GPH discussed here are roughly consistent with previous studies (e.g., Kodera et al., 2008). In particular, wave packets propagate upward and downward over different regions, zonal winds decelerate in the upper stratosphere and forms negative vertical shear before the downward propagation, and cold anomalies over North America around the day of downward propagation.

Next, we look at the composite results for the type 2 events in Figure 4-1-5, comparing them with those for the type 1 events in Figure 4-1-4. It is clear from the classification on the basis of the EOF analysis that the type 2 events have stronger downward propagation of wave packets in the Western Hemisphere (Fig. 4-1-5c). However, the zonal mean WAFz may not show any differences in the intensity of downward propagation between the type 1 and 2 events (Fig. 4a and 5a); this is because wave packets propagate upward and downward simultaneously around the event day to almost cancel out each other (Fig. 4-1-5c). Wave packets propagate upward around 180˚ from ten days before the event day to two days after the event day, in addition to the common feature of upward propagation in the Eastern Hemisphere with the type 1 events.

Focused on the zonal winds of the type 2 events, the maximum wind velocity ten days before the event day is stronger than in the type 1 events. After that, the rapid deceleration before the event day is more conspicuous (Fig. 4-1-5a). As a result, weak easterly winds appear in the upper stratosphere, which form statistically significant negative anomalies from the climatology (Fig. 4-1-5b). Easterly winds in the equatorial region are common to the type 1 events (Fig. 4-1-4b and 4.1.5b). Negative U(2-10) are developed widely in both event groups. However, corresponding to the significantly strong deceleration, U(2-10) in the type 2 events shows very strongly negative and a large time variation and has two clear peaks similar to the peaks of upward propagation (Fig. 4-1-5c). In the upper stratosphere, WN1 is dominant, and the Aleutian high is more developed (Fig. 4-1-5e through 4-1-5g). The stratospheric anticyclonic

anomalies hanging down from the stratospheric to the troposphere around 180˚ are clearer on the event day, and the cyclonic anomalies around 90˚W and their penetration are stronger (Fig. 4-1-5g). In the troposphere, anticyclonic anomalies around 180˚, cyclonic anomalies around 90˚W, and cold anomalies around 90˚W are significant around the event day (Fig. 4-1-5d).

The composite results for the type 3 events are shown in Figure 4-1-6. Corresponding to the classification of the events, downward propagation in the Western Hemisphere is considerably weaker in the type 3 events (Fig. 4-1-6c). Zonal mean WAFz has little difference from other event groups (Fig. 4-1-6a). On the other hand, wave packets propagate downward ubiquitously, which differs from other types of events. The upward propagation before the event day is weaker than in other events and not statistically significant (Fig. 4-1-6c). The zonal wind deceleration is much weaker than in other events, and the anomalies from climatology are much smaller, although U(2-10) is negative (Fig. 4-1-6a and b). In the stratosphere, wave amplitudes decrease as the event day approaches (Fig. 4-1-6e through g). In addition, the penetration of cyclonic anomalies in the troposphere around 90˚W are weaker. Compared to other event groups, the characteristics of GPH and temperature in the troposphere are not clear (Fig. 4-1-6d)

Finally, we focus on the composite results for the fourth category of NH events, the east events, in which wave packets propagate downward over 0˚ through 90˚E. Figure 4-1-7 shows their composite results. In this figure, the longitudinal axis is shifted 90 degrees. In the temporal variation of zonal mean WAFz, wave propagate downward at 200 hPa about three days before the event day(Fig. 4-1-7a). This preceded downward propagation contribute to weaken the wave

structure in the stratosphere. Wave packets propagate downward in the Eastern Hemisphere (Fig. 4-1-7c). Their longitude scale, the width of the negative WAFz in the longitude-time section, is smaller than that of the Western Hemisphere events (Fig. 4-1-7c and Fig. 4-1-4c). The peak of upward propagation exits nine days before the event day near 90˚W and seven days before the event day near 90˚E, but the latter is not statistically significant. (Fig. 4-1-7c).

Deceleration of zonal winds is similar to that in the type 1 and 2 events, but the westerly winds are already considerably decelerated ten days before the event day (Fig. 4-1-7a). Climatological wind anomalies are also negative in the upper stratosphere (Fig. 4-1-7b). The longitudinal distribution of U(2-10) has its peak near 45˚W, between the longitudes of the upward and downward propagation, around four days before the event day (Fig. 4-1-7c). This difference in the location of the peak of U(2-10) is consistent with that of the downward propagation. In the stratosphere, there is no sign of WN1 dominance nor Aleutian high development in the east type events. In contrast, there are signs of the development of other WN components on the event days. Correspondingly, neither the anticyclonic anomaly hanging down nor the cyclonic anomaly penetration are seen (Fig. 4-1-7d through f). The characteristics of GPH and temperature in the troposphere are unclear (Fig. 4-1-7d).

Figure 4-1-8 shows the interannual change in the event number colored for each event group. The type 1 events are widely distributed in many winters, while the type 2 events do not occur in the 1990s, and the type 3 events are very few in the 2000s and 2010s. For the east

events, it is difficult to discuss their interannual change because of the small number of the events.

4.1.3 Events in the Southern Hemisphere

We analyze the downward propagation events in the SH on the basis of the same analysis methods in the NH. Resultantly, we could obtain 37 events. This event number is larger than the number of events in the NH event, although the criterion value is 1.4 times more severe in the SH. Figure 4-1-9 shows the same figure as Fig. 4-1-1 for the number of events in the SH. Many SH events are also in the Western Hemisphere, but the SH events are widely distributed in the longitude direction, unlike the distribution in the NH events. The bar colors in Fig. 4-1-9 denote the month of occurrence. In the Northern Hemisphere, 90% of events occur in January and February (Fig. 4-1-1), while in the Southern Hemisphere, about 70 % of the SH events occur in September and October (Fig.4-1-9).

We make the EOF analysis for all the SH events since, as mentioned above, they are widely distributed in the longitude direction. Figure 4-1-10 shows results of the EOF analysis for the WAFz at 30 hPa during the downward propagation events in the SH. The NH events have a strongly negative peak in the Western Hemisphere (Fig. 4-1-2c). However, the longitude structure of the average wave packets for the SH event (blue line in Fig. 4-1-10c) has a negative peak around 135˚W and negative values throughout almost all longitudes. The contribution of the first principal component is about 40 % (Fig. 4-1-10b), which is smaller than that of the NH

events (Fig. 4-1-2b). The regressed distributions (orange and green lines in Fig. 4-1-10c) show that the peak longitudes are shifted each other. On the other hand, EOF2 (Fig. 4-1-10d) implies the strength of downward propagation with the contribution of about 30%. As in the NH events, we classify them as types 1 through 3 on the basis of the leading mode of EOF analysis (Fig. 4-1-10a and 10c). The event numbers are 17, 8, and 12, respectively.

Figure 4-1-11 is the same as Fig. 4-1-3 but for the SH events. In the NH events, the colors are neatly divided according to WAFz intensity in the Western Hemisphere (Fig. 4-1-3c); however, this does not hold in the SH events (Fig. 4-1-11), which clearly suggests the diversity of the longitude distribution.

Figures 4-1-12 through 4-1-14 show the composite results for types 1 through 3 of the SH events with the same panel configuration as in Fig. 4-1-4. First, we focus on the type 1 events (Fig. 4-1-12), which is the average pattern of the SH events. Waves propagate upward before the event day and downward around the event day throughout the stratosphere in the zonal mean fields, as in the NH events (Fig. 4-1-12a). However, wave packet propagation of the type 1 events also has different characteristics from those of the NH events. Before the event day, wave packets propagate upward at two locations around 90˚E and 45˚W (Fig. 4-1-12c), and those around 45˚W are statistically significant (Fig. 4-1-12c and 12e). Wave packets propagate downward in the Western Hemisphere mainly, but the slightly negative WAFz also exists in the Eastern Hemisphere. (Fig. 4-1-12c).

Zonal winds decelerate in the upper stratosphere as they approach the event day and have negative U(2-10) before the event day, but the minimum of wind speeds in the stratosphere is much larger than those of the NH events (Fig. 4-1-12a). The negative anomalies from the climatology of zonal winds in the upper stratosphere are common to the NH and SH events. Its negative anomalies are located closer to middle latitudes, and positive anomalies are also significant in high latitudes in the middle stratosphere (Fig. 4-1-4b and 4-1-12b). U(2-10) is already negative ten days before the event day, and it developed to more negative (Fig. 4-1-12c). The negative U(2-10) are distributed widely, and its peak position is around 180˚ (Fig. 4-1-12c). In the stratosphere, amplitudes of wave components in the SH events are smaller than in the NH events. The formation of a quasi-barotropic anticyclone toward the event day is a similar feature (Fig. 4-1-12e through 4-1-12g). Wave packets propagate downward at the east edge of this anticyclone. Despite the commonly quasi-barotropic anticyclone in the stratosphere, neither the anticyclonic anomaly hanging down nor the cyclonic anomaly penetration from the stratosphere to the troposphere is seen. In the troposphere, traveling waves are developed, but clear relationship with the downward propagation is unclear (Fig. 4-1-12d).

Next, we compare the type 2 events with the type 1 events in the SH. Wave packets of the type 2 events are characterized by a westward shift of the downward propagation peak compared to that of the type 1 events (Fig. 4-1-12c and 4.1.13c). Correspondingly, although overall features are similar to those of the type 1 events, some different points are also seen. The upward propagation around 90˚E and downward propagation around 180˚ are stronger than

those in the SH (Fig. 4-1-13c). The wind structure is also similar to the type 1 events (Fig. 4-1-13b), but the negative development of U(2-10) is more significant (Fig. 4-1-13c). In the stratosphere, wave amplitudes are larger than in the type 1 events (Fig. 4-1-13e through 4.1.13g).

We turn our attention to the type 3 events. The peak of downward propagation of this event group is shifted eastward in comparison with the type 1 events in the SH (Fig. 4-1-12c and 4.1.14c). The longitudes of upward and downward propagation in the type 3 events are shifted eastward than the type 2 events (Fig. 4-1-13c and 4-1-14c), and the ridge of the WN1 component on the event day is also shifted eastward (Fig. 4-1-13g and 4-1-14g). Zonal winds are also different from other types of events. Easterly winds are present in the upper stratosphere due to the deceleration of westerly winds beginning more than ten days before the event day (Fig. 4-1-14a). The common features for WN1 dominance in the stratosphere and the formation of a barotropic anticyclone toward the event day (Fig. 4-1-14e through 4-1-14g).

Finally, the interannual changes in the number of the events are shown in Figure 4-1-15. This figure shows that all types of the events are distributed widely throughout the analysis period, and no significant trend can be seen.

4.1.4 Discussion

We have extract significant downward propagation events in the NH and SH. Their events occurred mainly in the Western Hemisphere. After the extraction, we classified their

events on the basis of the longitudinal features of WAFz on the event day and made the composite analysis for their events. In the zonal mean fields, the features of each event group did not show any differences; waves propagated upward prior to the downward propagation, and the negative vertical shear of zonal winds was formed between them. On the other hand, the longitudinal features were found to differ each other. Here, we first discuss the longitudinal characteristics of the events, then the necessity of investigation on the basis of the wave packets.

Most of the NH events occur in the Western Hemisphere, especially over North America (Fig. 4-1-1). This distribution is consistent with the fact that many previous case studies examined the downward propagation over North America (e.g., Kodera et al., 2008 and Matthias and Kretschmer, 2020). Around the event day of those, the Aleutian high is developed quasi-barotropically in the stratosphere, and wave packets propagate downward at the east edge of the high (the longitude height sections in Figs. 4-1-4 through 4-1-6). This feature suggests that the quasi-barotropic development of the high or the WN1 component in the stratosphere with the ridge around 180˚ is necessary for the occurrence of the downward propagation in the Western Hemisphere. Moreover, the climatological location of the Aleutian high in the stratosphere is at least important for the longitudinal distribution tendency of the downward propagation events, i.e., the large occurrence number in the Western Hemisphere. Consistently, wave packets propagate downward at the east edge of the quasi-barotropic high around 0˚. In addition, the NH events have higher percentages of event numbers in the Western Hemisphere than the SH events. This fact also reflects the evidence that the NH has the stronger high in the

stratosphere, i.e., the Aleutian high, around 180˚ in the climatological sense than in the SH. Thus, the formation and longitude of the quasi-barotropic high has important role for occurrence and longitude of the wave packet downward propagation.

We next discuss the mechanism of the formation of the quasi-developed Aleutian high. Before the event day, upward propagation of wave packets decelerates zonal winds in the upper stratosphere and form the negative vertical shear of zonal-mean zonal winds. This wind structure is the favorable condition for the occurrence of downward propagation (e.g., Perlwitz and Harnik, 2003); it is difficult for waves propagate upward in this wind structure. Although not shown in figures and shown in the results in Section 4.2.2, the phase structures of both WN1 and WN2 components were quasi-barotropic on the event day. This phase indicates that each WN component propagate downward. The superposition of those waves forms the quasi-barotropic development of the Aleutian high. Therefore, the quasi-barotropically development of the Aleutian high might be generated by the negative vertical shear of winds.

As discussed above, the formation of the quasi-barotropical Aleutian high might contribute to the downward propagation in the Western Hemisphere. In addition, the leading component of the EOF analysis for the DP events in the Western Hemisphere indicate the strength of the downward propagation in the Western Hemisphere (Fig. 4-1-2c). We classified the events into three event groups, type 1 through 3 events. Among event groups, there are roughly proportional relationships between the intensity of downward propagation of wave packets in the Western Hemisphere and several indices, i.e., the intensity of the quasi-barotropic

developed Aleutian high, the magnitude of the deceleration of westerly winds, the negative vertical shear of zonal winds, the intensity of penetrated cyclonic anomalies to the troposphere there, and the magnitude of the cold anomalies below the DP region in the troposphere. These relationships imply that strong downward propagation is caused by the strong the Aleutian high and the strong upward propagation and contributed strong impact for the troposphere. Moreover, the zonal wind speeds ten days before the event day are different among the type 1 through 3 events; type 2 events have large velocity of the winds, and the type 3 events have small velocity. Such pre-condition might be important for the strength of downward propagation. Thus, the strength of downward propagation in the Western Hemisphere is controlled by strength of upward propagation and precondition of zonal winds in the stratosphere.

The analysis on the basis of the longitudinal structure of WAFz showed that some events occur in the Eastern Hemisphere. Those events also have commons with the events in the Western Hemisphere, for example, upward propagation and the deceleration of zonal winds and the quasi-barotropical high around 0˚. A longitude of upward propagation before the event day appears mainly in the Western Hemisphere, and the longitudinal relationship between upward and downward propagation was similar between the events in the Western and Eastern Hemispheres. (Fig. 4-1-4c and 4-1-7c). However, it is difficult to discuss them detailed because the event number is a few. Even for other event groups, the event number is not enough for statistical analysis, making it difficult to discuss their impact on the troposphere.

In this study, different features in EPFz and WAFz are found in analyses for the intensity of the downward propagation events. The leading mode based on the EOF analysis for the NH events represents the large intensity of downward propagation in the Western Hemisphere, which does not necessarily correspond to the intensity of downward propagation in EPFz when looking at scatter plots (Fig. 4-1-3). For example, the two events of the strongest downward propagation in the Western Hemisphere (two orange plots in Fig. 4-1-3) have EPFz values just exceeding the criterion value. The stratospheric features are intimately related to the intensity of WAFz over the Western Hemisphere. Furthermore, in the longitude-time sections of the east events, the peak day of downward propagation in WAFz appears one day before the event day determined on the basis of EPFz (Fig. 4-1-7c). These suggest that detailed consideration of downward propagation should be based on WAFz, like Kretschmer et al. (2018). In addition, EOF2 of the NH events represents differences in peak longitudes of downward propagation in the Western Hemisphere. However, our analyses are based on longitudinal averages of WAFz over 22.5 degrees longitude; perhaps a more detailed distribution of downward propagation events should be considered without longitudinal averaging of WAFz over the entire Western Hemisphere and North America.

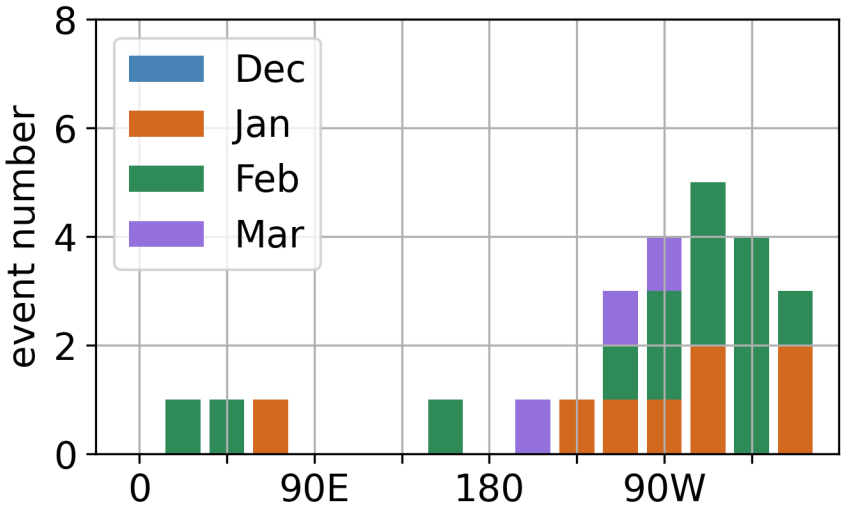

Figure 4-1-1: The extracted event numbers in the NH at each longitude in bar graphs. The event numbers are counted at 22.5˚ intervals, and the bar colors denote the month of occurrence.

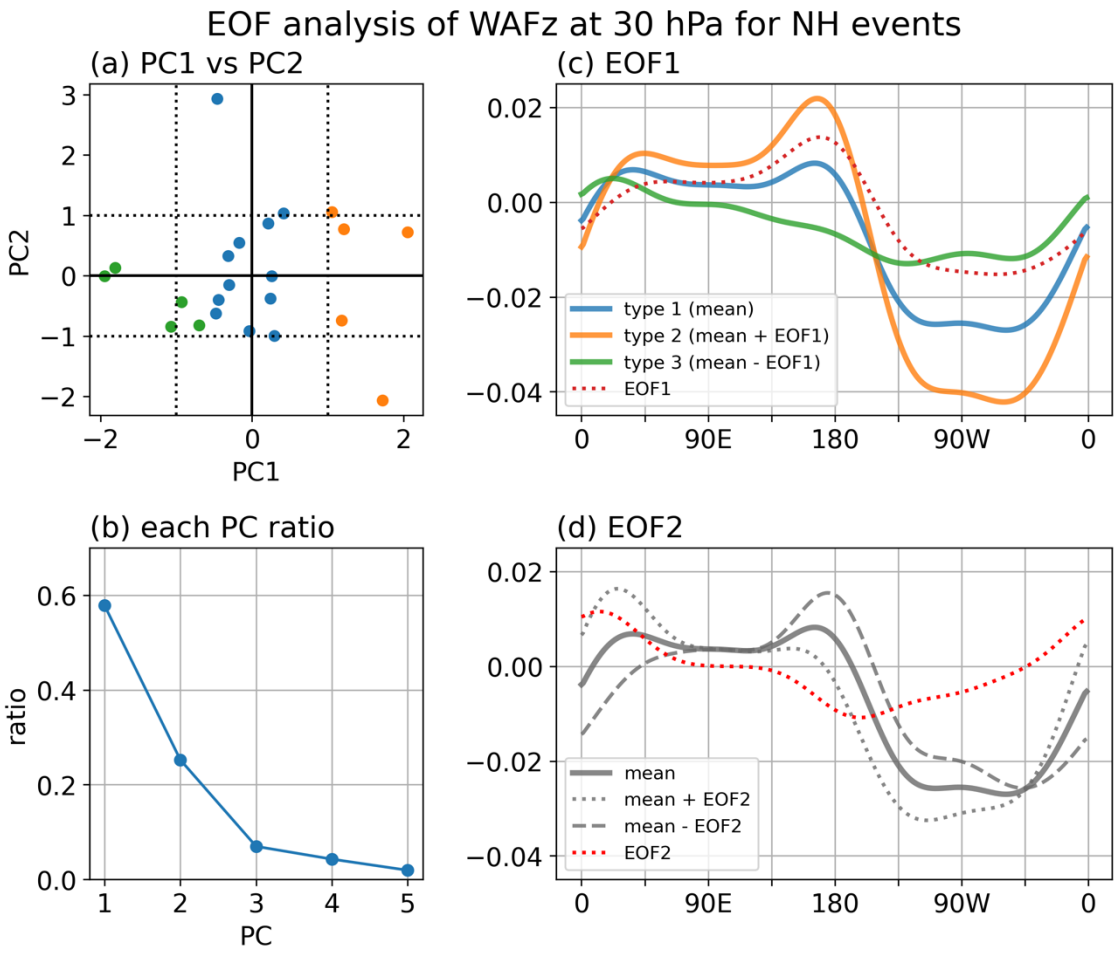

Figure 4-1-2: (a) Scatter plots of each event's first and second principal component scores for the EOF analysis. Dashed lines denote the standard deviations of each score. Plots are painted color according to the three event groups classificated on the basis of the first principal component scores, explained in Analysis Methods. (b) Each principal component is up to five for the EOF analysis. (c) The longitudinal structure of WAFz at 30 hPa regressed on the first principal component. A blue line is the mean of the events used in the EOF analysis, and an orange (green) line is calculated by adding (subtracting) the mean and EOF1 (a broken red line). (d) Similar panel to (c) but about EOF2. A solid line is the mean of the NH events, and a broken (dotted) line is calculated by adding (subtracting) the mean and EOF2 (a broken red line).

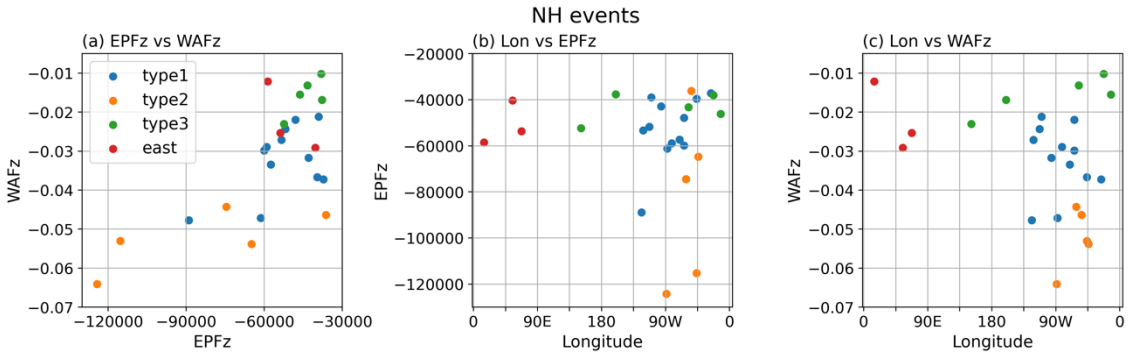

Figure 4-1-3: (a) Scatter plots of EPFz versus WAFz, averaged 50 N˚ through 80 N˚ at 30 hPa, of the NH downward propagation events. Plots are painted color based on the classification using the EOF analysis and the east events. (b) A similar panel to (a), but its x-axis is the occurrence longitude of downward propagation events based on WAFz, and the y-axis is EPFz. (c) A similar panel to (a), but its x-axis is the occurrence longitude.

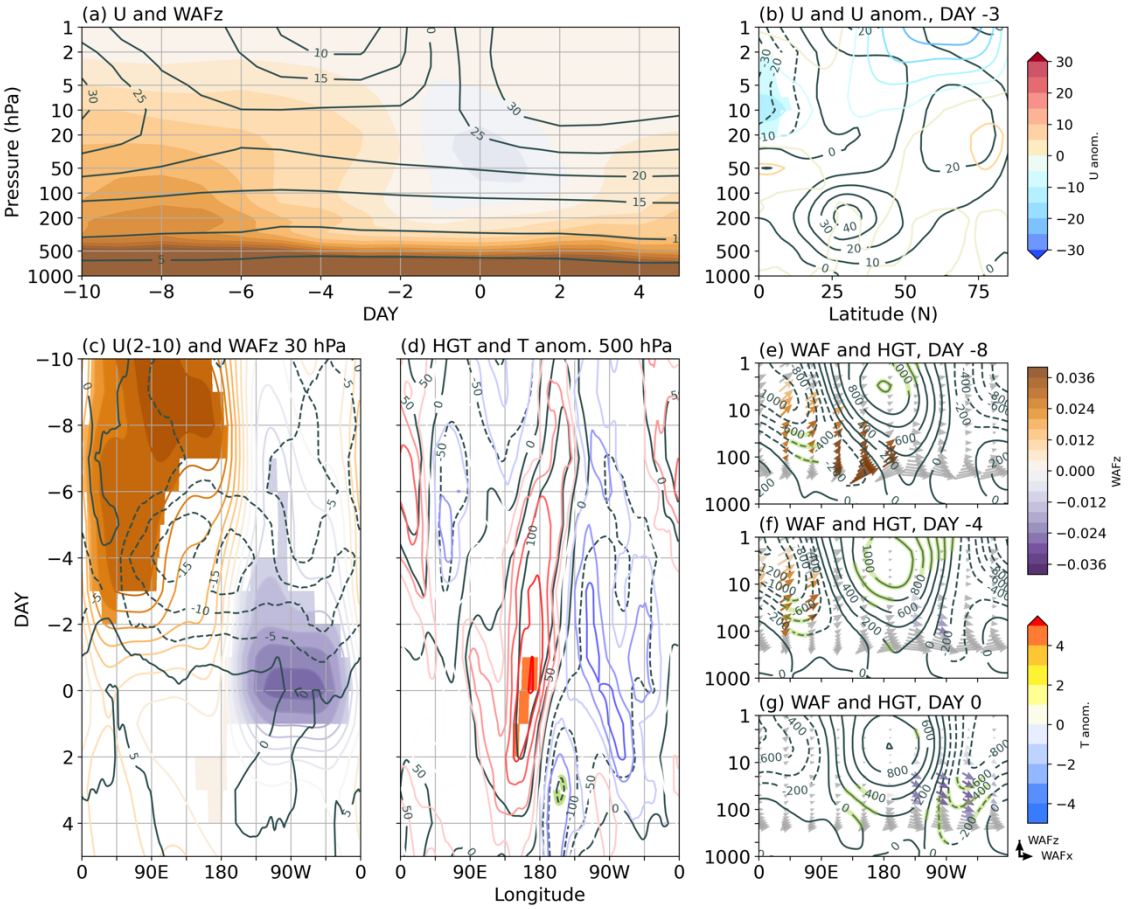

Figure 4-1-4: The composite results of the type 1 event in the NH. All variables in this figure except panel (b) are averaged middle-high latitude (50˚N through 80˚N). Color bars of each panel are shown together on the right side of this figure. (a) Time-height section of zonal mean zonal winds (m s^{-1}, contours) and WAFz (m^2 s^{-2}, shadings). (b) Latitude-height section of zonal mean zonal winds (m s^{-1}, contours) and their anomalies from the climatology (m s^{-1}, color contours and shadings) three days before the event day, with the shading depicting only the statistically significant parts. (c) Longitude-time sections of U(2-10) (m s^{-1}, contours) and WAFz at 30 hPa (color contours and shadings), with the shading depicting only the statistically significant parts. (d) Longitude-time sections of the geopotential height anomalies (m, black and green contours) and temperature anomalies from their climatology at 500 hPa (K, color contours and shadings). The green contours and shading depicting only the statistically significant parts. (e) Longitude-height section of geopotential height anomalies from zonal averages (m, contours), WAF (m^2 s^{-2}, vectors), for eight days before the event day. The green contours and colored vectors are statistically significant. The unit vector is bottom of this figure, and its

length is 10 m^2 s^{-2} in the horizontal direction and 0.5 m^2 s^{-2} in the vertical direction. (f) Same panel as (e), but on four days before the event day. (g) Same panel as (e), but on the event day.

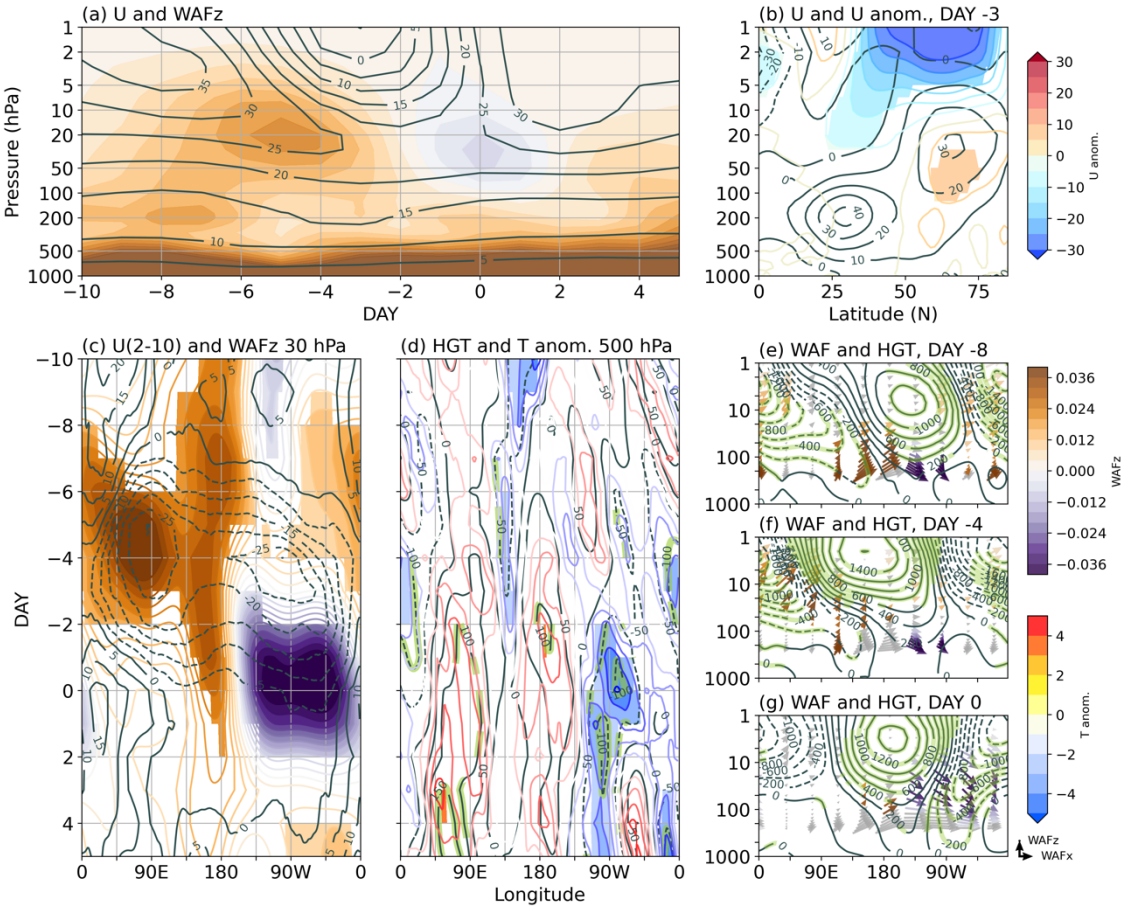

Figure 4-1-5: Same figure as Fig. 4-1-4, but for the type 2 event in the NH.

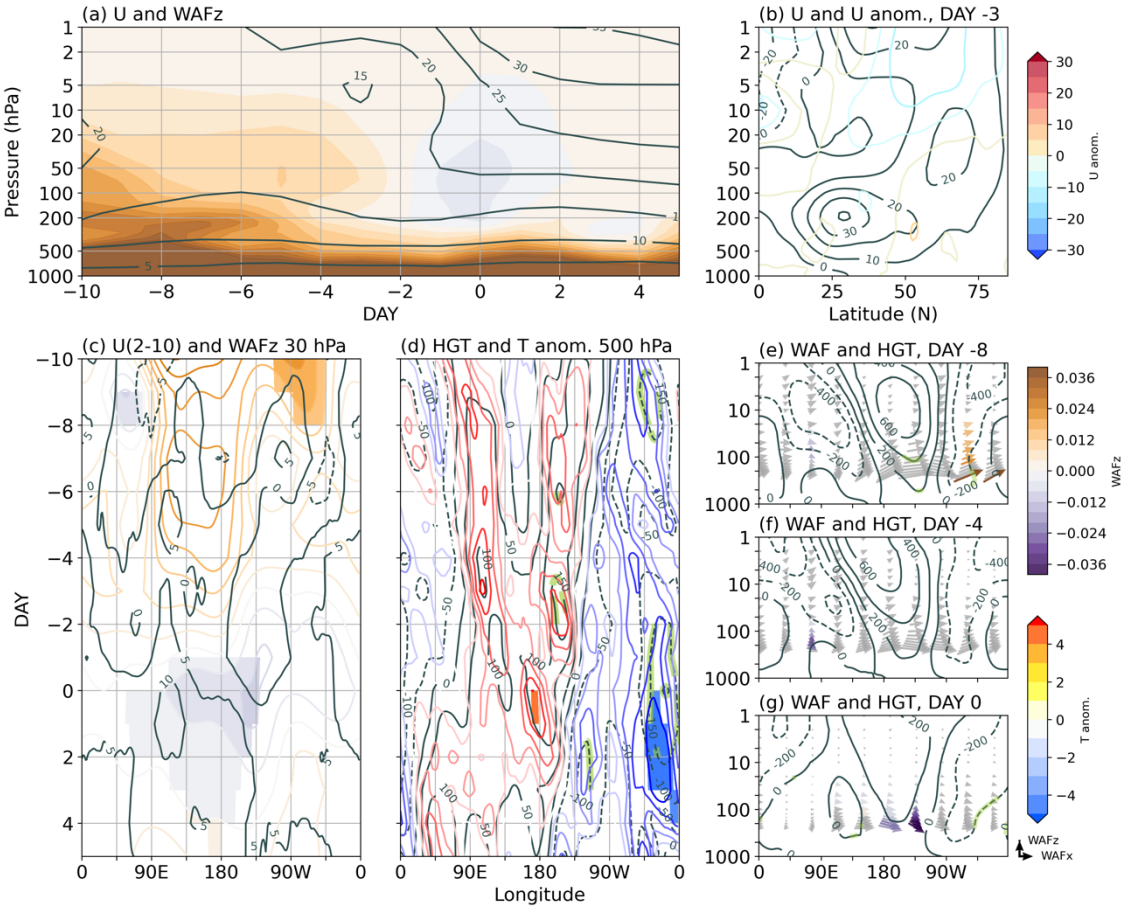

Figure 4-1-6: Same figure as Fig. 4-1-4, but for the type 3 event in the NH.

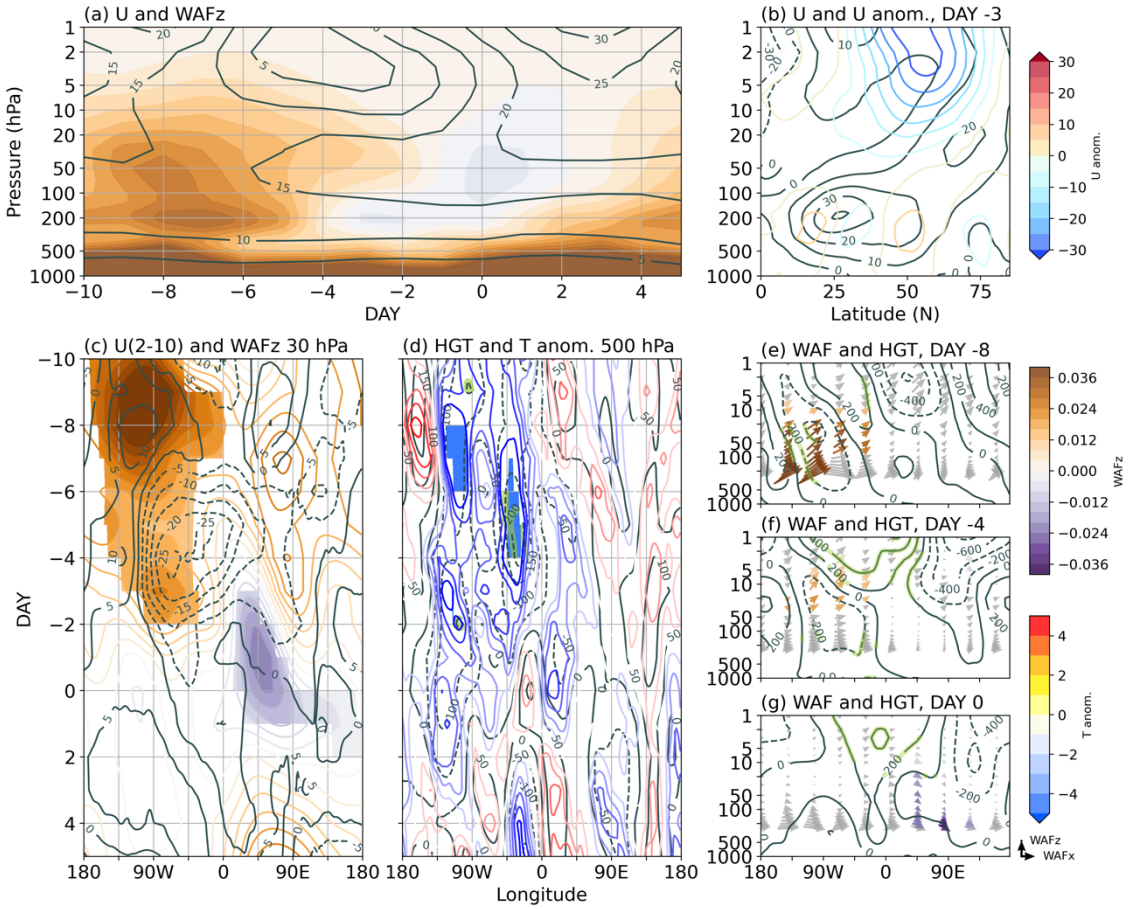

Figure 4-1-7: Same figure as Fig. 4-1-4, but for the east event in the NH. The longitudinal axis is shifted 90 degrees.

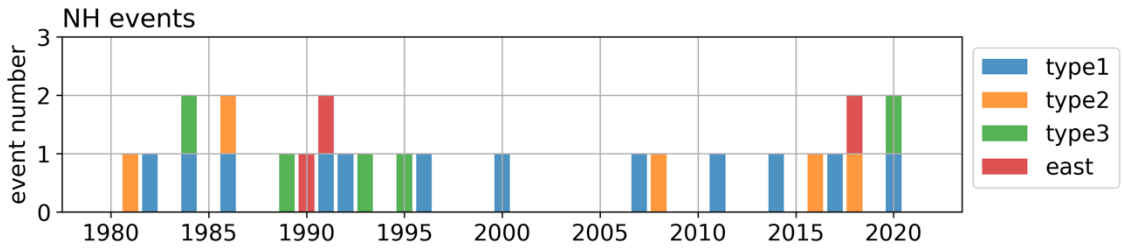

Figure 4-1-8: The interannual change in the event number of each event group. Colors denote the event group.

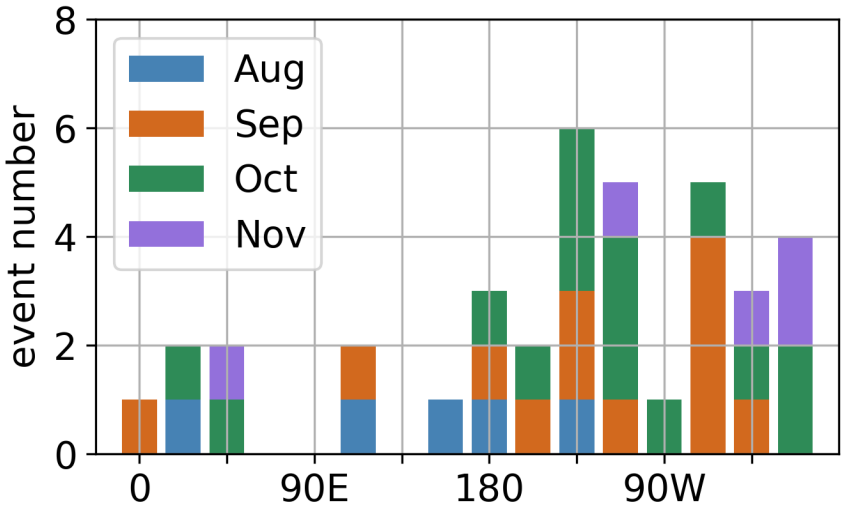

Figure 4-1-9: Same figures as Fig. 4-1-1, but for the downward propagation events in the Southern Hemisphere.

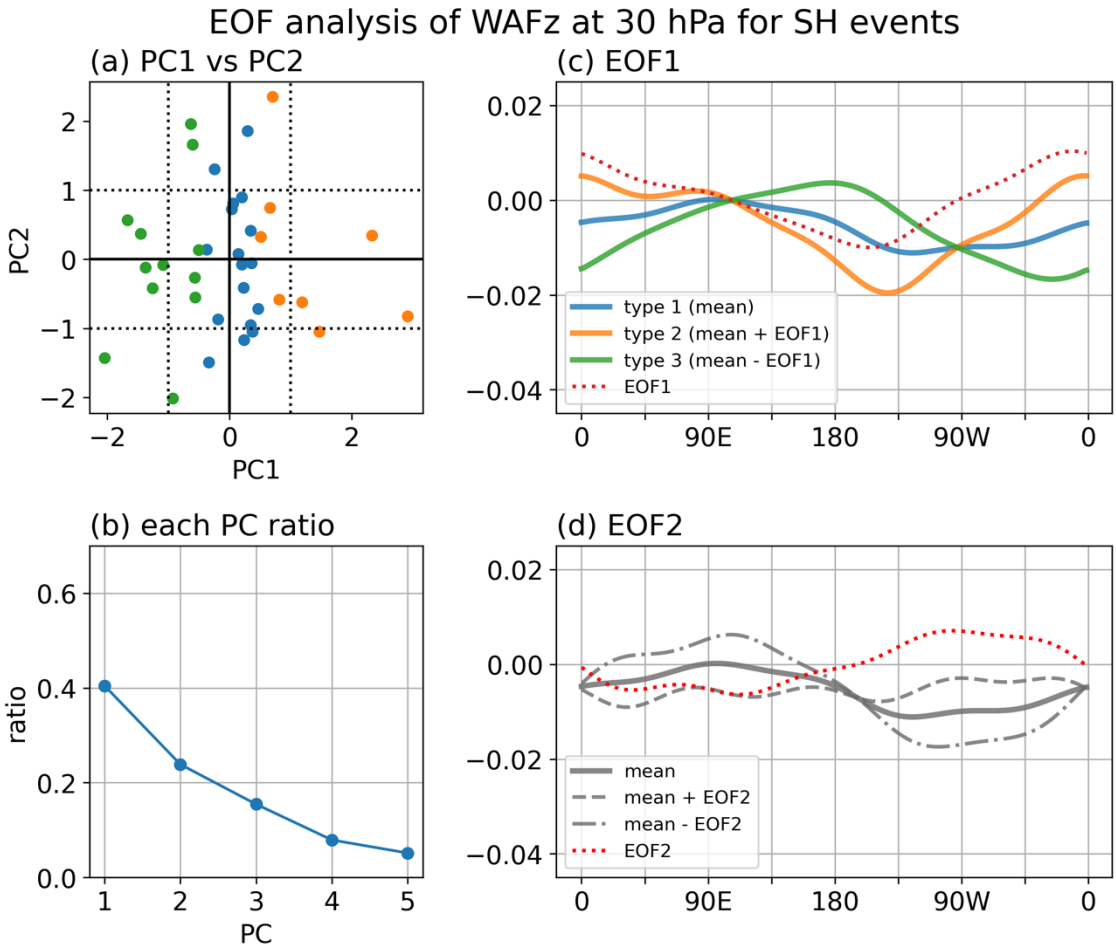

Figure 4-1-10: Same figures as Fig. 4-1-2, but for the downward propagation events in the Southern Hemisphere.

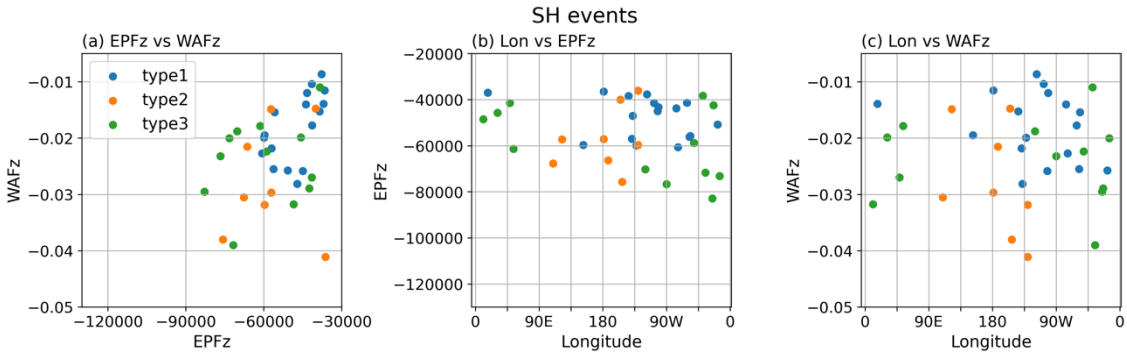

Figure 4-1-11: Same figures as Fig. 4-1-3, but for the downward propagation events in the Southern Hemisphere.

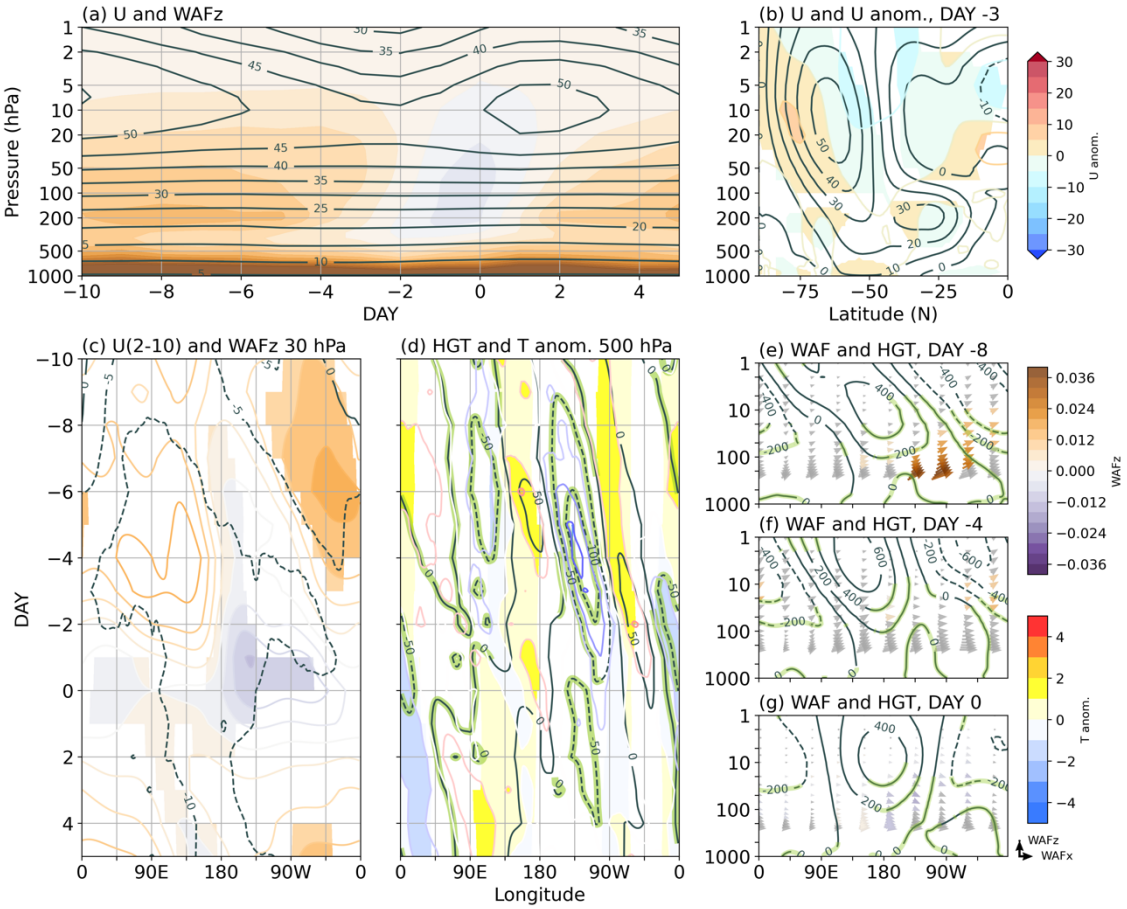

Figure 4-1-12: Same figure as Fig. 4-1-4, for the type 1 event in the SH. The variables in panels expect latitude-height section are averaged over 50˚S through 80˚S.

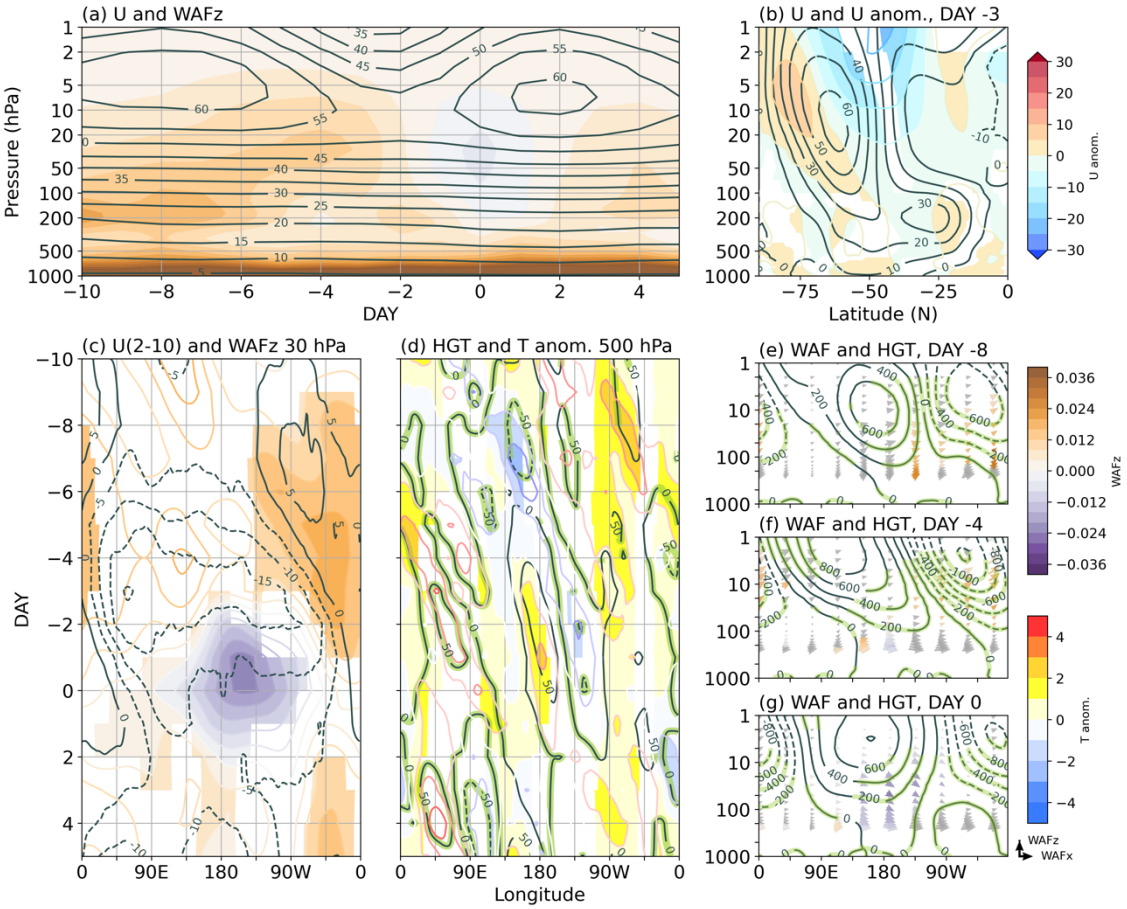

Figure 4-1-13: Same figure as Fig. 4-1-4, but for the type 2 event in the SH.

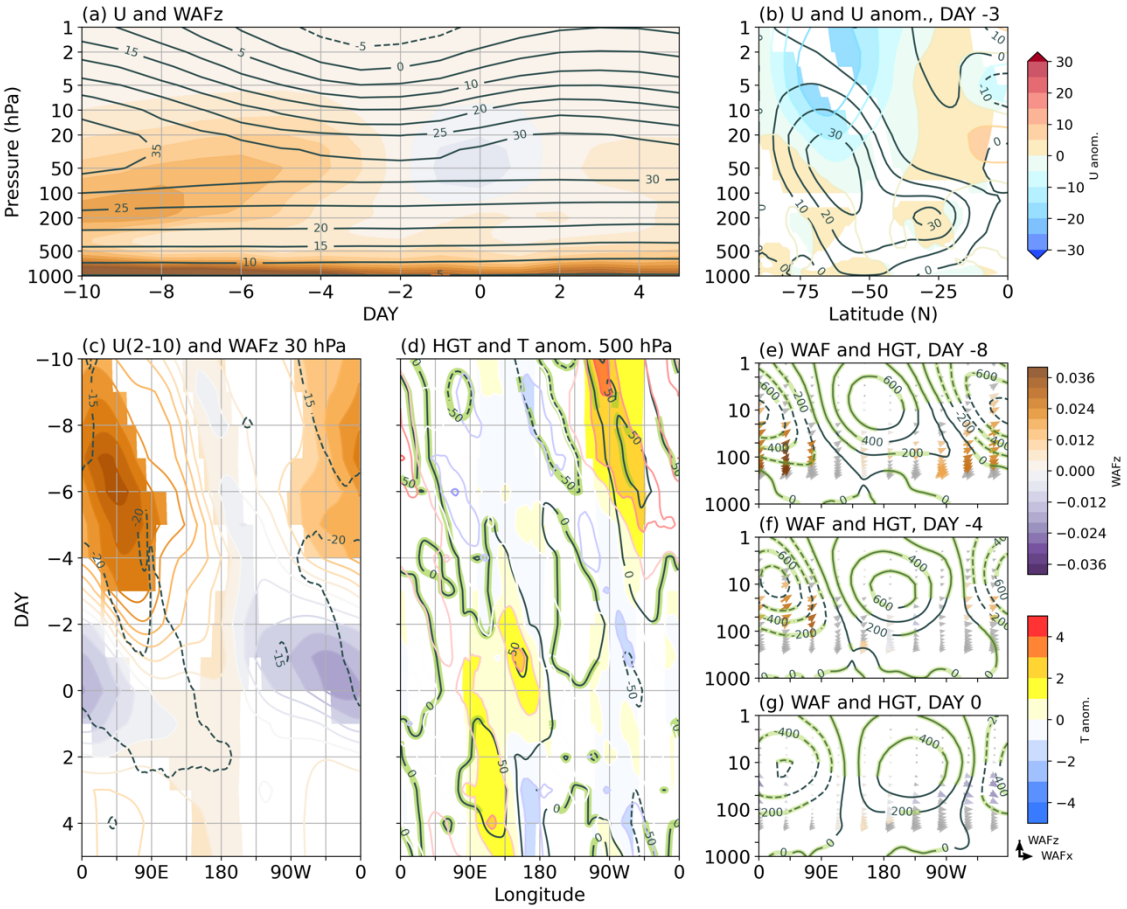

Figure 4-1-14: Same figure as Fig. 4-1-4, but for the type 3 event in the SH.

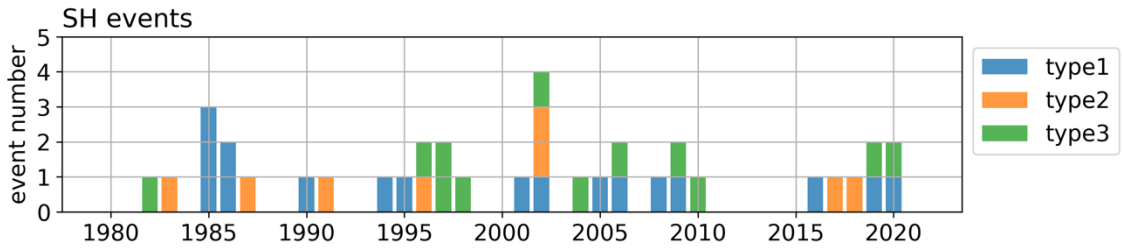

Figure 4-1-15: Same figures as Fig. 4-1-8, but for the downward propagation events in the Southern Hemisphere.

4.2 Events in the Large Ensemble Data

In Section 4.1, we performed a composite analysis for the DP events in the NH and SH. The NH events had a possibility of downward propagation affecting the tropospheric circulation; however, the number of their events was small for statistical analysis to show their impact. In particular, there are only three events in the Eastern Hemisphere. Therefore, we investigate the downward propagation events in the NH using d4PDF.

4.2.1 Analysis Methods

We also extract DP events for d4PDF in the same way as in Section 4.1.1, but the criterion value in the extraction is zonally averaged WAFz, not EPFz. We set a criterion value in the same way as in Section 4.1.1, and its value is $-4.23 \times 10^{-3}\ \mathrm{m^2\ s^{-2}}$. After the extraction, we classify the events on the basis of the longitudinal characteristics and make a composite analysis for them.

4.2.2 Results

Resultantly, we obtain 4746 events during 6000 years in the NH. This number of events which is converted to the analysis period of 40 years in JRA-55 is about 33. This event number is larger than that in JRA-55. Figure 4-2-1 shows a bar graph of extracted event numbers in the NH at each longitude. In this graph, the event numbers are counted at 11.25˚ intervals, although the d4PDF longitudinal grid spacing is 2.5˚. This interval is half that of the analysis for JRA-55.

We compare this bar graph with that of the event number of the DP events in JRA-55 (Fig. 4-1-1). We could obtain a smooth distribution using d4PDF. Most of the events occur in the Western Hemisphere in both data, but the longitude of occurrence in d4PDF has two large peaks. There is a single peak in the Eastern Hemisphere, consistent with the isolated peak in the Eastern Hemisphere in JRA-55 (Fig. 4-1-1). The bar colors indicate the month of occurrence. The event number in February is large, and some events occur in December, although events do not occur in December in JRA-55 (Fig. 4-1-1).

Before classifying events, we show a figure similar to Figure 4-1-3, which compares the strength of downward propagation in EPF and WAF. Figure 4-2-2 is the two-dimensional histogram of EPFz vs. WAFz averaged over middle-high latitudes at 30 hPa, occurrence longitude vs. EPFz, and occurrence longitude vs. WAFz on the event day, from left to right. Note that EPFz in this figure is the zonally averaged WAFz. The horizontal and vertical axes show that the magnitude of WAFz is greater than that of EPFz (Fig. 4-2-2a). The strong events tend to have strong downward propagation in WAFz, but this tendency is not absolute because some weak events in EPFz have strong WAFz (Fig. 4-2-2a). In the longitudinal distribution, there are strong events in EPFz or WAFz in both the Western and Eastern Hemispheres (Figs. 4-2-2b and 4-2-2c).

In the analysis for JRA-55, we classified the events into four groups on the basis of the longitudinal distribution and an EOF analysis for WAFz at 30 hPa. In the current analysis for

d4PDF, we classify the events on the basis of the longitudinal distribution, because the two peaks in the Western Hemisphere are noteworthy and different from the distribution in JRA-55.

We make three groups on the basis of the three peaks in the histogram. Each longitude of the groups is 45˚. The first group is the DP events with occurrence longitude from 135 ˚W to 90˚W ("west1"), the second group is those with occurrence longitude from 67.5 ˚W to 22.5 ˚W ("west2"), and the third group is those with occurrence longitude from 45 ˚E to 90˚E ("east"). The longitudinal range of the east events in d4PDF is slightly different from that of the east events in JRA-55. Their event numbers are 1297, 1595, and 443, respectively.

In addition, upward propagation before the event day is different for each event in the east events, i.e., upward propagation in the Western Hemisphere or Eastern Hemisphere before the event day. Therefore, we classify the east events into two groups; one is "east-west" events which have upward propagation in the Western Hemisphere four days before the event day, and the other is "east-east" events which have those in the Eastern Hemisphere. The event numbers of the east-west and east-east events are 285 and 158, respectively. Therefore, we make a composite analysis for four groups.

Figure 4-2-3 shows time-height sections of the lag composite results for zonal-mean zonal winds (contours) and zonal-mean WAFz (color shadings) averaged over middle-high latitudes. For all event groups, zonal winds decelerate mainly in the upper stratosphere, reaching a deceleration peak about three days before the event day; this feature is consistent with the results in JRA-55. The deceleration forms a negative vertical shear of the zonal winds which is

favorable condition for the downward propagation. The differences between the west1 and west2 events are small, but the zonal winds of the east-west and east-east events are different from those. The wind speeds are greater in the east-west events from ten days before the event day and smaller in the east-east events.

We focus on the wind structures three days before the event day because the peak deceleration exists on that day. Figure 4-2-4 is latitude-height sections of composite results for zonal mean zonal winds (contours) and their anomalies from the climatology (color shadings and color contours) three days before the event day. By the deceleration, the negative anomalies are developed in the upper stratosphere in all event groups. As seen in the time-height sections (Fig. 4-2-4), there are differences in the speeds of zonal winds. In the east-west events, the wind speeds are large, and positive anomalies exist over high latitudes in the stratosphere. Anyways, the negative vertical shear of zonal winds is clear three days before the event day.

We next focus on the longitudinal characteristics of the events. Figure 4-2-5 shows longitude-time sections of the lag composite results for U(2-10) (contours) and WAFz at 30 hPa (color shadings and color contours), averaged over middle-high latitudes. The overall characteristics of the west1 and west2 events are similar to those of the west events in JRA-55, and we could obtain smooth and statistically significant features. Wave packets propagate upward in the Eastern Hemisphere before the event day and propagate downward in the Western Hemisphere around the event day, and the negative U(2-10) is formed between the upward and downward propagation. The longitudinal regions of upward and downward propagation are

almost the same in the west1 and west2 events, but the longitudinal peaks of downward and upward propagation are different. In the west1 events, there is the peak of downward propagation on the event day around 110˚W and the peak of upward propagation between 90˚E and 180˚ from four to six days before the event day (Fig. 4-2-5a). In the west2 events, there is the peak of downward propagation on the event day at 45˚W and the peak of upward propagation at 45˚E from four to six days before the event day (Fig. 4-2-5b). Their longitudinal peaks of wave packets propagation are different in the west1 and west2 events, but the length of the periods between upward and downward propagation are almost the same.

The results in the east events are also clear and significant because d4PDF has a large ensemble. The characteristics of the east-west events are similar to the east events in JRA-55. Wave packets propagate in the Western Hemisphere before the event day and downward in the Eastern Hemisphere around the event day, and negative U(2-10) is located between their propagation, As discussed for the east events in JRA-55, the features of the east-west events are qualitatively similar to those of the west1 and west2 events, i.e., the positional relationship of upward and downward propagation and the negative U(2-10) between upward and downward propagation. However, the east-east events have different characteristics from the others. Wave packets propagate upward and downward in the Eastern Hemisphere, and negative U(2-10) is ubiquitous before the event day.

We next focus on the tropospheric circulation during the events. Figure 4-2-6 shows longitude-time sections of lag composite results for geopotential height anomalies (contours)

and temperature anomalies (color shading and color contours) at 500 hPa from their climatology. In the analysis for JRA-55, the statistical characteristics were unclear because the event number is small, but we could obtain them in d4PDF. For the west1 and west2 events, the cyclonic and cold anomalies are developed over the almost same region, covering the Western Hemisphere around the event day (Fig. 4-2-6a and 4-2-6b), although the longitudinal peaks of downward propagation in their events are different (Fig. 4-2-5a and 4-2-5b). The anticyclonic and warm anomalies also develop around 180˚, but on different days. The magnitudes of their anomalies are larger in the west1 events than in the west2 events.

In the east-west events, cyclonic and cold anomalies in the troposphere exist below the DP region in the stratosphere. This feature is not seen in JRA-55 and is qualitatively consistent with the features of the west1 and west2 events. Prior to the event day, anticyclonic anomalies develop around 180˚ in the troposphere; these anomalies force upward propagation in the Western Hemisphere (Fig. 4-2-6c). In the east-east events, the cyclonic and cold anomalies are not as strong as in the east-west events, but the anticyclonic and warm anomalies are developed around 135˚E.

Figure 4-2-7 shows the anomalies of geopotential height from zonal averages and WAF vectors for the composite results averaged over the middle-high latitudes of each event group. The left, center, and right panels are the composite results on the event day, four days before the event day, and eight days before the event day. The characteristics of the west1 and west2 events are similar to the west events in JRA-55, i.e., the downward propagation of wave

packets at the east edge of the Aleutian high, the quasi-barotropic development of the Aleutian high, and the penetration of the cyclonic anomalies from the stratosphere into the troposphere. The Aleutian high develops more barotropically in the west1 events.

The characteristics of the east-west events are qualitatively similar to those of the west1 and west2 events; this fact is estimated in longitude-height sections in JRA-55, but we could obtain clear results using d4PDF. Wave packets propagate at the east edge of the high around 0˚. This high develops after the upward propagation in the Western Hemisphere, and the Aleutian high is weak. The east-east events have weaker wave structures on the event day, but the very weak high is located around 0˚. Wave packets propagate downward at the east edge of the high.

To discuss the wave structure in more detail, we show the WN1 and WN2 components in longitude-height sections on the event day, Figure 4-2-8. The left panels of this figure are same as those of Fig. 4-2-7, and the center and right panel shows the WN1 and WN2 components of geopotential height in the longitude-height sections on the event day. For west1 and west2 events, the WN1 and WN2 components have quasi-barotropic wave structures in the stratosphere. The longitude of ridge of WN1 has a small difference between their events. The east-west events have a smaller amplitude of WN1 and a larger amplitude of WN2 than the west1 and west2 events. The phase of WN2 tilt eastward, and the phase of WN1 is tilted eastward at 30 hPa. The east-east events also have barotropic phases, but the amplitudes of the

waves are very small. The overlapping of these waves in each event group produces the features of wave packets.

The analysis for d4PDF allows us to examine interannual changes and the trend in occurrence dates. Figure 4-2-9 shows the ensemble means and standard deviations of the interannual changes of each event group; event numbers are counted from December to March each winter. There are no increasing or decreasing trends in any of the event groups. The standard deviations are large and the perturbations of each ensemble, i.e. sea surface temperature, change the event number.

Figure 4-2-10 shows histograms of the occurrence dates of the event numbers in each event group. The west1, west2, and east-west events have a large peak around February, but the east-east events peak around March.

4.2.3 Discussion

We obtained similar composite results about downward propagation in d4PDF as in JRA-55, and their results are more statistical. On the other hand, there are two different points; one is the two large peaks of the occurrence longitude of the events in the Western Hemisphere, and the other is the characteristics of the events in the Eastern Hemisphere. In this section, we discuss their differences and the causal mechanism of the events.

The occurrence longitude of DP events in d4PDF have two large peaks in the Western Hemisphere (Fig. 4-2-1), which is not seen in JRA-55 (Fig. 4-1-1). We made a composite

analysis for the event groups classified on the basis of distribution. There are several common features between the west1 and west2 events, i.e., the longitudinal region of downward propagation, the penetration of the cyclonic and cold anomalies in the Western Hemisphere, and the quasi-barotropic development of the Aleutian high. On the other hand, the upward propagation before the event day and the phase of the WN1 components are different. In the phases of the waves, the ridges of the WN1 components in the west2 events are farther west than those in the west1 events (Fig. 4-2-8), and the appearances of the geopotential heights eight days before the event day have no differences in the west1 and west2 events (Fig. 4-2-7). Therefore, these differences in the phases of WN1 are considered to be generated by the differences in the longitudinal peaks of upward propagation. Moreover, the longitudes of the anticyclonic anomalies six through eight days before the event day are different between the west1 and west2 events (Fig. 4-2-6). The anomalies are located around 25˚E and 0˚ in the west1 and west2 events. This difference in the anticyclonic anomalies generate the difference of the longitudes of upward propagation discussed above.

The results of the west1 and west2 events discussed above were not observed in JRA-55. This may be because the analysis period of the reanalysis data is short, or this is the tendency of the model calculating the ensemble data. On the other hand, we get a similar result for the LDP events in JRA-55 and d4PDF, as shown in Chapter 5. Therefore, the former possibility might be high.

The characteristics of the east events are different from those in JRA-55. First, the events in JRA-55 are located over 0˚ to 90˚, and we could get a smooth distribution in d4PDF, which has a peak around 45˚E to 90˚E. Next, the diversity of upward propagation before the event day is clarified by the analysis in d4PDF. There are two groups of events; they have upward propagation in the Western and Eastern Hemispheres, the east-west and east-east events. In JRA-55, it was difficult to show such results, but the characteristics of the wave packets in one of the east events in JRA-55 were similar to the east-east events in d4PDF. Therefore, the east-east events can occur in the real atmosphere.

The east-east events have different characteristics from the west1, west2, and east-west events. The main differences are the smaller amplitude of the waves in the stratosphere on the event day and the slow westerly winds. The east-east events might occur after something decelerate zonal winds, for example, stratospheric warming. In stratospheric winters, the amplitude is large and decreases toward the end of the winter, and the velocity of the westerly winds decreases; therefore, the occurrence dates of the east-east events were later than other event groups. Because the amplitude is small, the penetration of cyclonic anomalies seen in other event groups is unclear and has less impact on the troposphere.

The following causal mechanisms are considered for the four groups of events.

(1) Wave packets propagate upward from the troposphere into the stratosphere. Note that the longitudes of upward propagation are different for the different event groups.

(2) Upward propagation decelerates westerly winds and forms the negative vertical shear of zonal

winds. It is difficult for waves to propagate upward in the formed wind structure (Perlwitz and Harnik, 2003).

(3) Wave phases are changed to quasi-barotropic.

(4) Overlapping of waves, i.e., WN1 and WN2, produces downward propagation of wave packets.

(5) Downward propagation enhances wave trains or entrainment of cyclonic anomalies.

(6) The cyclonic and cold anomalies in the troposphere are enhanced below the region of downward propagation. Note that the strength of their anomalies is different for different groups of events.

Here, we discuss the mechanism of the impacts on the troposphere. Downward propagation causes blocking events in the stratosphere, and blocking events cause advection, resulting cold spells (Matthias and Kretschmer, 2020). However, the anticyclonic and cyclonic anomalies are developed in the troposphere in the west1 and west2 events (Fig. 4-2-6a and 4-2-6b), and the cold spells are located over the almost same region of the cyclonic anomalies. Hence, the enhancement of their anomalies causes cold spells in the troposphere. This enhancement implies the enhancement of wave structure in the troposphere. Because wave packets propagation stretches the wave trains, it is easy to estimate that the wave structures are strengthened in the region of the downward propagation. Same characteristics are observed in the east-west and east-east events (Fig. 4-2-6c and 4-2-6d).

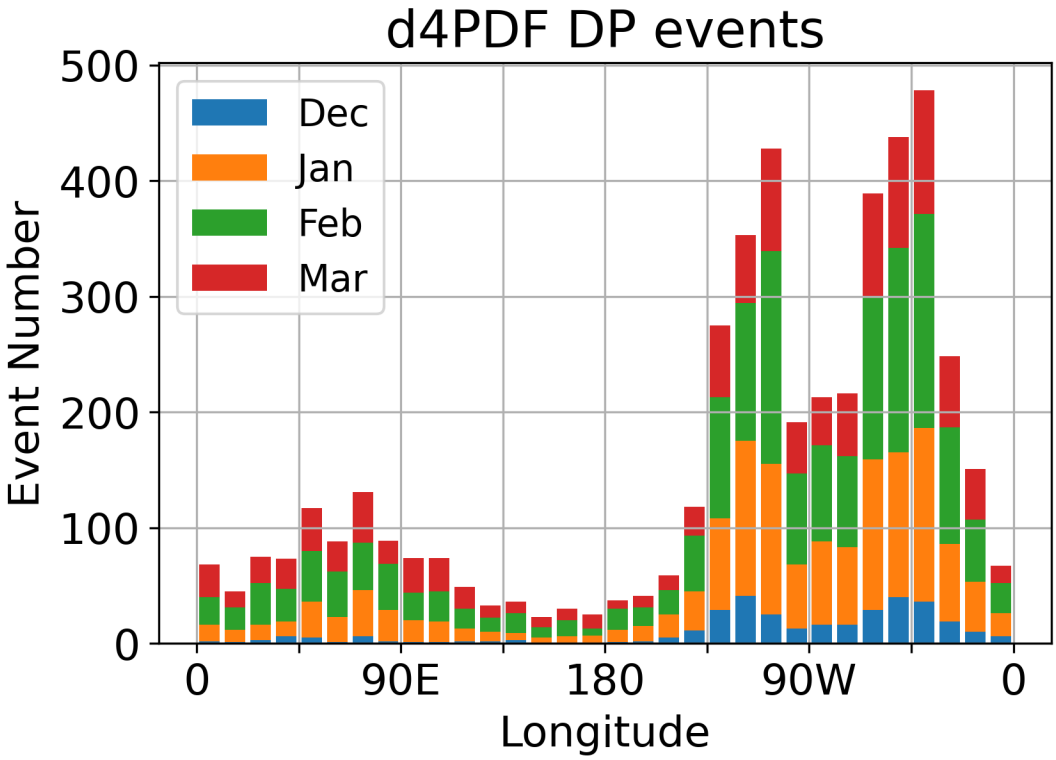

Figure 4-2-1: The extracted event numbers in d4PDF at each longitude in bar graphs. The event numbers are counted at 11.25˚ intervals, and the bar colors denote the month of occurrence.

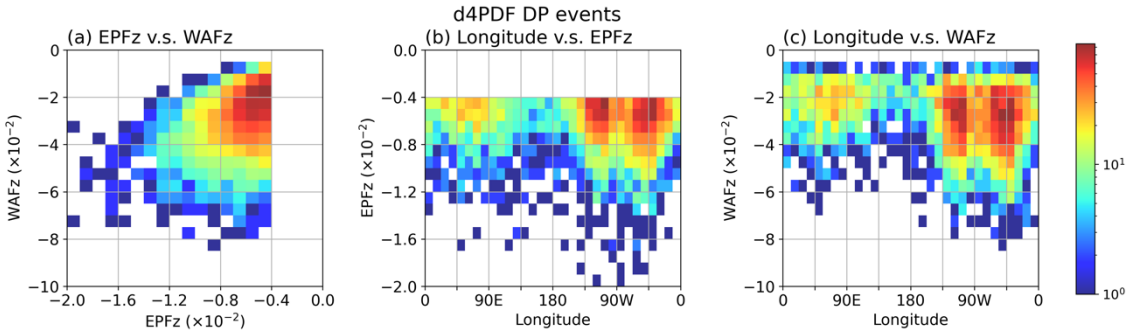

Figure 4-2-2: (a) Two-dimensional histogram of EPFz, which is WAFz averaged zonally, versus WAFz, averaged 50 N˚ through 80 N˚ at 30 hPa, of the DP events in d4PDF. (b) A similar panel to (a), but its x-axis is the occurrence longitude based on WAFz on the event day of DP events, and the y-axis is EPFz. (c) A similar panel to (a), but its x-axis is the occurrence longitude.

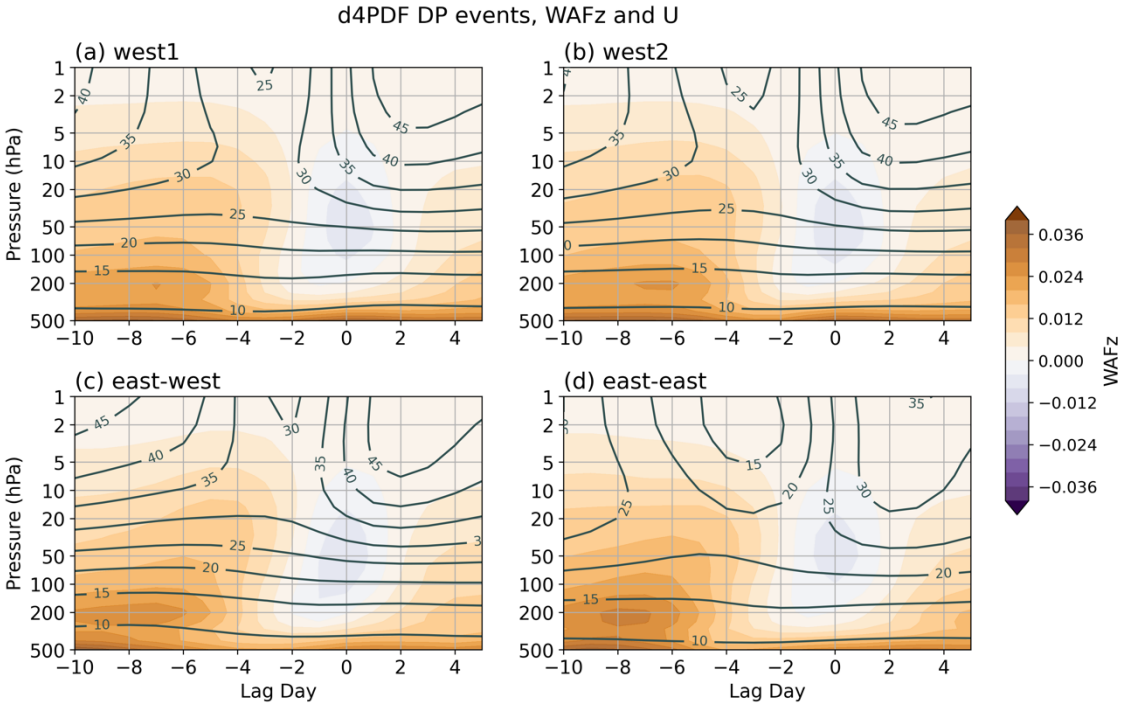

Figure 4-2-3: Time-height sections for zonal mean zonal winds (m, contours) and zonal mean WAFz (m^2 s^{-2}, color shadings) averaged over 50˚N through 80˚N of the lag composite results for the west1 events (a), the west2 events (b), the east-west events (c), the east-east events (d) in d4PDF. The horizontal axis denotes the lag day from the event day.

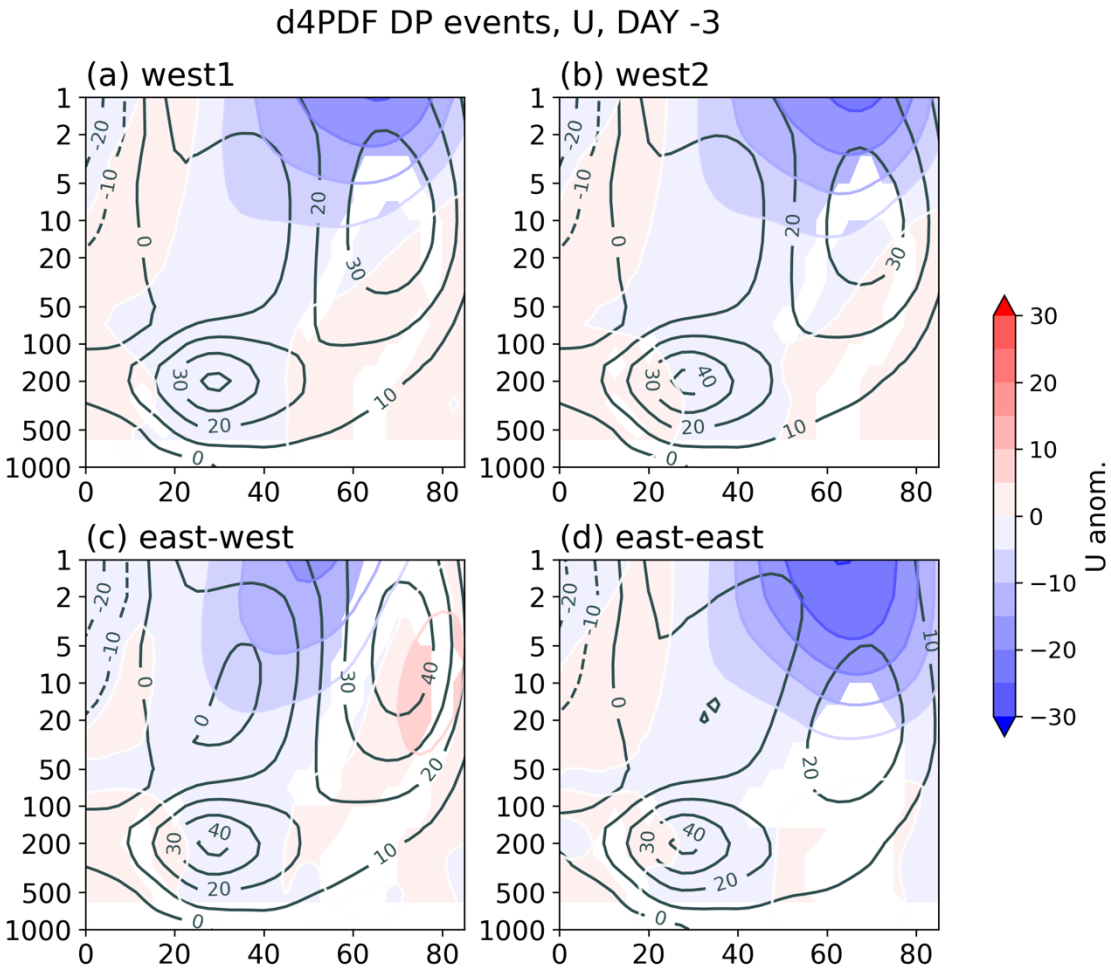

Figure 4-2-4: Latitude-height sections for zonal mean zonal winds (m, contours) and their anomalies from the climatology (m, color shadings and color contours) of the composite results three days before the event day for the west1 events (a), the west2 events (b), the east-west events (c), the east-east events (d) in d4PDF.

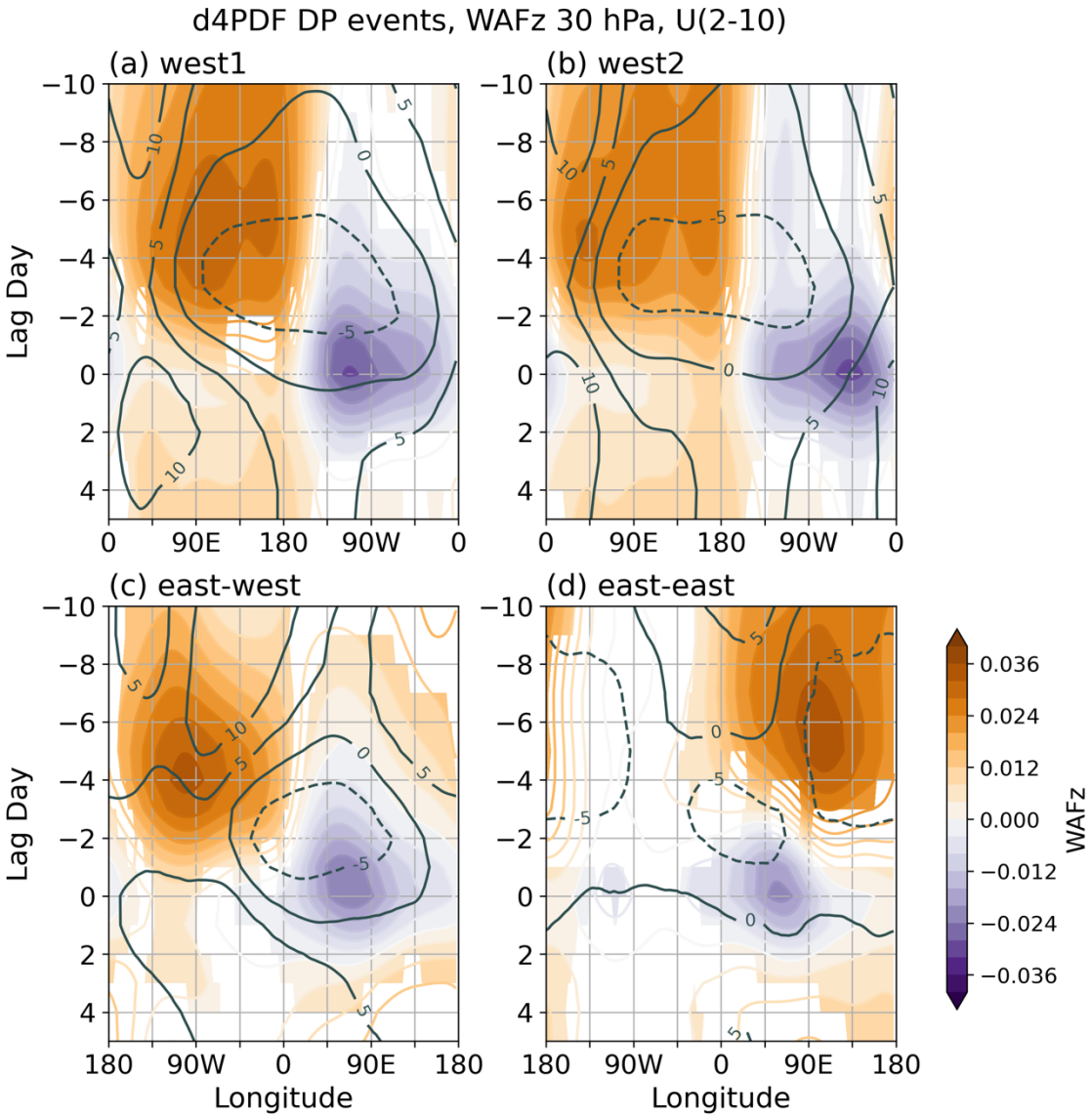

Figure 4-2-5: Longitude-time sections for U(2-10) (m, contours) and WAFz at 30 hPa (m^2 s^{-2}, color shadings and color contours) averaged over 50˚N through 80˚N of the lag composite results for the west1 events (a), the west2 events (b), the east-west events (c), the east-east events (d) in d4PDF.. The panel configuration is the same as Fig. 4-2-4. The color shadings are drawn only in the region where WAFz is statistically significant of 99.9 % confidence level.

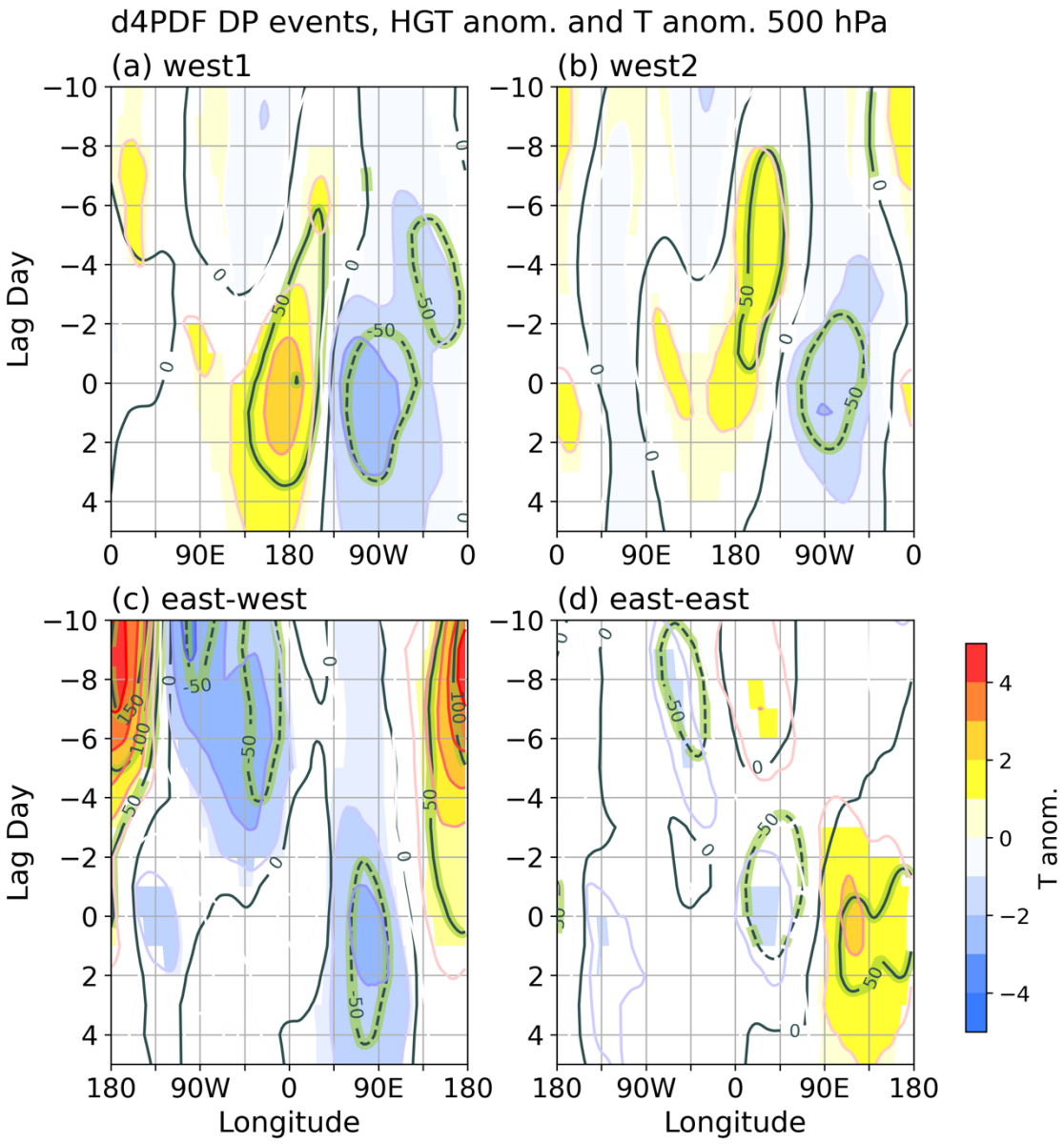

Figure 4-2-6: Same as Fig. 4-2-5 but for the geopotential heigh anomalies from the climatology (m, black and green contours) and the temperature anomalies from the climatology (K, color shadings and color contours) at 500 hPa. The color shadings and green contours are drawn only in the region where WAFz is statistically significant of 99.9 % confidence level.

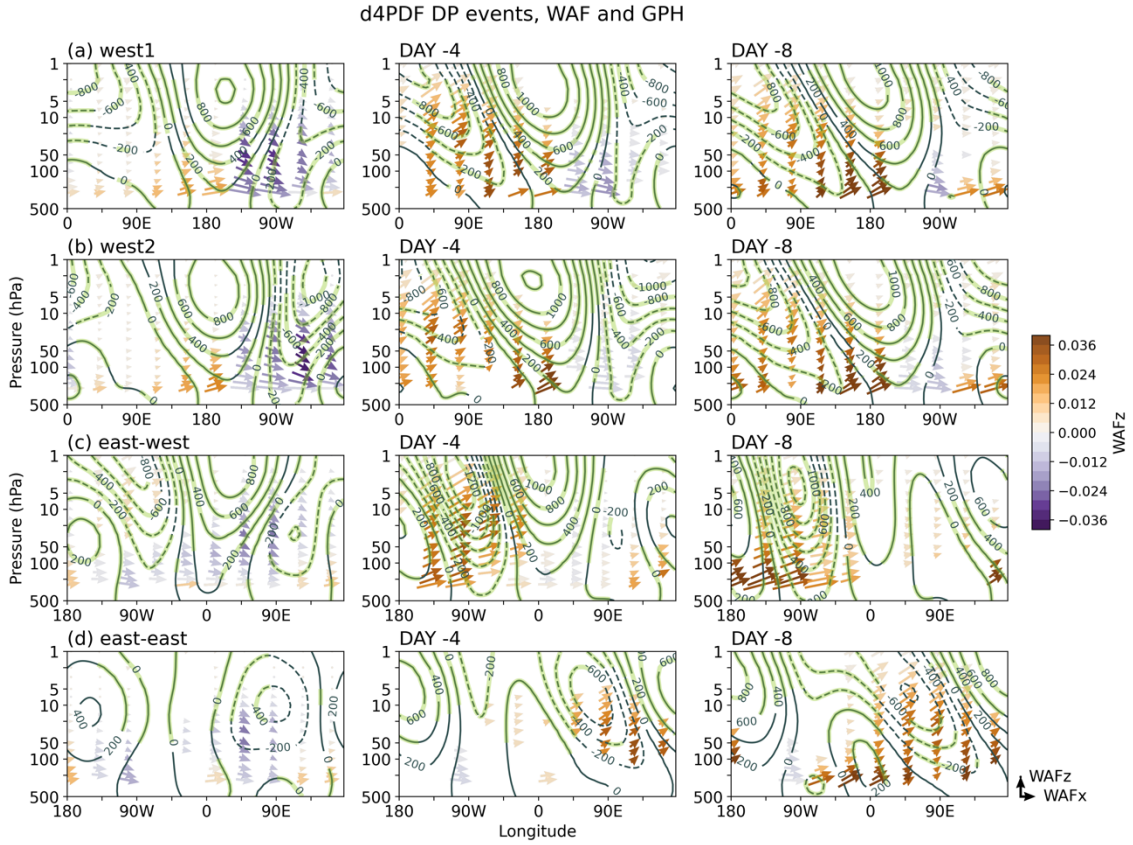

Figure 4-2-7: Longitude-height sections for the anomalies of geopotential height from the zonal averages (m, black and green contours) and WAF (m^2 s^{-2}, vectors) averaged over 50˚N through 80˚N of the composite results on the event day (left panels), four days before (center panels), and eight days before the event day (right panels) for the west1 events (a), the west2 events (b), the east-west events (c), the east-east events (d) in d4PDF. The value of WAFz colors the vectors. The green contours and color vectors are drawn only in the region where WAFz is statistically significant of 99.9 % confidence levels in the t-test. The unit vector is bottom of this figure, and its length is 10 m^2 s^{-2} in the horizontal direction and 0.5 m^2 s^{-2} in the vertical direction.

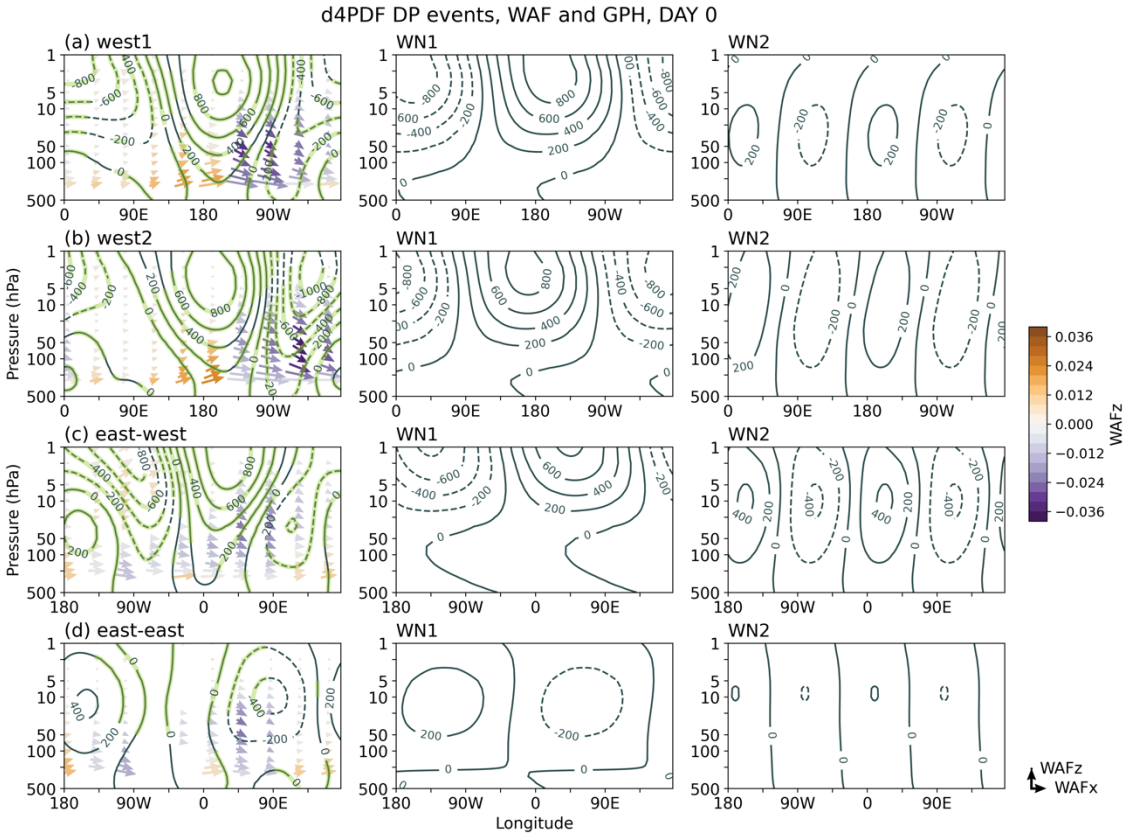

Figure 4-2-8: (Left) Same panels as left panels in Fig. 4-2-7. (Center) Longitude-height sections for WN1 components of geopotential height averaged over 50˚N through 80˚N of the composite results on the event day for each event group. (Right) Same panels as center panels, but for WN2 components.

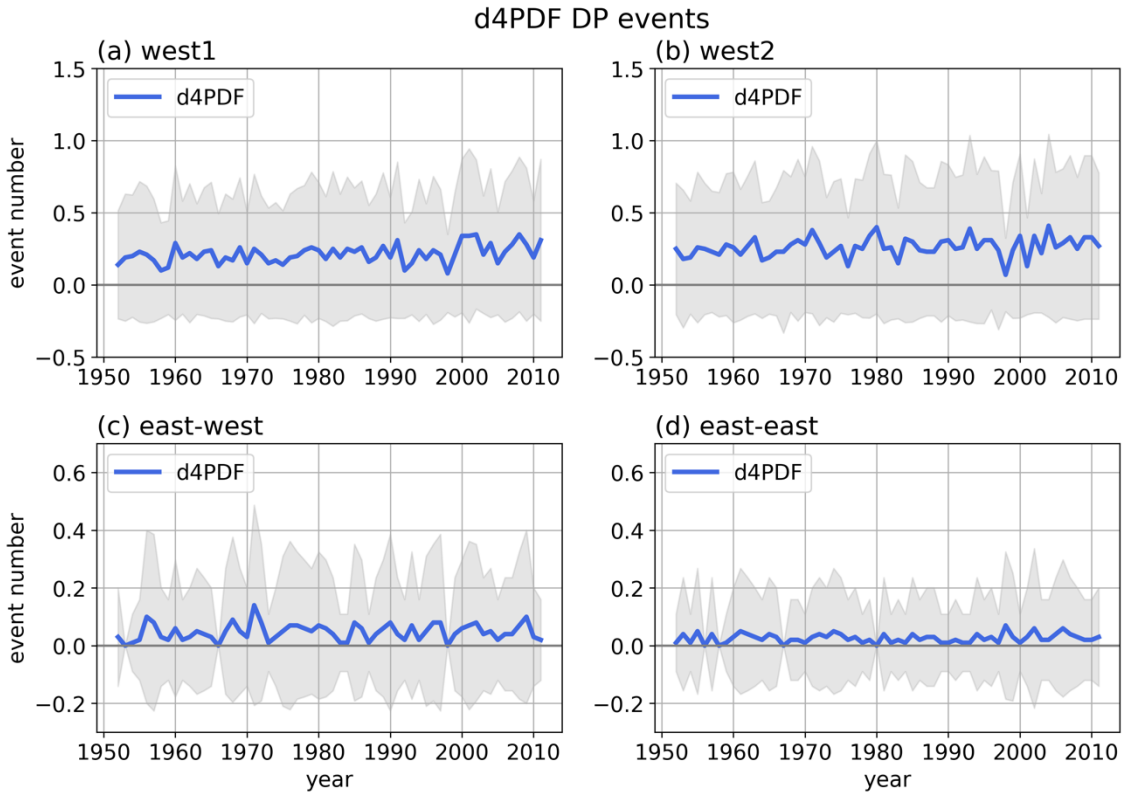

Figure 4-2-9: The interannual change in the event number for the west1 events (a), the west2 events (b), the east-west events (c), the east-east events (d) in d4PDF. Blue lines show the ensemble means of event number, and gray shadings show the standard deviations of them.

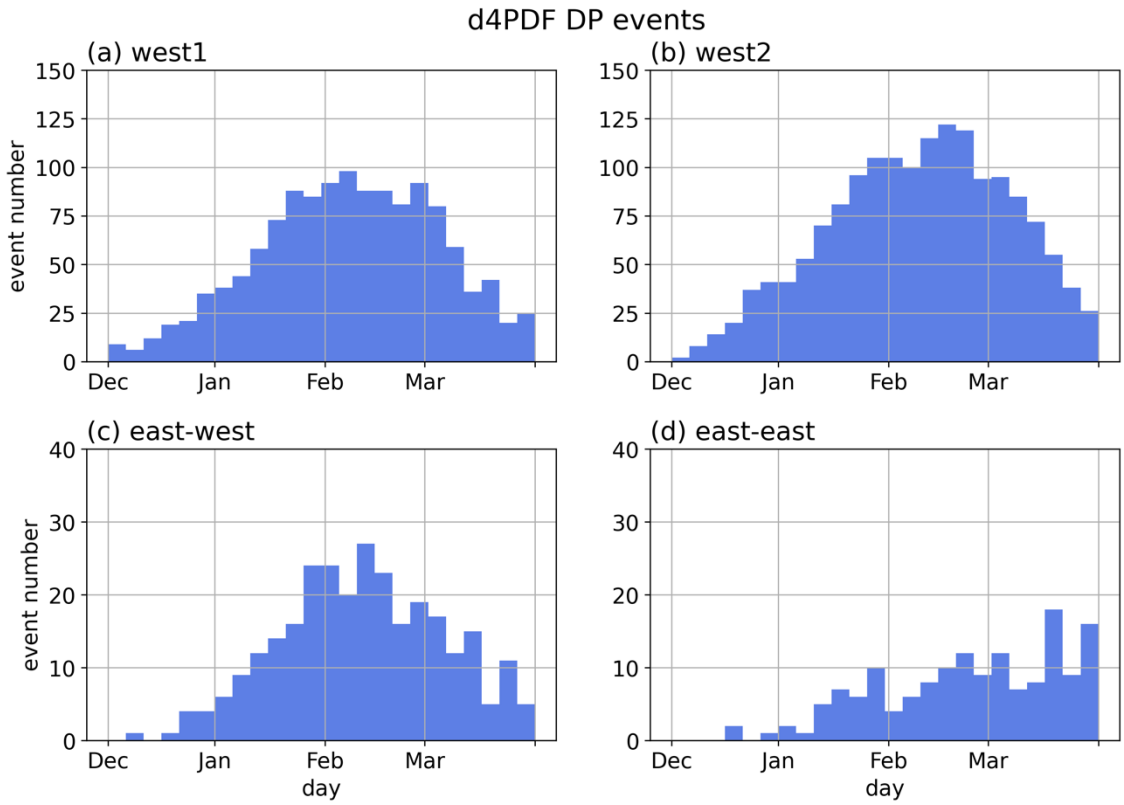

Figure 4-2-10: Histograms of the occurrence date of events in each event group. Events are counted at 5 days intervals.

5. Downward Propagation of planetary wave packets in the Northern Hemisphere

Partially reflection (PR) events are being investigated by several studies (e.g., Nath et al., 2014; Matthias and Krestchmer, 2020), but their characteristics, such as longitude scale and distribution, are still unknown, and statistical analyses are lacking. Therefore, the current study proposes and implements a method for extracting LDP events independent of longitude scale and region. Furthermore, in this study, the events extracted by that method are classified according to several perspectives to clarify the stratospheric and tropospheric characteristics of each group of LDP events.

This section is also composed by two parts: The first part is about the investigation of the LDP events in the reanalysis data. In the second part, we investigate the events more detail by using a large ensemble dataset on the basis of the results from the reanalysis data.

5.1 Events in the Reanalysis Data

5.1.1 Analysis Methods

The method of detecting LDP events is as follows. We average WAFz at 30 hPa over 50˚N through 80˚N. In this calculation, WAFz is a two-dimensional value in longitude-day. For each day in the analysis period, we search for the minimum value of averaged WAFz and its longitude; we define the occurrence longitude as this longitude. The day with negative values and negative WAFz peak in the time dimension at the occurrence longitude are added to event

candidates. At the occurrence longitude, we define the event start (end) day as the day when WAFz changes from positive to negative (negative to positive) and the event period as term between them. If event periods overlap among the event candidates, we leave event candidates with the most negative WAFz among the overlapping events. By applying the above method to JRA-55, we obtain 340 LDP events. These include very weak LDP events, i.e., LDP events with a minimum WAFz slightly less than 0. Therefore, we redefine the LDP events as stronger than the mean minimum of 340 events. Finally, we obtain 194 events and use them for statistical analysis. This number of events seems a bit large, but we use them all for statistical significance.

The longitude scale of the LDP events is a continuously negative WAFz. The event latitude is a latitude that has the minimum WAFz at the occurrence longitude on the event day.

5.1.2 Results

First, we examine the longitude scale, occurrence longitude, and occurrence latitude of each detected event. Figure 5-1-1 shows their histograms. Note that shown intervals of longitude scale and occurrence longitude are 22.5˚, and those of occurrence latitude are 2.5˚. The upper right panel (Fig. 5-1-1d) is the two-dimensional histogram of the occurrence latitude and longitude scale. The occurrence latitude has a single peak (Fig. 5-1-1b); this result suggests that we can discuss downward propagation in the field averaged over 50˚N through 80˚N. The longitude scale has two peaks at 150˚ and 75˚ (Fig. 5-1-1a). The occurrence longitude has two

large peaks at 112.5˚W and 45˚W and a weak peak at 67.5˚E (Fig. 5-1-1c). These longitudes can be shown because we do not average WAFz longitudinally. In the two-dimensional histogram (Fig. 5-1-1d), the occurrence longitude peak at 112.5˚W has equivalent distinct peaks at the longitude scale. The occurrence longitude peak at 45˚W also has two peaks at the same longitude scales, but the peak at 75˚ is weaker than that at 150˚. Two peaks are unclear at the 67.5˚E peak because of its low number of events.

To examine the event characteristics of the occurrence longitude and the longitude scale, we classify the events by features seen in the histograms. For the longitude scale, the events are classified by a threshold of 112.5˚. For the occurrence of three longitude intervals, i.e. 67.5˚ centered from the three peaks in the histogram, 112.5˚W, 45˚W, and 67.5˚E are considered as one category. As a result, the detected events are divided into six groups. The first group is the LDP events with occurrence longitude from 135˚W to 90˚W and longitude scale less than 112.5˚ ("west1-narrow"), and the second group is those with the same occurrence longitude range and longitude scale greater than 112.5˚ ("west1-wide"). The third group is the LDP events with occurrence longitude from 67.5˚W to 22.5˚W and longitude scale less than 112.5˚ ("west2-narrow"), and the fourth group is those with the same occurrence longitude range and longitude scale greater than 112.5˚ ("west2-wide"). The fifth group is the LDP events with occurrence longitude from 45˚E to 90˚E and longitude scale less than 112.5˚ ("east-narrow"), and the sixth group is those with the same occurrence longitude range and longitude scale greater than 112.5˚ ("east-wide"). We could divide the events into six groups; however, it is difficult to statistically

investigate the east-narrow events because their number of events is small. Therefore, we show the composite results for five groups, excluding the east-narrow events.

We perform a lag composite analysis for each classified group of events to compare them and clarify the time evolution of the dynamical fields in the stratosphere and troposphere during the events. We first show the zonal mean fields, followed by the longitudinal structures.

Figure 5-1-2 shows time-height sections of zonal mean winds and zonal mean WAFz for the lag composite results. Again, note that the zonal mean WAFz is equal to the vertical components of the EPF. All event groups have no negative zonal mean WAFz around the event day, although it is minimized around the event day. The westerly winds at upper stratosphere in all event groups decrease two or three days before the event day, forming the negative vertical shear of the zonal winds.

To investigate general features of the event occurrence, we plot longitude-time sections for several quantities. Figure 5-1-3 shows the time evolution of WAFz and U(2-10) for the lag composite results. The color shadings are drawn only in the regions with statistically significant WAFz at the 95% confidence level. We first focus on the west1-wide (Fig. 5-1-3a) and west2-wide (Fig. 5-1-3b) events. Wave packets propagate upward in the Eastern Hemisphere before downward propagation in the Western Hemisphere. Although the peaks of negative WAFz are at different longitudes, the overall regions are similar. The upward propagation before the event day is also slightly different, with the longitudinal peak of the west2-wide events being further east than that of the west1-wide events. The negative U(2-10)

has also slightly differences. The region of negative U(2-10) in the west2-wide events is narrower than that in the west1-wide events, and its peak is located further east than in the west1-wide events.

The east-wide events (Fig. 5-1-3c) have relatively similar characteristics to the west1- and west2-wide events. Wave packets propagate upward in the Western Hemisphere before propagating downward in the Eastern Hemisphere. Negative regions of U(2-10) are centered around 0˚. As can be seen in Fig. 5-1-1, the longitude scale of the east events is smaller than that of the west1- and west2-wide events.

The narrow events have different characteristics from the wide events. The most important difference is that WAFz is negative in the narrow region of the Western Hemisphere on the event day. The west1-narrow events (Fig. 5-1-3d) have stronger upward propagation in the Western Hemisphere than the west1-wide events (Fig. 5-1-3a), and their peak is further east. On the event day, wave packets propagate upward at 180˚ and 0˚, with narrow downward propagation between them. The longitude scale of the west2-narrow events (Fig. 5-1-3e) is similar to that of the west1-narrow events (Fig. 5-1-3d), but the upward propagation is weak and less statistically significant. There are two regions of upward propagation at the 95% confidence level prior to the day of the event, and one in the east is very close to the regions of downward propagation. Thus, the intensities and characteristics of the longitudinal peaks of upward propagation before the day of the event differ depending on the longitudinal peaks and scales of the LDP.

To investigate the characteristics of the wave appearance in the stratosphere and troposphere, we present longitude-height sections of various quantities of each event group. Figure 5-1-4 shows the zonal structure of anomalies of geopotential height (GPH) from the zonal mean and x- and z-components of the WAF vectors for the composite results of each event group on the event day. The green contours and color vectors are drawn only in statistically significant regions. The middle (right) panels denote the WN1 (WN2) components of GPH. Figure 5-1-5 is the same as Fig. 5-1-4, but on the peak day of upward propagation in each event group: Four days before the event day in the west1-wide, west2-wide, and east-wide events and two days before the event day in the west1-narrow and the west2-narrow events. Figure 5-1-6 is the same as Fig. 5-1-4, but on ten days before the event day to investigate the wave structures before the upward propagation. In both wide events (Figs. 5-1-4a and 5-1-4b), the quasi-barotropically developed Aleutian high is observed on the event day, but the west1-wide events have one more developed than the other. The strong penetration of the downstream cyclonic anomalies from the stratosphere into the troposphere occurs in the Western Hemisphere in the wide events on the event day (Figs. 5-1-4a and 5-1-4b) compared to before the event day (Fig. 5-1-5 and 5-1-6). Wave packets propagate downward at the east edge of the Aleutian high in the west1 events (Fig. 5-1-4a) and at the center of the cyclonic anomalies in the west2 events (Fig. 5-1-4b). These differences are caused by differences in the longitude of ridge for WN1 rather than WN2. The WN1 component are quasi-barotropically developed from ten days before the event day, and the amplitude of WN2 component changes larger. Ten days

before the event day, there is no significant difference between the west1- and west2-wide events (Fig. 5-1-6a and 5-1-6b). On the peak day of the upward propagation, the differences of the phase of WN1 start to appear (Fig. 5-1-5a and 5-1-5b).

The west1-narrow events also have the quasi-barotropically developed Aleutian high (Fig. 5-1-4d); however, there are several different features from the west1-wide events (Fig. 5-1-4a). The longitudinal width of the stratospheric anticyclonic anomaly is wider, and the penetration of the cyclonic anomaly is not seen. Wave packets propagate downward at the bottom of the high instead of at the east edge of the high as in the west1-wide events. Ten days before the event day, the wave structures do not appear to differ much between the west1-wide and narrow events. As the event day approaches, the differences in WN1 and WN2 structures between the two groups become large, especially in WN2 (Fig. 5-1-5 and 5-1-6).

The west2-narrow events (Fig. 5-1-4d) also have different characteristics from the west2-wide event (Fig. 5-1-4b). The development of the Aleutian high is weak, but only the penetration of the cyclonic anomaly is observed. As a result, wave packets locally propagate downward around the penetrated cyclonic anomalies. Similar to the above groups of events, the wave structures ten days before do not show any significant differences (Fig. 5-1-6), and the differences become large to the event day (Fig. 5-1-5).

On the other hand, the east events (Figs. 5-1-4c, 5-1-5c, and 5-1-6c) have different characteristics from the west events throughout the period shown. On the event day, the WN1 amplitude becomes very small, and the Aleutian high is weakened. However, the WN2

amplitude does not show much difference. As a result, the anticyclonic anomalies appear around 0˚, and wave packets propagate downward on the east edge of these anomalies. The penetration of the cyclonic anomaly is not seen. Ten days before the event day, the amplitude of WN1 component appears to be smaller than other event groups and decreases to the peak day of the upward propagation. The amplitude of WN2 component increase to the event day. Therefore, the superposition of WN1 and WN2 forms quite different features from other event groups, which could make the time evolution of the east events very different afterwards.

Each group of events on the event day shows different phases of WN1 from each other as described above. In particular, the phase difference of WN1 in the west1-wide and west2-wide events could determine the peak longitude of downward propagation. We then statistically examine the phase of the WN1 components of these events. Histograms of the maximum longitude of the WN1 component at 5 hPa for the event days of the west1-wide and west2-wide events are shown in Figure 5-1-7, with dashed lines for the means of each event group. A t-test of the difference between the two means indicates that they are significantly different at the 95% confidence level. This significant difference means that the phase of WN1 is important in determining the longitude of occurrence of downward propagation, even though the difference is somewhat small.

Finally, we focus on the tropospheric characteristics during the LDP events. Figure 5-1-8 is the same as in Fig. 5-1-3, but the contours denote GPH anomalies from the climatology at 500 hPa, and the color shadings denote temperature anomalies from the climatology at 500 hPa.

These panels show that only the west1 and west2-wide events have low-temperature anomalies in the troposphere below the LDP region on the event day. In the west1-wide events, the anticyclonic anomalies are developed at 180˚ before the event day, corresponding to the development of Aleutian high and its hanging down into the troposphere seen in Figs. 5-1-4a and 5-1-4b. This feature is considered to be caused by the upward propagation of wave packets in the Western Hemisphere prior to the event day (Fig. 5-1-3). Around the event day, cyclonic and cold anomalies develop in the troposphere in the Western Hemisphere. These features are consistent with the strong cyclonic anomaly penetration on the event day in Fig. 5-1-4. Cyclonic anomalies could enhance cold advection from high latitudes to generate cold anomalies. Note that these anomalies in the west1-wide event are apparently stronger than in the west2 event.

The narrow and east-wide events do not have the above features, consistent with weak or nonexistent cyclonic anomalies penetration. Only the west2-narrow event has relatively weak entrainment, thus the cyclonic and low-temperature anomalies exist around 90˚W, although they are not statistically significant.

5.1.3 Discussion

We extracted the LDP events on the basis of WAFz, which are not zonally averaged. The LDP events had several peaks in their longitudinal distribution and occurrence longitude (Fig. 5-1-1b). We classified the LDP events based on their characteristics and performed a composite analysis; the event groups had different characteristics in upward propagation, zonal

winds, geopotential height in the stratosphere and troposphere, and temperature in the troposphere. In this section, we consider the reason for their longitudinal characteristics. Then, we evaluate the possibility of effects on the tropospheric circulation. Finally, we describe the notification of the extraction method and the differences between the LDP and DP events.

Most of the LDP events occurred in the Western Hemisphere. This tendency is same as that of the DP events. In the Western Hemisphere, LDP events had two distinct peaks. These peaks are considered to be generated by small but significant differences in the WN1 components on the event day. Differences in the quasi-barotropical development of the Aleutian high are also thought to be generated by these differences, since this high is expressed by the superposition of mainly WN1 and WN2. These differences were not seen ten days before the event day. Therefore, these differences could be generated by the upward propagation and zonal wind structures before to the event day.

The LDP events had a weak peak in the Eastern Hemisphere; this fact is common to the DP events. The characteristics of the wave packets and zonal winds in the east events were qualitatively similar to those in the west events; however, the amplitude of the WN1 components from ten days before the event day to the event day was small. For the occurrence of LDP in the Eastern Hemisphere, it may be necessary that the weak amplitude of WN1 components and the development of the high at 0˚.

Next, we focus on the longitudinal scale of LDP events. The events had two large peaks, consisting mainly of the events in the Western Hemisphere. Here, we compare the west1-

wide and west1-narrow events here. The largest difference was the upward propagation around the event day; in the west1-narrow events, waves packets propagate upward around 0˚ on the event day. From the longitude-height and longitude-time sections, this upward propagation was considered to be caused by anticyclonic anomalies in the troposphere around 0˚. It is difficult to conclude that wave packets propagate downward to enhance these anomalies. However, this upward propagation from the troposphere may narrow the regions of the downward propagation in the stratosphere. These facts in the west1-wide and narrow events are similar to those in the west2-wide and west2-narrow events, although the longitude of upward propagation was different from each other.

As discussed above, there are several differences between the event groups in the stratosphere. In addition, the effects on the tropospheric circulation are also important. The west1-wide and west2-wide events had cold anomalies below the LDP region in the troposphere. These cold anomalies are thought to be generated by cyclonic anomalies there; the penetration of the anomalies from the stratosphere into the troposphere enhances these cyclonic anomalies. The cold anomalies of the west1-wide events were larger than those of the west2-wide events; this fact suggests that the DP events with a western peak in the Western Hemisphere tend to affect the tropospheric circulation. This consideration is consistent with the longitudinal peak of downward propagation in the west1-wide events being west of the cold anomalies in the troposphere, because the longitudinal component of the WAF is eastward.

Composite results of other event groups that had weak penetration of the cyclonic anomalies did not show cold anomalies in the troposphere like the west1-wide events. However, there is a possibility that some events in these event groups may have strong penetration and cold anomalies. It is difficult to show their statistical characteristics because the number of events is small.

The LDP events that have the longitudinal characteristics discussed above were extracted based on WAFz, not zonally averaged. The threshold for event extraction is the mean of all LDP events; therefore, the events include weak events and the number of events is large. When we want to get more strong events, we can set strict thresholds, e.g., the mean minus the standard deviation. Note that the strong threshold significantly reduces the number of available events and makes it difficult for us to perform statistical analysis.

Finally, we should note the differences between LDP and DP events; not all LDP events are the same as DP events. For example, the zonal mean WAFz was not negative in the stratosphere on the event day. In the longitude-height sections, the phase of the GPH was tilted to the west, not to the east, on the day of the event. Not all events have such features because these are the composite results; however, these must be statistical features. Wave packets propagate downward in the Western Hemisphere in the DP events (e.g., Jadin, 2011) and also in most of the LDP events; therefore, the method of detecting events in Matthias and Kretschmer (2020) is ultimately correct. On the other hand, the LDP events had a more detailed longitudinal distribution in the Western Hemisphere, and some occurred in the Eastern Hemisphere. These

facts are essential characteristics of the LDP events, which are first found in the unique method of the current study.

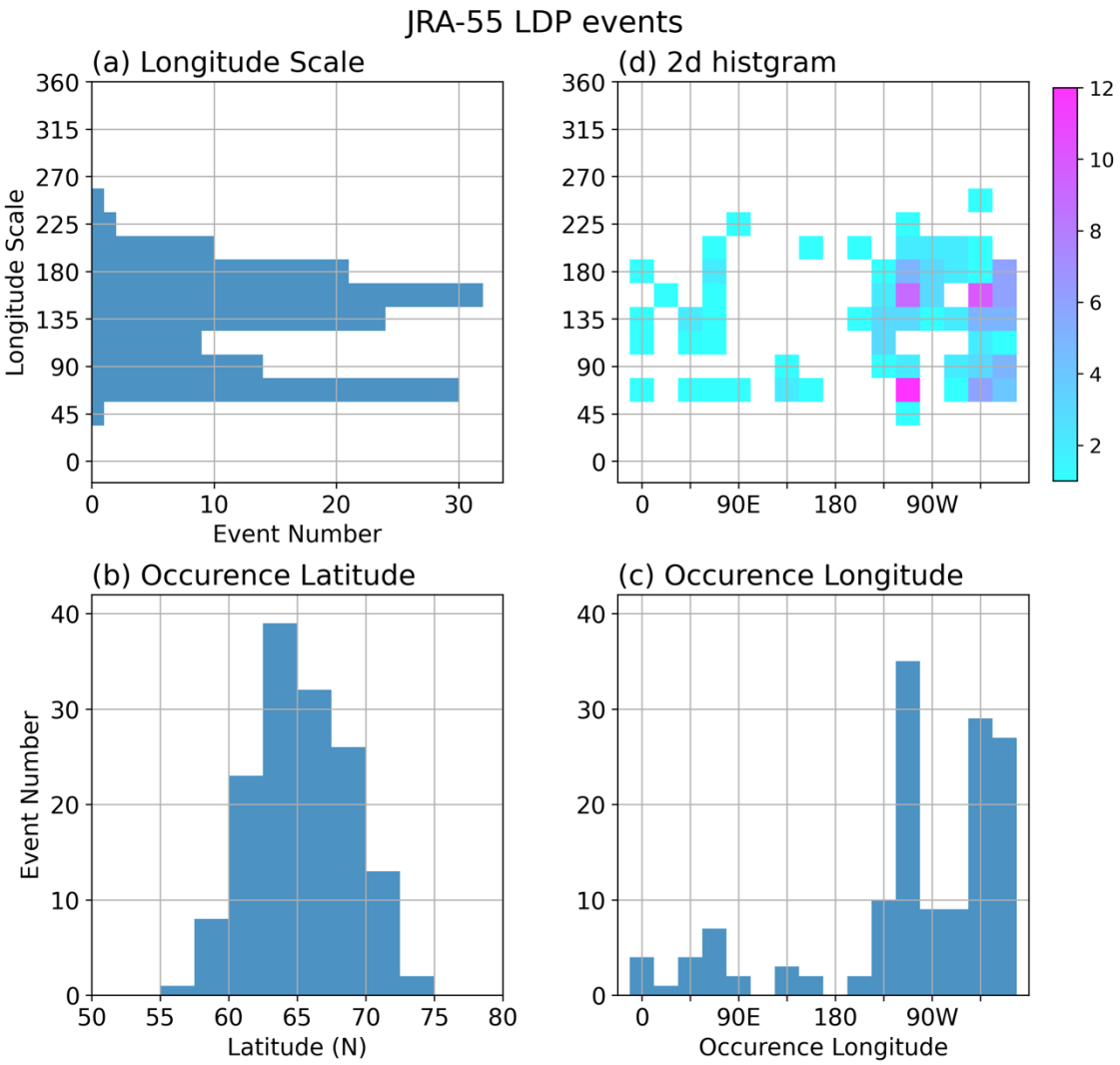

Figure 5-1-1: Histograms of the longitude scale (a), the occurrence latitude (b), the occurrence longitude (c), and occurrence longitude versus longitude scale (d) of the LDP events in JRA-55.

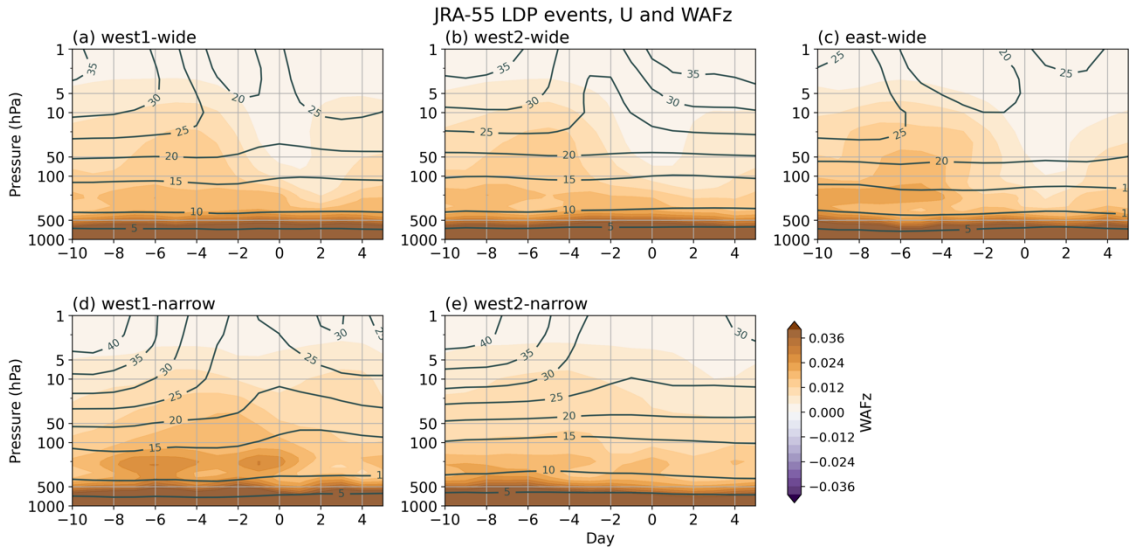

Figure 5-1-2: Time-height sections for zonal mean zonal winds (m, contours) and zonal mean WAFz (m^2 s^{-2}, color shadings) averaged over 50˚N through 80˚N of the lag composite results for the west1-wide event (a), the west2-wide event (b), the east event (c), the west1-narrow events (d), the west2-narrow event (e) in JRA-55. The horizontal axis denotes the lag day from the event day.

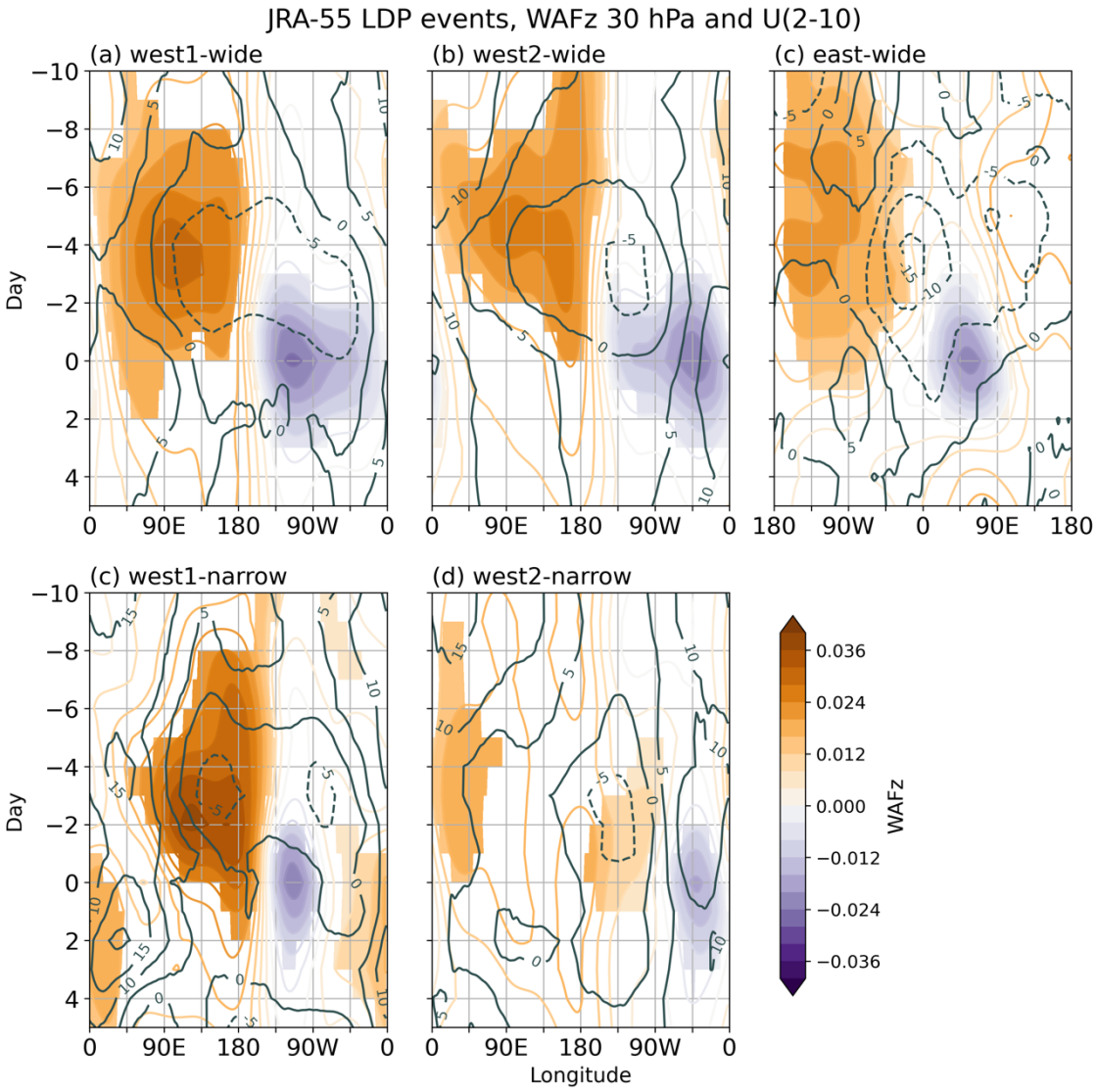

Figure 5-1-3: Longitude-time sections for U(2-10) (m, contours) and WAFz (m^2 s^{-2}, color shadings) averaged over 50˚N through 80˚N of the lag composite results for each event group. The panel configuration is the same as Fig. 5-1-2. The colors are drawn only in the region where WAFz is statistically significant of 95 % confidence level in the t-test.

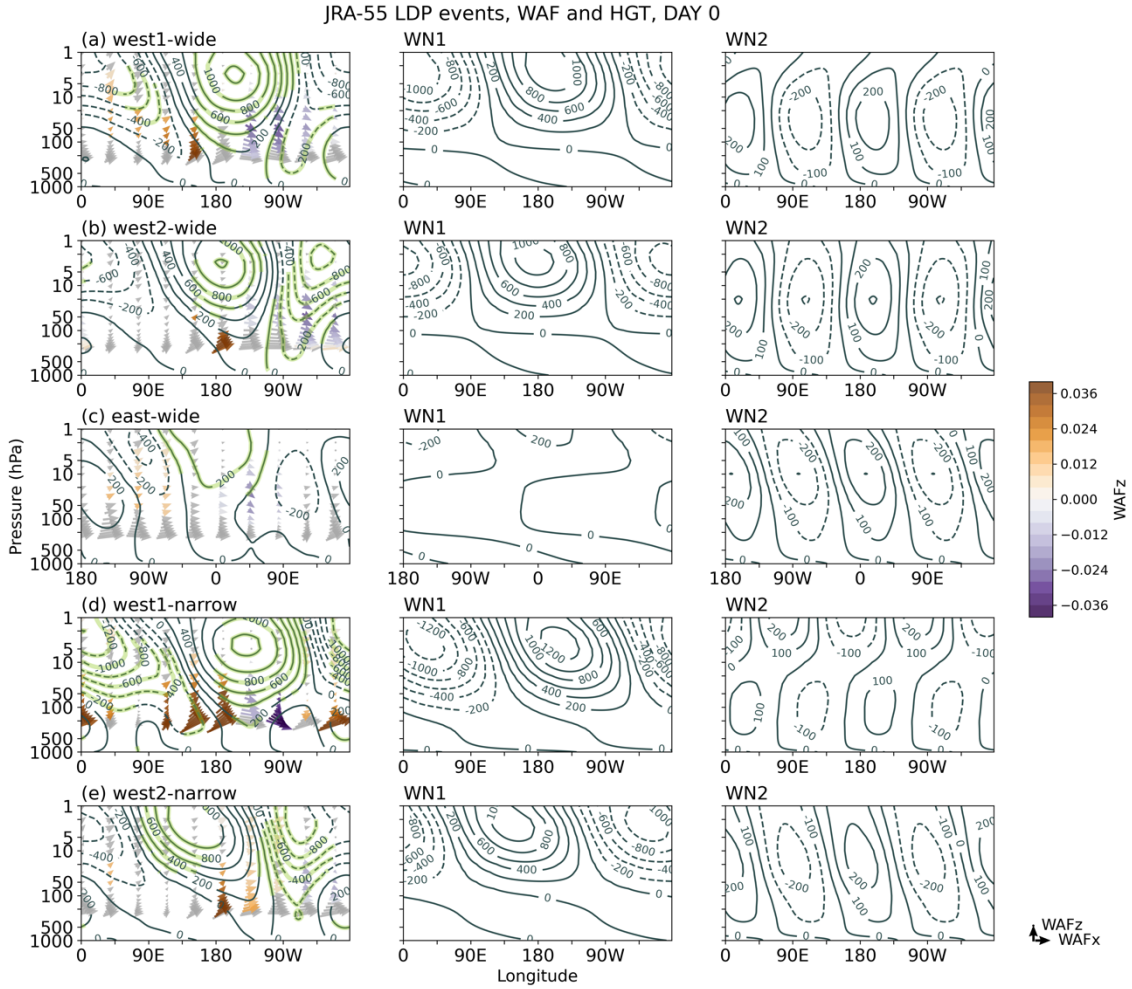

Figure 5-1-4: Longitude-height sections for geopotential zonal mean anomaly (m, contours) and WAF (m^2 s^{-2}, vectors) averaged over 50˚N through 80˚N of the composite results on the event day for the west1-wide event (a), the west2-wide event (b), the east event (c), the west1-narrow events (d), the west2-narrow event (e) in JRA-55. The green contours and color vectors are drawn only in the region where WAFz is statistically significant in the t-test. The unit vector is bottom of this figure, and its length is 10 m^2 s^{-2} in the horizontal direction and 0.5 m^2 s^{-2} in the vertical direction.

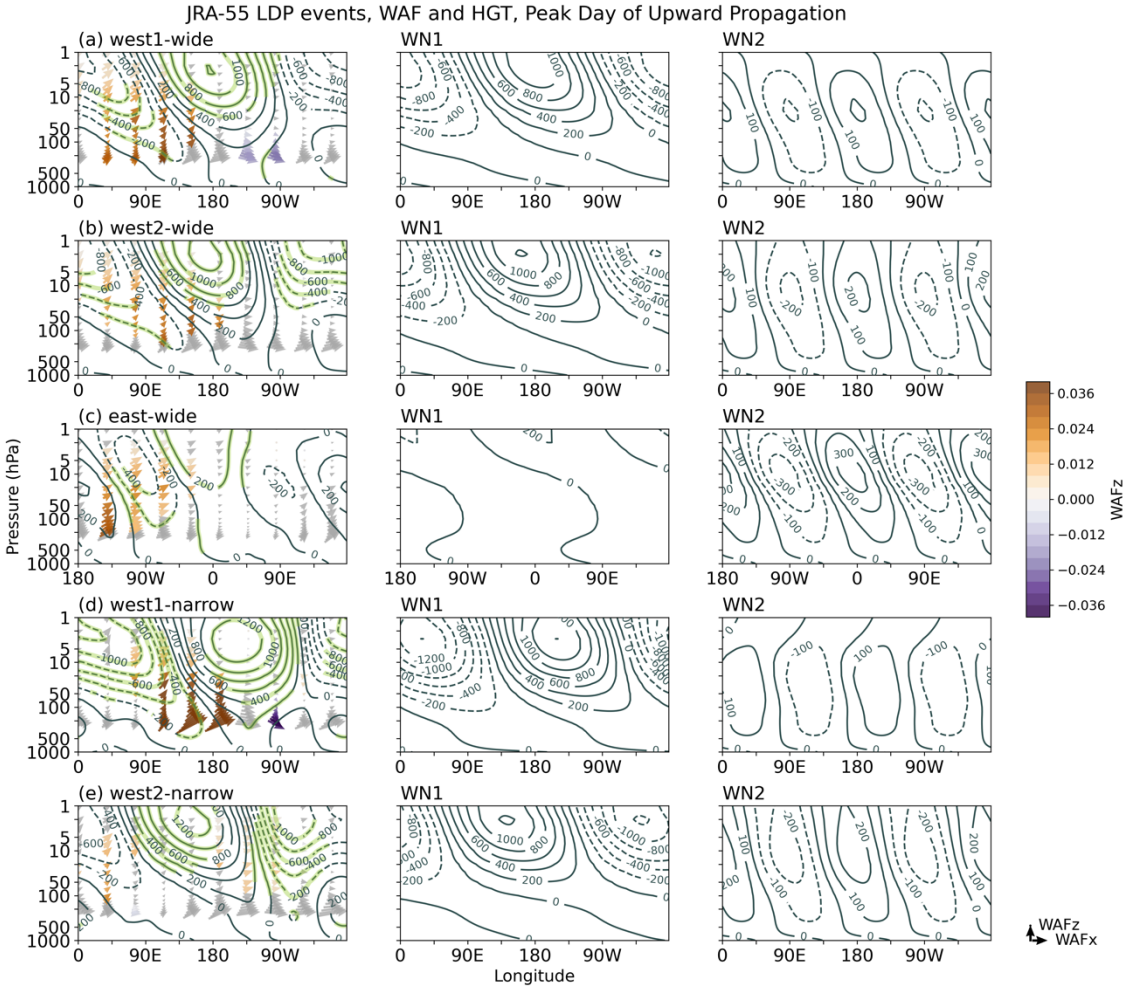

Figure 5-1-5: Same as Fig. 5-1-4 but on the peak day of upward propagation in each event group: four days before the event day in the west1-wide, west2-wide, and east-wide events and two days before the event day in the west1-narrow and the west2-narrow events.

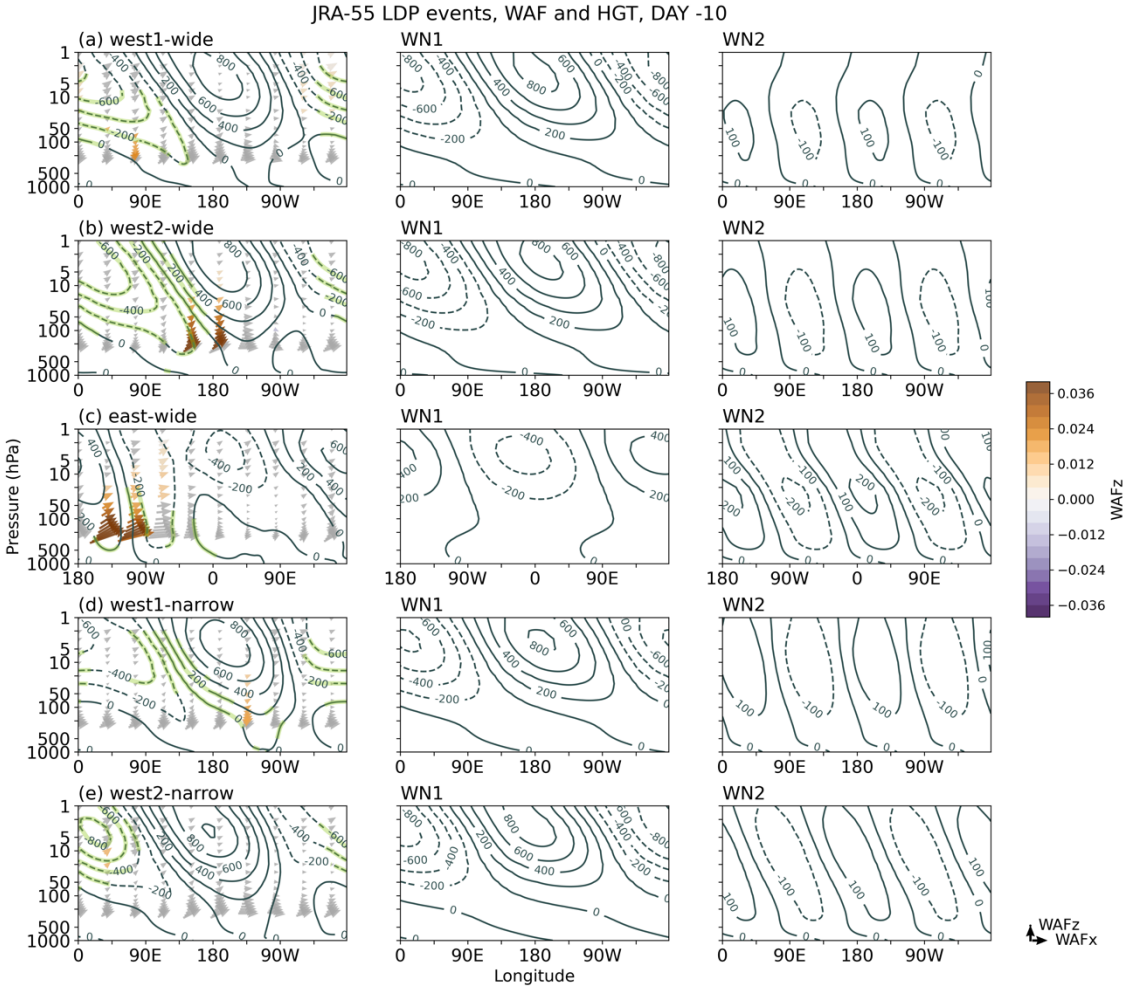

Figure 5-1-6: Same as Fig. 5-1-4 but ten days before the event day.

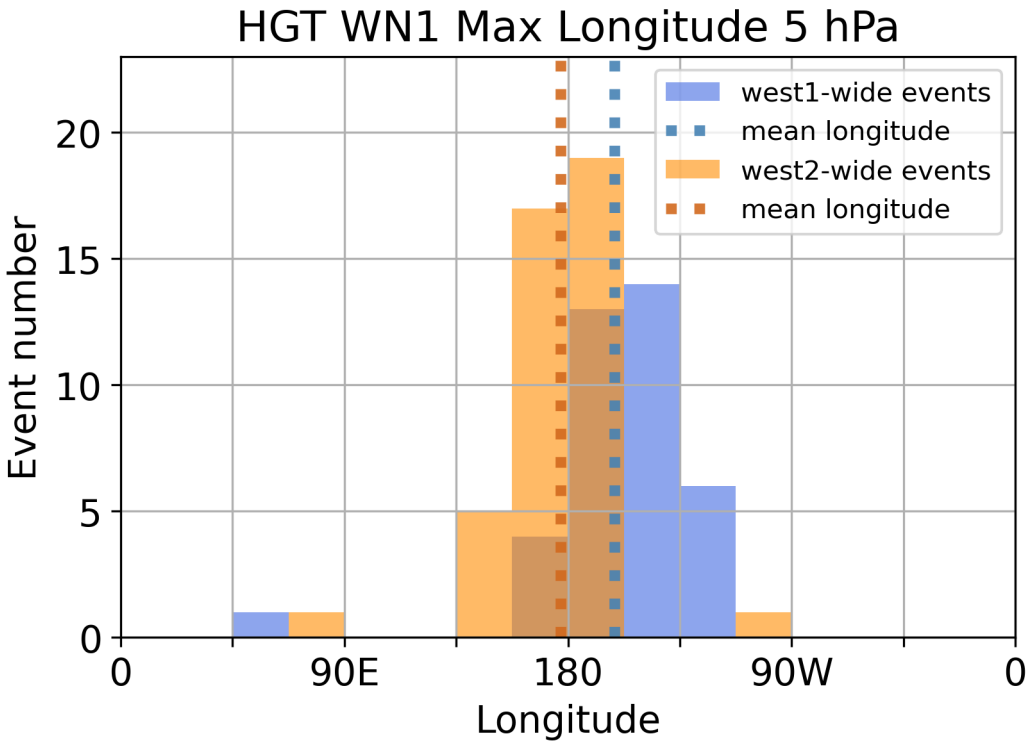

Figure 5-1-7: Histogram of the maximum longitude of the WN1 component for the geopotential height at 5 hPa for each event day of the west1-wide and west2-wide events.

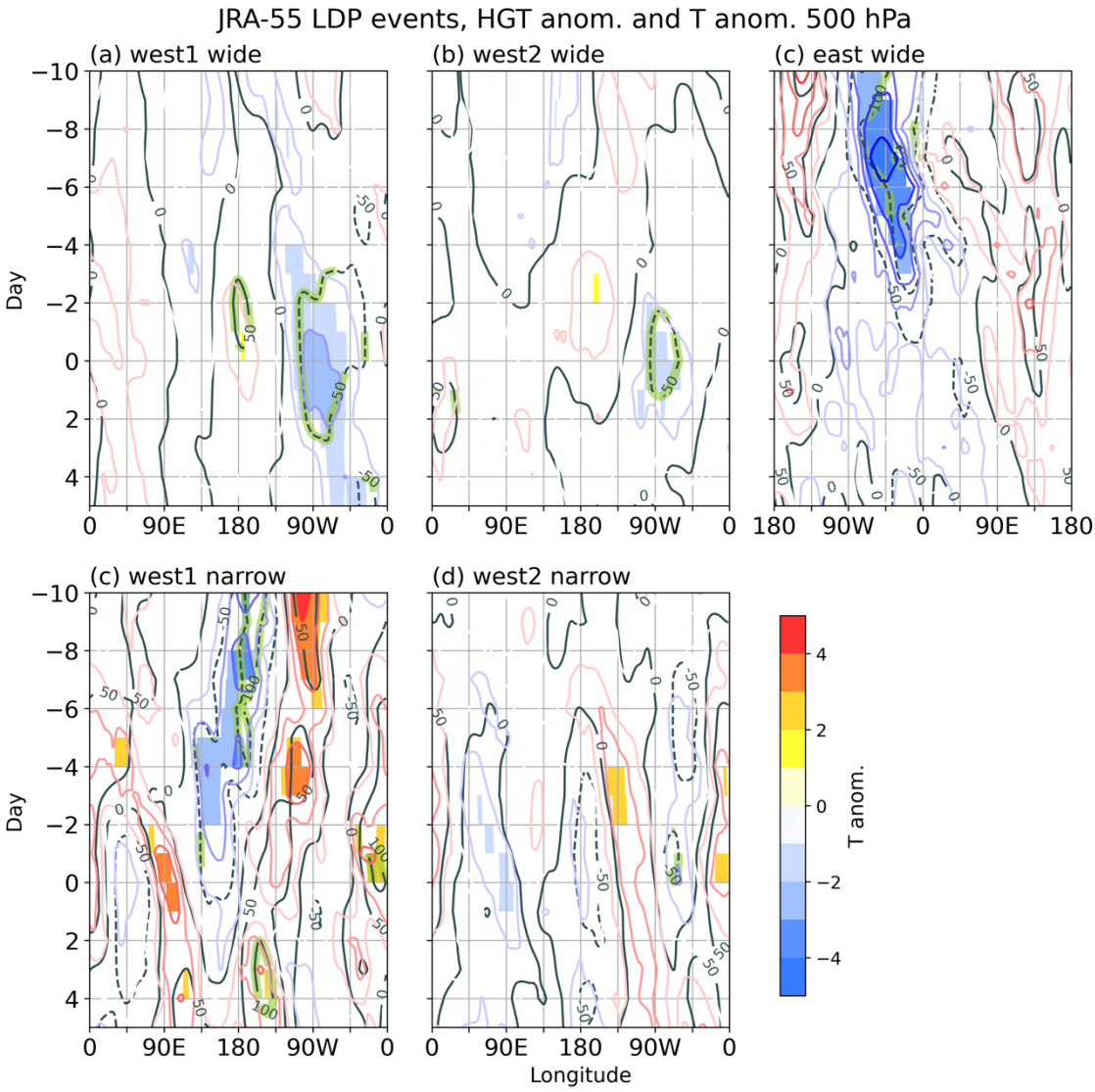

Figure 5-1-8: Same as Fig. 5-1-4 but for geopotential height anomalies (m, contours) and temperature anomalies (K, color shadings) from the climatology at 500 hPa.

5.2 Events in the Large Ensemble Data

The longitudinal distribution of the LDP events in JRA-55 were similar to those of the DP events in d4PDF. On the other hand, it was difficult to show the statistical features of downward propagation and the tropospheric circulation, as same as the analysis of the DP events in JRA-55. In particular, the event numbers of the events in the Eastern Hemisphere and the events which have the narrow region of the downward propagation are small. Thus, we examined the LDP events by using d4PDF to show more statistical characteristics. When we regard the event days occurring within five days to be included in the same events between the DP and LDP events in d4PDF, about 20 % of the LDP events are common with the DP events.

5.2.1 Analysis Methods

The method of the LDP event detection is the same as those in JRA-55, but the criterion value is different. By conducting the same analysis methods in JRA-55, we get 44529 LDP events, including very weak LDP events. We redefine the LDP events as those that are stronger than the mean minimum minus the standard deviation of all events. Finally, we get 7416 events and use these for the statistical analysis. The event number converted to the analysis period in JRA-55 is about 52, which is smaller than that in JRA-55, 194 events because the criterion value in the analysis of d4PDF is stricter.

5.2.2 Results

First, we examine the longitude scale and the longitude of occurrence of each detected event. Figure 5-2-1 shows their histograms. Note that the depicted intervals of longitude scale and occurrence longitude are 11.25˚. The appearances in the longitudinal scale and occurrence longitude are similar to those in JRA-55, but their distributions are smoother. The numbers of their peaks are the same as in JRA-55, but the longitudes of the peaks are slightly different. This may be because d4PDF can show a more accurate distribution.

Figure 5-2-2 shows the same figure as Fig. 4-2-2 but for the LDP events in d4PDF, which are two-dimensional histograms of EPFz vs. WAFz averaged over middle-high latitudes at 30 hPa, occurrence longitude vs. EPFz, and occurrence longitude vs. WAFz on the event day, from left to right. Half or more of the events have positive EPFz on the event day, illustrating that the waves in these events propagate upward, not downward (Fig. 5-2-2a). There is no correlation between the strength of downward propagation in EPFz and that in WAFz.

As in the analysis for JRA-55, we classify the events according to the features shown in the histograms in Fig. 5-2-1. For the occurrence longitude, there are three groups colored in the bottom panel of Fig. 5-2-1; "west1" events are from 135˚W to 90˚W, "west2" events are from 67.5˚W to 22.5˚W, and "east" events are from 22.5˚E to 67.5˚E. The longitudes of the west1 and west2 events are almost the same as those of the LDP events in JRA-55, and those of the east events are different from those in JRA-55. For the longitude scale, the events are classified by a threshold of 110˚.

On the other hand, there are large differences in the east events classified on the basis of upward propagation longitudes rather than those classified on the basis of the longitudinal scale. Therefore, the east events are classified only on the basis of the upward propagation longitude; this classification method is the same as that for the DP east events in d4PDF. As a result, the detected events are classified into six groups: They are "west1-wide", "west1-narrow", "west2-wide", "west2-narrow", "east-west", and "east-east". All event groups have enough events for statistical analysis.

We make lag composite results for the six groups of events classified above. First, we focus on the zonal mean fields. Figure 5-2-3 is the same as Fig. 5-1-2, but for the composite results of the six event groups in d4PDF, i.e., time-height sections of zonal mean zonal winds and zonal mean WAFz. As seen in Fig. 5-1-2, all event groups have no negative zonal mean WAFz around the event day. The westerly winds in all event groups decrease two or three days before the event day, forming the negative vertical shear of the zonal winds. On the other hand, there are some differences in the recovery and the speeds of the westerly winds. In the west1-wide, west2-wide, east-west events, the westerly winds recover after the deceleration. The recovery is weak in the west1-narrow and west2-narrow events, and the wind speeds are small throughout the period in the east-east events.

We investigate the LDP events in d4PDF using the same figures as the analysis in JRA-55. Figure 5-2-4 is the same figure as Figure 5-1-3, but for the results in d4PDF and the confidence level is 99.9%, which are longitude-time sections of U(2-10) and WAFz at 30 hPa.

In particular, the features of the narrow events and the east events are clearer than the results in JRA-55. The features in the west1-wide and west2-wide events are similar to those in JRA-55; the wave packets propagate upward in the Eastern Hemisphere before downward propagation, and the vertical shear of the zonal winds is negative between their propagations. On the other hand, there are two peaks in the upward propagation and negative U(2-10) of the west2-wide events around 45˚E and 180˚E (Fig. 5-2-4b).

The strength and longitude of upward propagation before the event day are different for the west1-wide and west1-narrow events in JRA-55 (Figs. 5-1-6a and 5-1-6b); however, there are no such differences for the west1-wide and west1-narrow events in d4PDF (Figs. 5-2-4a and 5-2-4b). Around and after the event day, wave packets propagate upward around 45˚E, making the region of downward propagation narrow. In the west2-narrow events, there are two peaks of upward propagation and negative U(2-10) before the event day, consistent with the results of the west2-narrow events in JRA-55 and the west2-wide events in d4PDF. The upward propagation at 180˚ in the west2-narrow events is stronger than that in the west2-wide events, and this region extends eastward (Figs. 5-2-4b and 5-2-4d).

The east-west events in d4PDF are similar to the east-wide events in JRA-55 (Figs. 5-2-4e and 5-1-3c); wave packets propagate upward in the Western Hemisphere before downward propagation in the Eastern Hemisphere, and the negative vertical shear of the zonal winds is negative between their propagations. The characteristics of the east-east events are similar to the

DP east-east events in JRA-55; wave packets propagate upward and downward in the eastern hemisphere, and negative U(2-10) is ubiquitous.

As described above, the west1-wide, west2-wide, east-west, and east-east events in d4PDF LDP events have similar characteristics of time variation in WAFz to the west1, west2, east-west, and east-east events in d4PDF DP events, respectively. On the other hand, EPFz is positive in most of the LDP events. The main difference between the DP and LDP events is that the wave packets continue to propagate upward around the event day, and the date peaks of upward and downward propagation are close together.

Next, we focus on the tropospheric characteristics during the LDP events in d4PDF. Fig. 5-2-5 is the same as Fig. 5-1-8, but for the LDP events in d4PDF and its confidence level is 99.9%; this figure shows longitude-time sections of the lag composite results for anomalies of geopotential height (contours) and those of temperature (color shading and color contours) at 500 hPa from their climatology. Compared to the results of the DP events in d4PDF (Fig. 4-2-6), the longitudinal features are much more apparent in the LDP events in d4PDF.

The general features of the tropospheric circulation in the west1-wide and west2-wide events in d4PDF are similar to those in JRA-55 (Fig. 5-1-8), but are clearer; their features are the cyclonic and cold anomalies below the LDP region, the anticyclonic anomalies at 180˚, and the date of their anomalies. Anticyclonic anomalies before the event day are significant in the west1- and west2-wide events, and the anomalies in the west1-wide events are further west in

the west2-wide events. This difference is consistent with the longitude of upward propagation (Fig. 5-2-4).

In JRA-55, it is difficult to clarify the statistical features of the tropospheric circulation during the west1-, west2-narrow, and east events (Fig. 5-1-8), but d4PDF allows us to do so. The west1-narrow events have similar characteristics to the west1-wide events: the anticyclonic and cold anomalies below the LDP region on the event day, the anticyclonic anomalies around 180˚ on the event day, and the anticyclonic anomalies at 45˚E before the event day. On the other hand, the anticyclonic anomalies at 0˚ are significantly large in the west1-narrow events. This fact is consistent with the upward propagation of wave packets at 45˚E on the event day (Fig. 5-2-4c).

Cyclonic and cold anomalies below the LDP region are weaker in the west2-narrow events than in the west2-wide events, and their anomalies at 45˚E are more significant in the west2-narrow events. The anticyclonic anomalies at 180˚ in the west2-narrow events are stronger in the west2-wide events, and this fact is consistent with the fact that the upward propagation at 180˚ is stronger in the west2-narrow events.

The east-west events have significant cyclonic and cold anomalies at 45˚W before the event day, which is a common feature with the east events in JRA-55. The general characteristics of the east-west events are similar to those of the DP east events in d4PDF; the cyclonic and cold anomalies develop below the LDP region, and the anticyclonic anomalies develop at 180˚ before the event day. As expected from the differences in downward

propagation, the characteristics of the east-east events are different from those of the east-west events. The cyclonic anomalies in the east-east events are located farther west than in the east-west events, and the anticyclonic anomalies develop around 90˚E.

Next, we compare longitude-height sections for the LDP events in d4PDF and those in JRA-55. Figure 5-2-6 is the same figure as Fig. 5-1-4 but for the LDP events in d4PDF and the confidence level is 99.9%; the figure shows longitude-height sections for the zonal structure of geopotential height anomalies from the zonal mean and x- and z-components of WAF vectors for the composite results of each event group on the event day. Figure 5-2-7 is the same figure as Fig. 5-2-6, but on the peak day of upward propagation in each event group: three days before the event day in the west1-wide, west2-wide, and east-west events, two days before the event day in the west1-narrow and the west2-narrow events, and the four days before the event day in the east-east events. Figure 5-2-8 is the same figure as Fig. 5-2-6, but on ten days before the event day. In all event groups, the phase of each WN change from the westward tilting to the quasi-barotropic structure from ten days before the event day to the event day. Note that they are not barotropic compared to those of the DP events in d4PDF (Fig. 4-2-8). There are no differences among the west event groups on ten days before the event day (Fig. 5-2-8). The differences start to increase with the upward propagation (Fig. 5-2-7), and phases and amplitudes of waves are different on the event day (Fig. 5-2-6).

As discussed in Section 4.2.3 and 5.1.3, the longitudes of the ridge of WN1 component are different on the event day between the west1- and west2-wide events. Moreover, WN2

component have differences in the upper stratosphere and is more barotropic in the west2-wide. These wave differences and superposition of waves generate the differences in the enhancement of the Aluetian high and the longitudinal peak of the upward propagation. These differences are almost the same between the west1- and west2-narrow events; however, the ridges of WN1 are more different.

In the east-west events, the phase of WN1 component is shifted about 180˚ from the west events, and its ridge is located about 45˚E. The amplitude of WN2 is about twice that of other event groups. These differences are observed already on ten days before the event day. The superposition of these waves form the quasi-barotropic high around 0˚E on the event day.

The characteristics of the east-east events are much different from other event groups. The phase of WN1 is similar to that of the west1 events, but its amplitude is smaller. WN2 component has smaller amplitude in the middle stratosphere and larger amplitude in the upper stratosphere. In the east-east events of the DP events in d4PDF, the amplitudes were dramatically smaller than other event groups (Fig. 4-2-8), but the differences are not that large in the east-east events in the LDP events.

Finally, we show the interannual changes and tendency of occurrence dates of the LDP events in d4PDF. Figure 5-2-9 shows the same figure as Fig. 4-2-9, but for the LDP events in d4PDF; ensemble averages and standard deviations of interannual changes of each event group. As in the interannual changes of the DP events in d4PDF (Fig. 4-2-9), there are no tendencies of increasing and decreasing, and standard deviations are large.

Figure 5-2-10 shows histograms of occurrence dates of event numbers in each event group. Blue bars depict the event number of the LDP events in d4PDF, and yellow bars depict that in JRA-55. There are two kinds of tendencies. The west1-wide, west2-wide, east-west, and west2-narrow have the peak in February, which is similar to the distribution of the west1, west2, and east-west events in JRA-55. The west1-narrow and east-east events peak in March or increase with date, which is similar to the distribution of the east-east events in JRA-55.

5.2.3 Discussion

d4PDF allowed us to statistically investigation the longitudinal characteristics of the LDP events. We classified the LDP events based on their characteristics and performed a composite analysis; there were differences in the characteristics of the upward propagation in the stratosphere and the tropospheric circulation. In particular, the statistical characteristics of the narrow LDP events were first established. In this section, we discuss the causal mechanism and impacts of the LDP events and the narrow LDP events in detail.

From the overall results, the causal mechanism is assumed to be the same as that discussed in Section 4.3.2, but the phases of the waves are not barotropic. This phase indicates that EPFz is not negative in the LDP events, but the superposition of waves generates the LDP. In addition, the LDP have impacts on the troposphere, which are cold anomalies, although EPFz was not negative. This result is consistent with that of Matthias and Kretschmer (2020); however, this current study shows that the impacts differ depending on the longitudinal

characteristics of the LDP. In particular, the LDP events that peak relatively west in the Western Hemisphere have large impacts on North America. The LDP events in the Eastern Hemisphere also have impacts on the troposphere approximately below the LDP region.

The longitudinal characteristics of the narrow LDP events have been clarified in this study. Here, the west1- and west2-narrow events are discussed in detail. The causal mechanism is assumed to be the same as that mentioned above, since the wave structure was similar to that of the other groups of events. However, the LDP region was made narrow by upward propagation from the troposphere. The anticyclonic anomalies, which are parts of the wave train enhanced by downward propagation, may trigger this upward propagation in the troposphere.

In addition, the effects of the west1-narrow and west2-narrow events were different. As described earlier, the west1-narrow events had stronger cold anomalies over North America; this region is below the LDP region. This characteristic is almost the same as that of the DP and LDP events; thus, mechanism of cold anomalies is considered to be same as in Section 4.2.3 in perspective of the wave enhancement in the troposphere. The west2-narrow events have cold anomalies in the Eastern Hemisphere, far from the LDP region. Wave packets propagate horizontally east of the downward propagation in the upper stratosphere (Fig. 5-2-6d). This propagation can enhance wave trains in the troposphere. Downward propagation and subsequent horizontal propagation might generate the cold anomalies in the region away from the LDP region.

We have raised cold anomalies in the troposphere as an impact of the LDP; however, it is not known that the LDP events contribute significantly to the cold events in the troposphere because the anomalies were about -3℃. The reality of the impact of the LDP on cold events in the troposphere should be investigated.

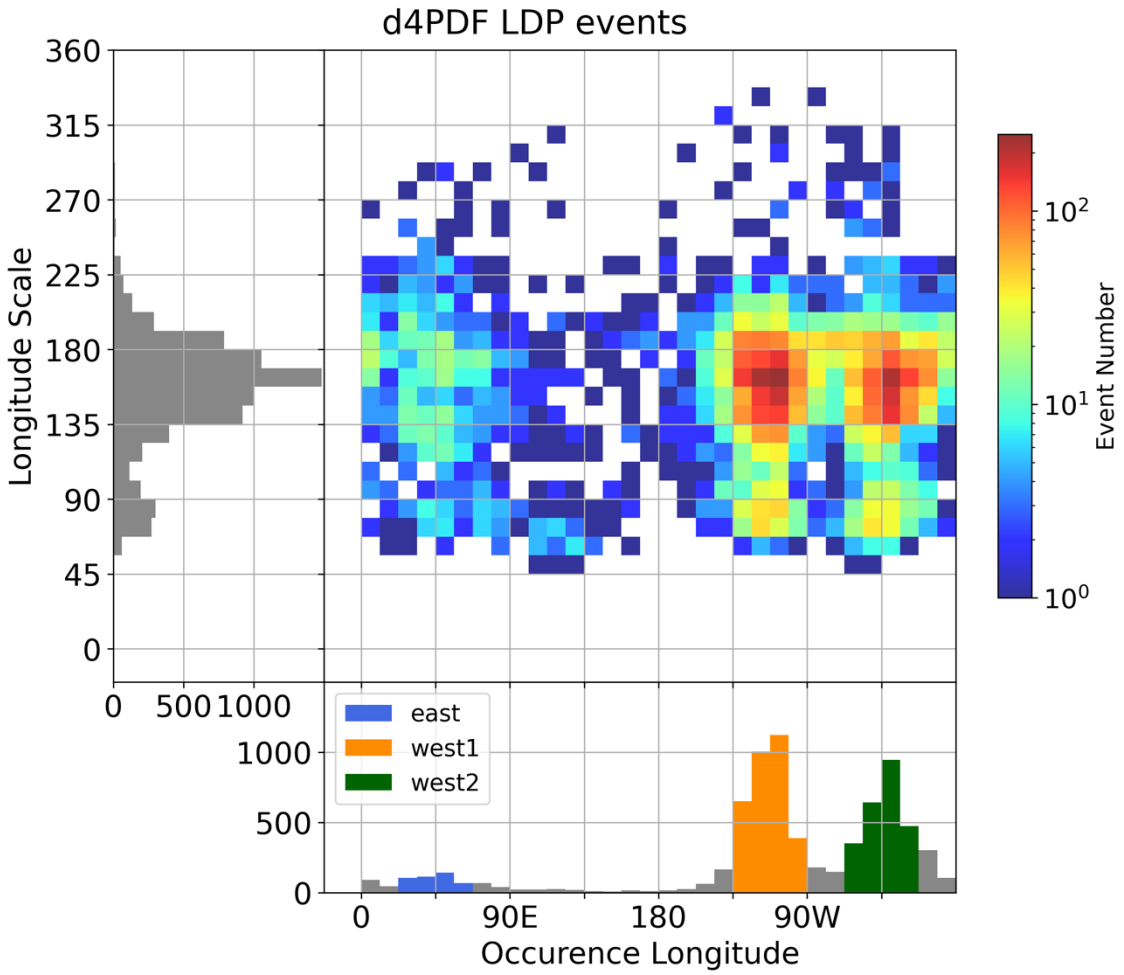

Figure 5-2-1: Histograms of the longitude scale, the occurrence latitude, and occurrence longitude versus longitude scale of the LDP events in d4PDF.

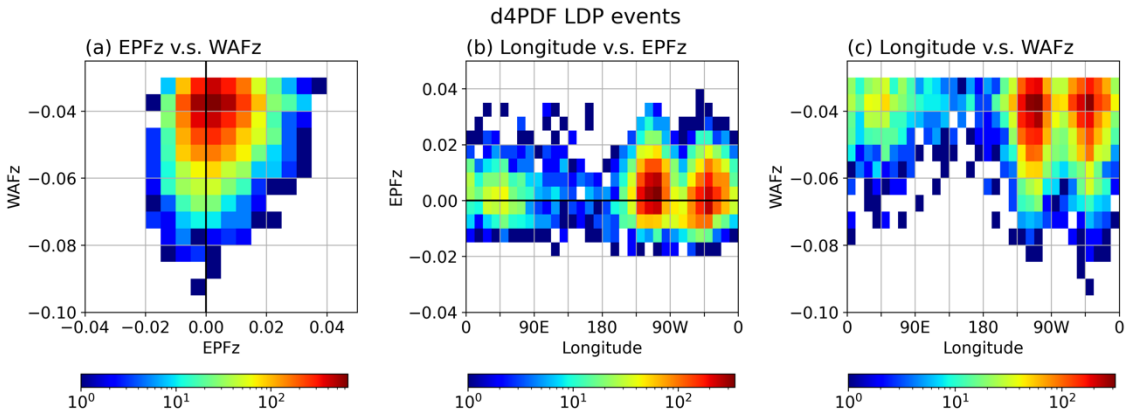

Figure 5-2-2: (a) Two-dimensional histogram of EPFz, which is WAFz averaged zonally, versus WAFz, averaged 50 N˚ through 80 N˚ at 30 hPa, of the LDP events in d4PDF. (b) A similar panel to (a), but its x-axis is the occurrence longitude of downward propagation events based on WAFz, and the y-axis is EPFz. (c) A similar panel to (a), but its x-axis is the occurrence longitude.

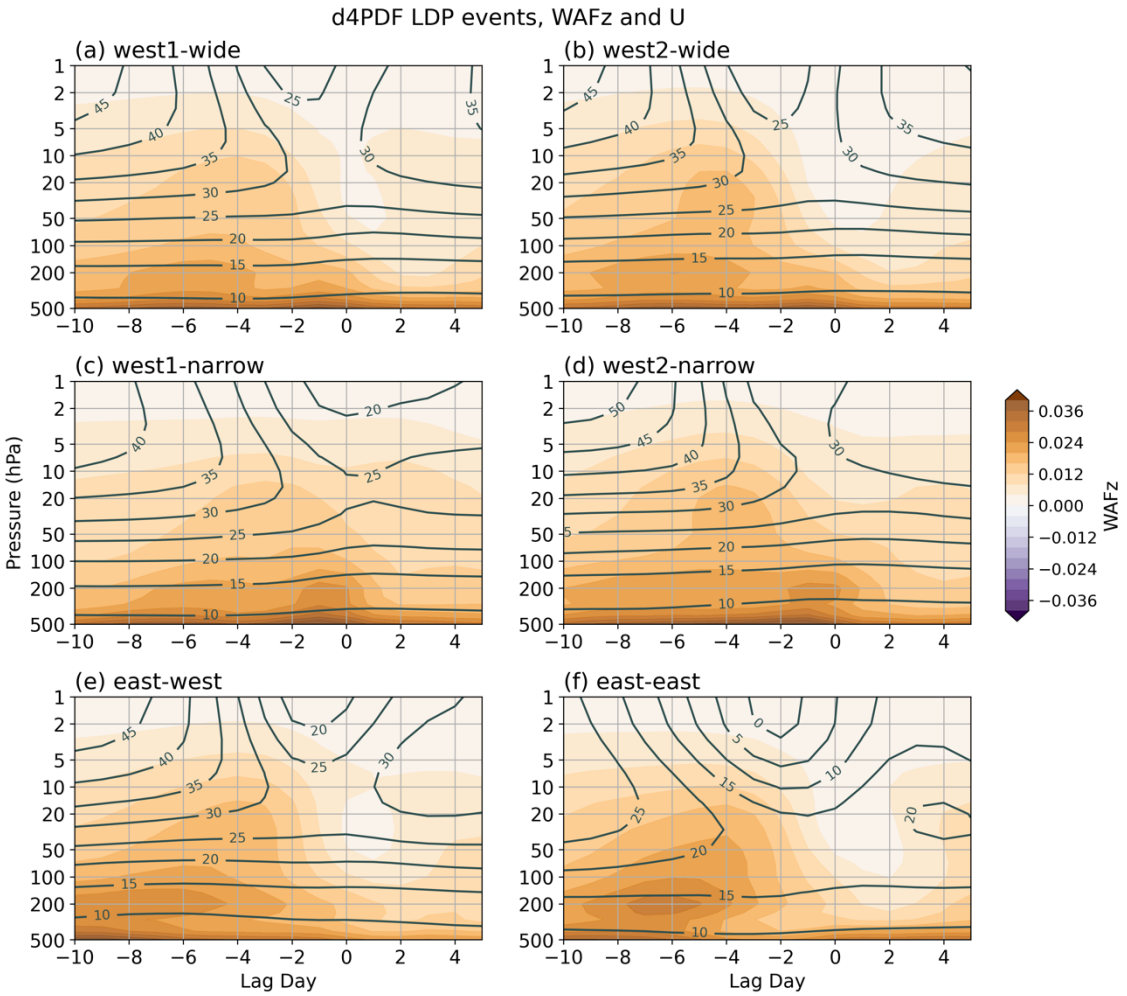

Figure 5-2-3: Time-height sections for zonal mean zonal winds (m, contours) and zonal mean WAFz (m^2 s^{-2}, color shadings) averaged over 50˚N through 80˚N of the lag composite results for the west1-wide event (a), the west2-wide event (b), the west1-narrow events (c), the west2-narrow event (d), the east-west events (e), and the east-east events (f) in d4PDF. The horizontal axis denotes the lag day from the event day.

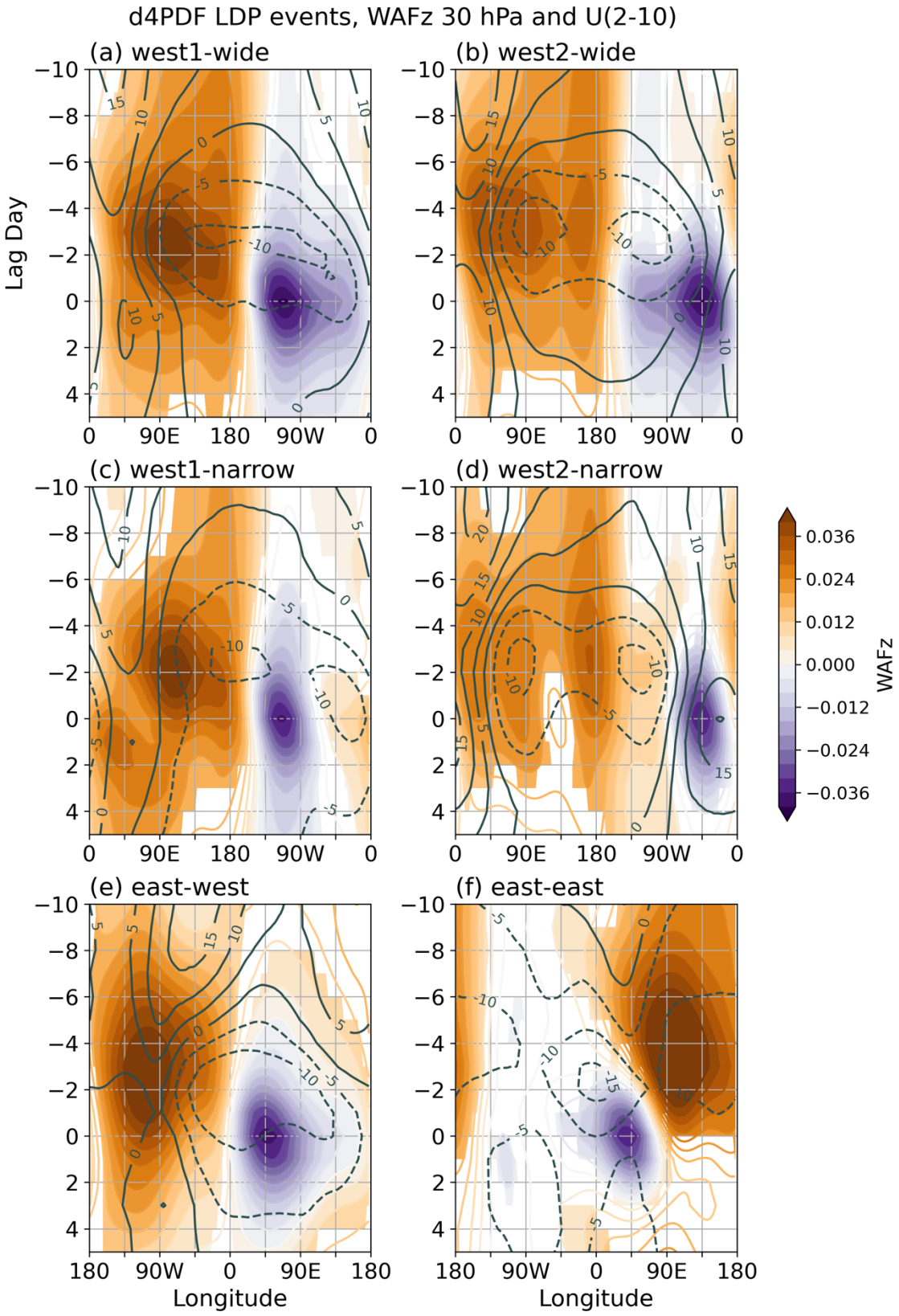
d4PDF LDP events, WAFz 30 hPa and U(2-10)
(a) west1-wide
(b) west2-wide
(c) west1-narrow
(d) west2-narrow
(e) east-west
(f) east-east
Lag Day
Longitude
WAFz
0.036
0.024
0.012
0.000
−0.012
−0.024
−0.036

Figure 5-2-4: Longitude-time sections for U(2-10) (m, contours) and WAFz (m^2 s^{-2}, color shadings) averaged over 50˚N through 80˚N of the lag composite results for the west1-wide event (a), the west2-wide event (b), the west1-narrow events (c), the west2-narrow event (d), the east-west events (e), and the east-east events (f) in d4PDF. The colors are drawn only in the region where WAFz is statistically significant of 99.9 % confidence level in the t-test.

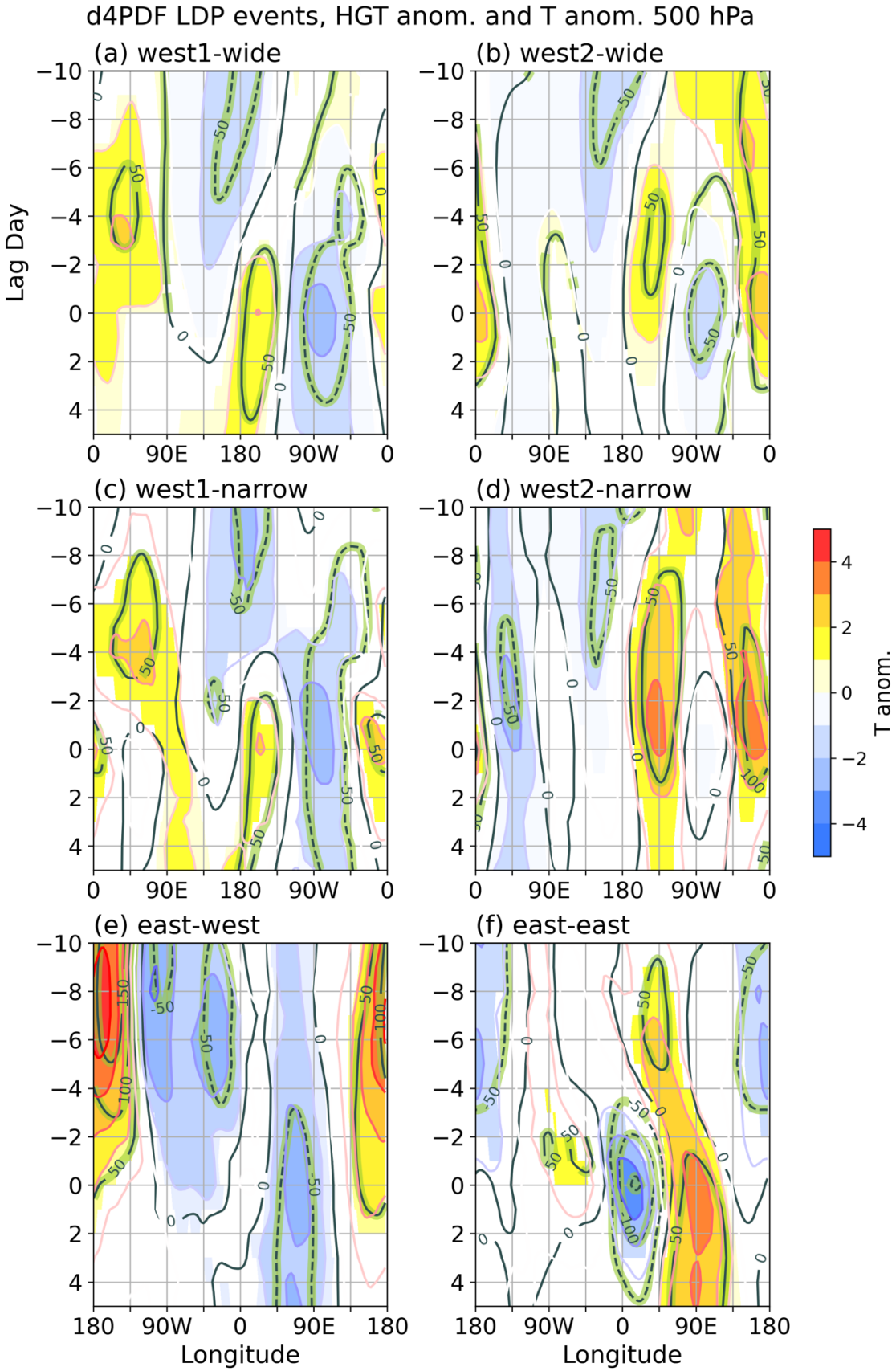
d4PDF LDP events, HGT anom. and T anom. 500 hPa
(a) west1-wide
(b) west2-wide
(c) west1-narrow
(d) west2-narrow
(e) east-west
(f) east-east
Lag Day
Longitude
T anom.

Figure 5-2-5: Same as Fig. 5-2-4 but for geopotential height anomalies (m, contours) and temperature anomalies (K, color shadings) from the climatology at 500 hPa

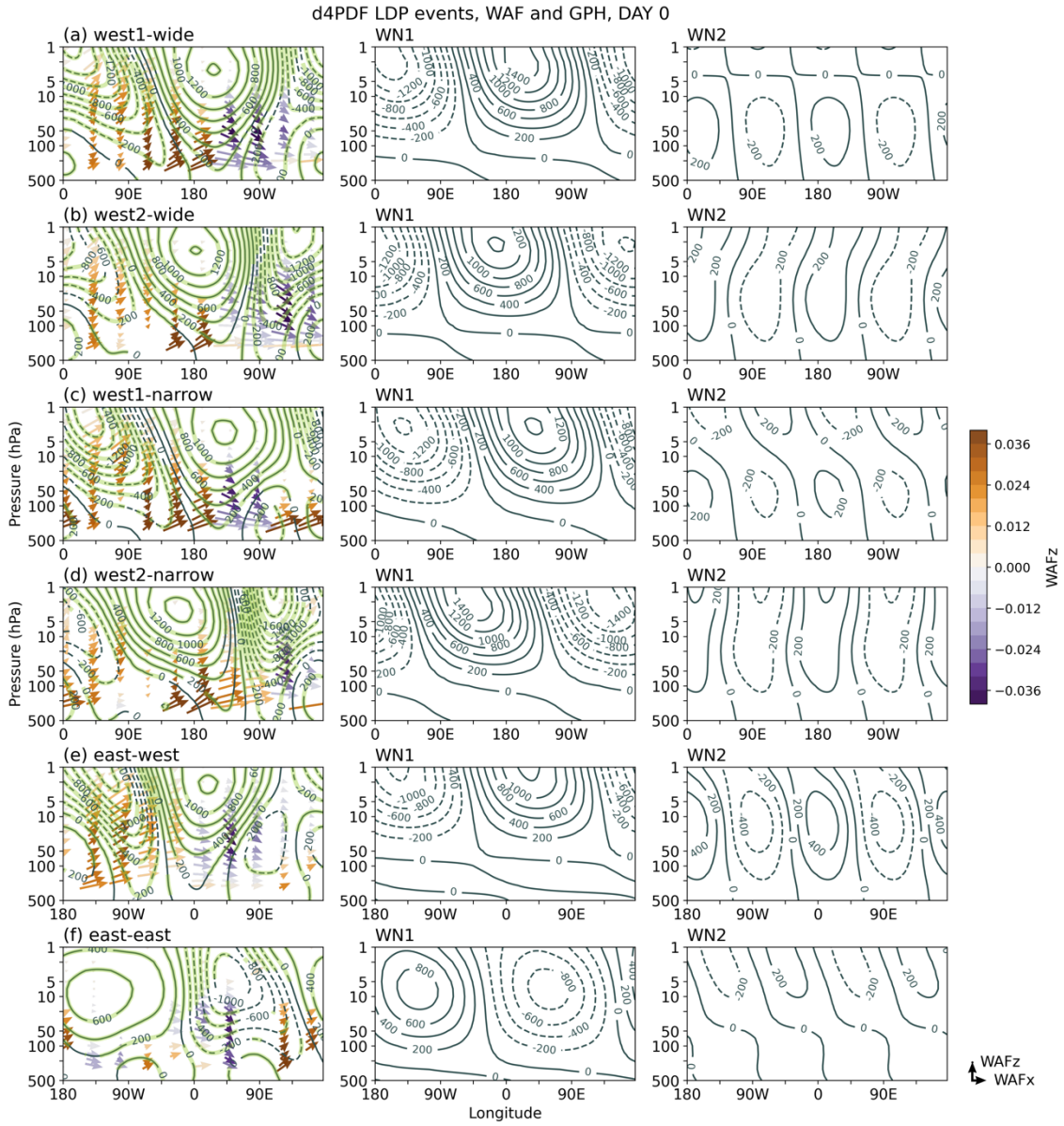

Figure 5-2-6: (Left) Longitude-height sections for the anomalies of geopotential height from the zonal averages (m, black and green contours) and WAF (m^2 s^{-2}, vectors) averaged over 50˚N through 80˚N of the composite results on the event day for the west1-wide event (a), the west2-wide event (b), the west1-narrow events (c), the west2-narrow event (d), the east-west events (e), and the east-east events (f) in d4PDF. The value of WAFz colors the vectors. The green contours and color vectors are drawn only in the region where WAFz is statistically significant of 99.9 % confidence levels in the t-test. The unit vector is bottom of this figure, and its length is 10 m^2 s^{-2} in the horizontal direction and 0.5 m^2 s^{-2} in the vertical direction. (Center) Longitude-height sections for WN1 components of geopotential height averaged over 50˚N

through 80˚N of the composite results about the event groups of the LDP events in d4PDF on the event day for each event group. (Right) Same panels as center panels, but for WN2 components.

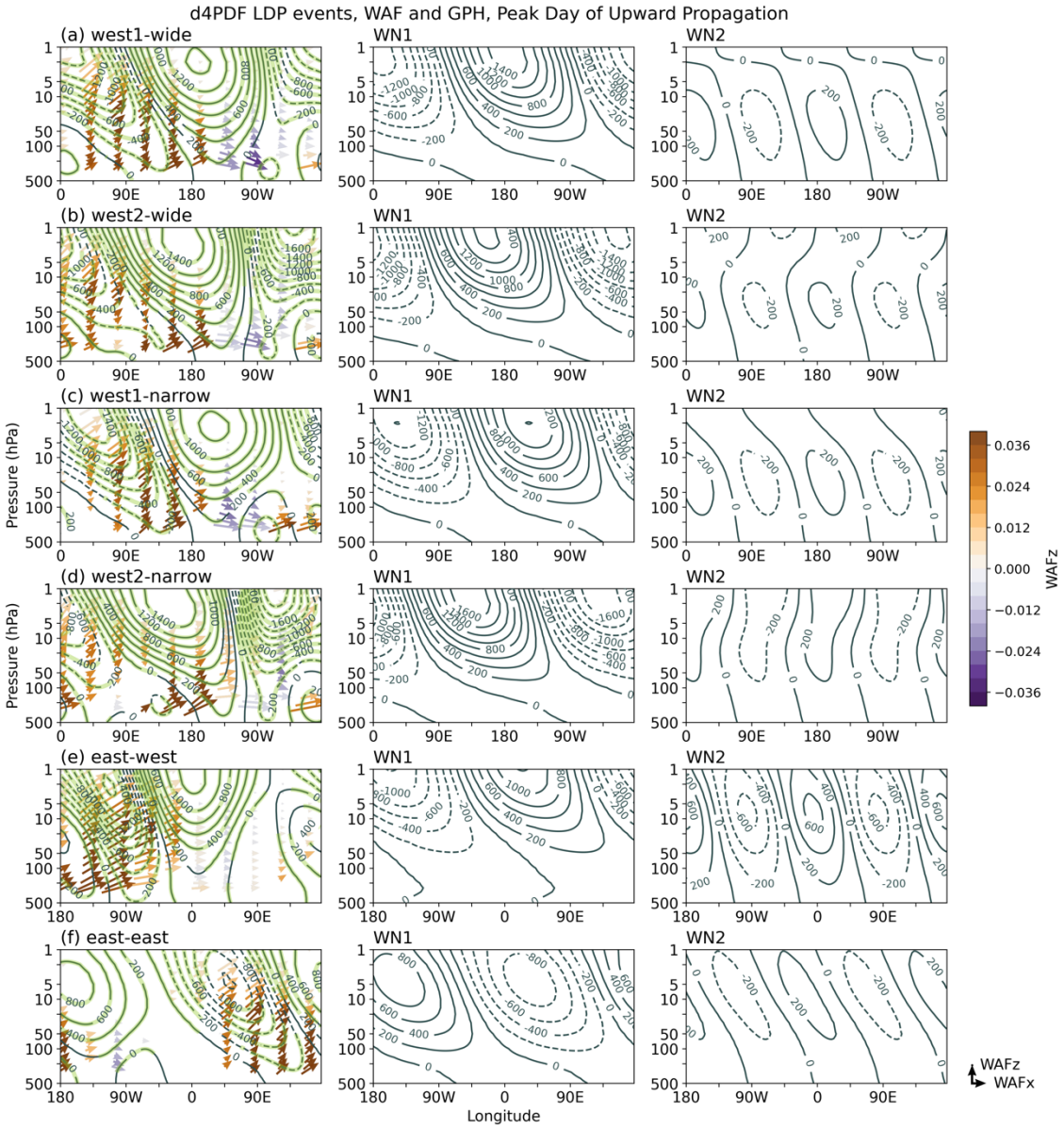

Figure 5-2-7: Same figure as Fig. 5-2-6, but for the peak day of the upward propagation: three days before the event day in the west1-wide, west2-wide, and east-west events, two days before the event day in the west1-narrow and the west2-narrow events, and the four days before the event day in the east-east events.

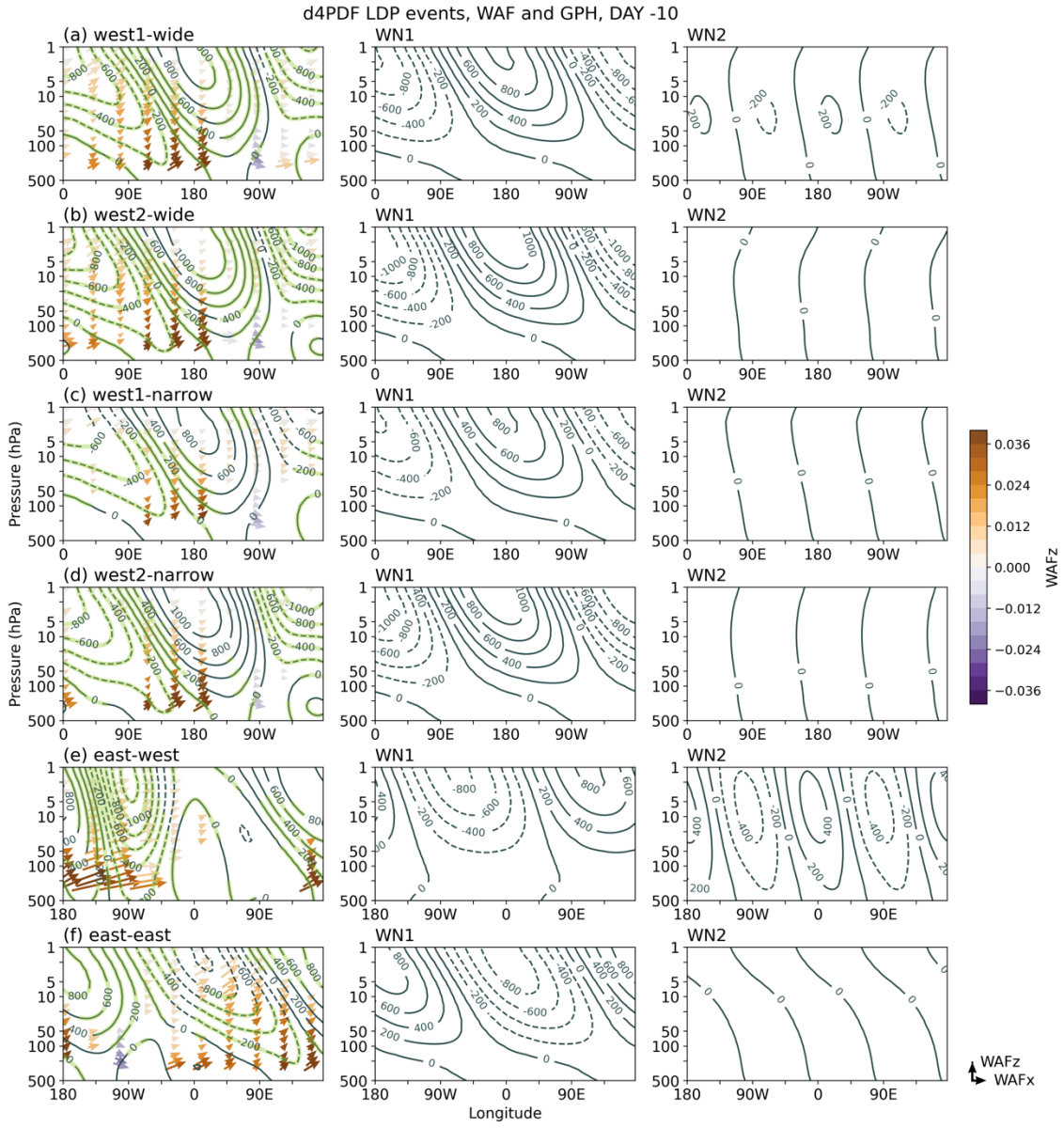

Figure 5-2-8: Same figure as Fig. 5-2-6, but for ten days before the event day.

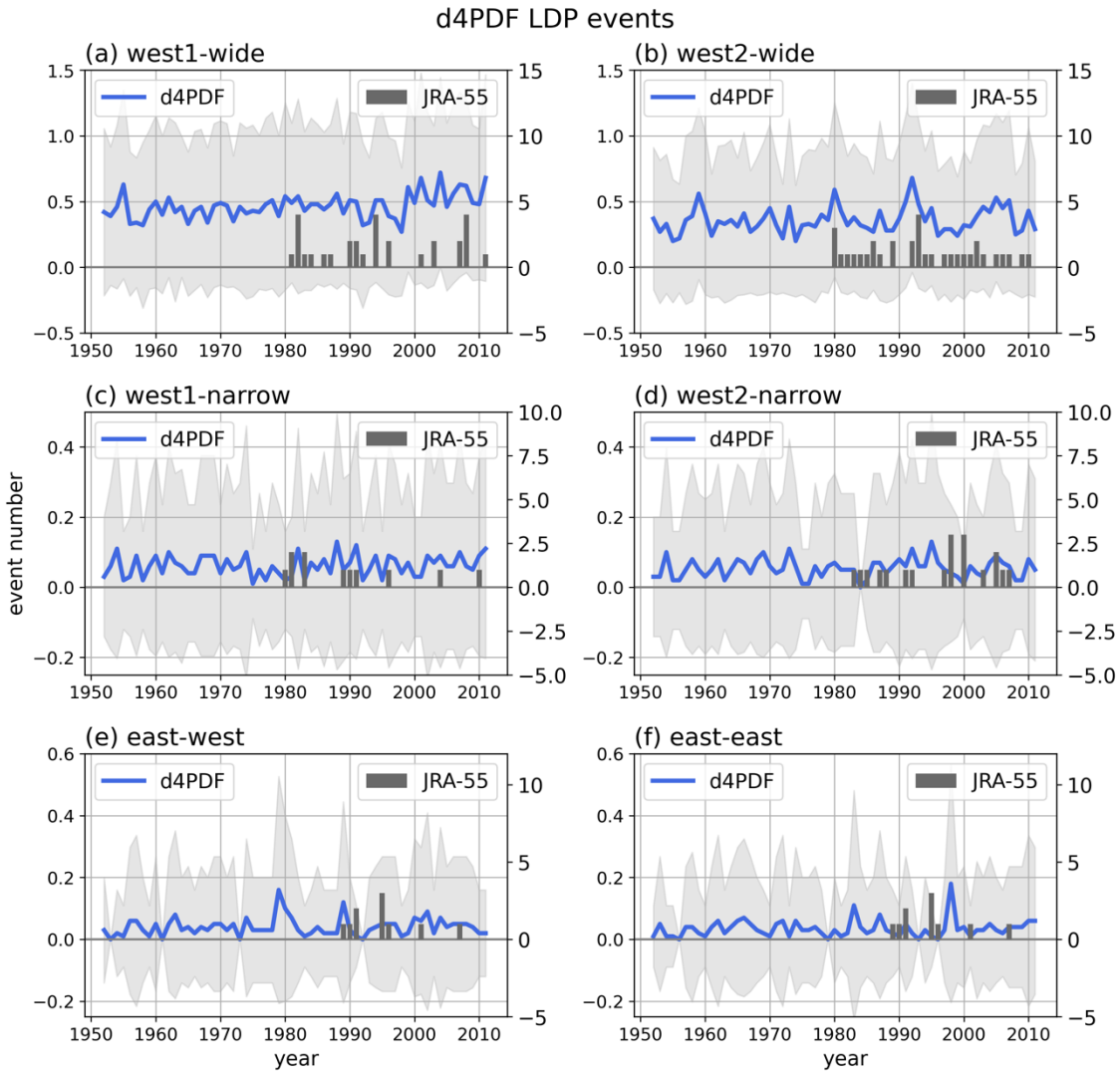

Figure 5-2-9: The interannual change in the event number of for the west1-wide event (a), the west2-wide event (b), the west1-narrow events (c), the west2-narrow event (d), the east-west events (e), and the east-east events (f) in d4PDF.Blue lines show the ensemble means of event number in d4PDF, and gray shadings show the standard deviations of it. Gray bars show the event number of corresponding groups of LDP events in JRA-55; in the panel (e) and (f), gray bars show the event number of the LDP east events in JRA-55.

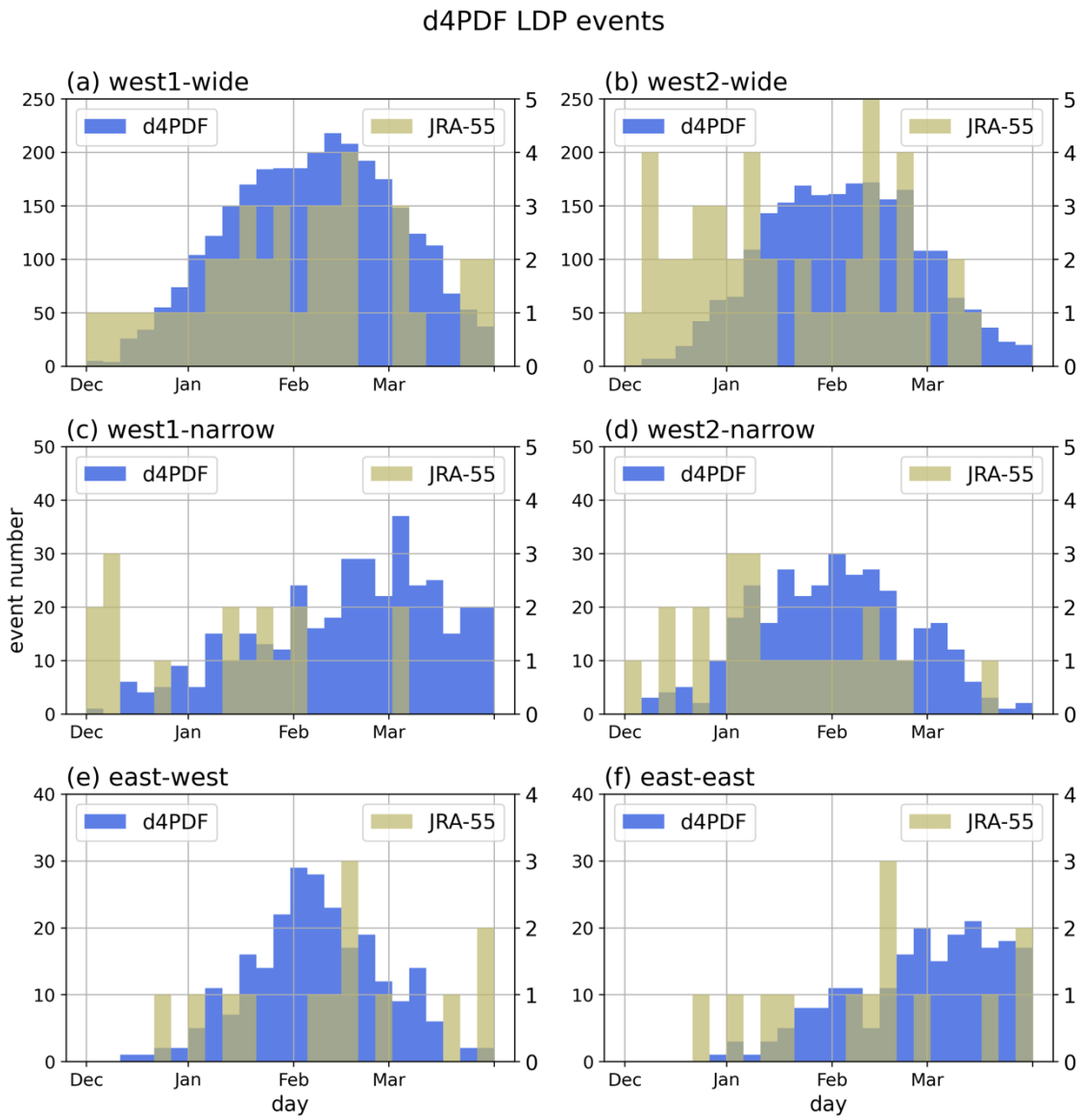

Figure 5-2-10: Histograms of the occurrence date of events in each event group. Events are counted at 5 days intervals. Blue bars show the event number in d4PDF. Gray bars show the event number of corresponding groups of LDP events in JRA-55; in the panel (e) and (f), gray bars show the event number of the LDP east events in JRA-55.

6. Summary and Conclusions

In this study, the downward propagation events (DP events) and the localized downward propagation events (LDP events) were investigated by using the reanalysis data (JRA-55) and a large ensemble dataset (d4PDF) to clarify their occurrence features and plausible mechanism.

The DP events were extracted from EPFz and indicated the downward propagation of planetary waves. The event days of the DP events were defined as the day that EPFz averaged over 50˚N through 80˚N (or 50˚S through 80˚S) at 30 hPa are more negative than -3.6×10^4 kg^2 s^{-2}. Resultantly, we obtained 25 events in the NH and 37 events in the SH for the analysis period from 1980 to 2020. The occurrence longitude of the events was investigated on the basis of WAFz on the event day. In the NH, 84 % of events occurred in the Western Hemisphere, and 16 % occurred in the Eastern Hemisphere.

We classified the event in the Western Hemisphere into three groups on the basis of the EOF analysis for WAFz on the event day; the leading component denoted the strength of the downward propagation in the Western Hemisphere. The composite results showed the upward propagation of wave packets in the Eastern Hemisphere before the downward propagation, the deceleration of zonal winds in the upper stratosphere, and the quasi-barotropic development of the Aleutian high. Moreover, they exhibited cyclonic anomalies penetrated from the stratosphere to the troposphere and cold anomalies in the troposphere below the DP region. The strength of these characteristics during the events was positively correlated with the strength of

downward propagation in the Western Hemisphere. In particular, the strength of downward propagation was considered to be controlled by the strength of upward propagation.

In the SH, 70 % of events occurred in the Western Hemisphere. The evolution of the events is similar to that of the NH events described above. Thus, the analysis for JRA-55 showed the longitudinal characteristics of the DP events and the temporal evolution of their events.

Characteristics of the DP events in the Eastern Hemisphere and those of the tropospheric circulation during the DP events were unclear in the analysis of JRA-55. We applied the same analysis to d4PDF in order to obtain more statistically clear characteristics of the events in the NH. Resultantly, although we obtained similar longitudinal distribution for the DP events, there were two discrete peaks of the event number around 120˚W and 45˚W. Composite results of the classified events on the basis of the longitudinal distribution indicated that differences in occurrence longitudes of the upward propagation four days before the event day and differences in location of the Aleutian high formed these two peaks.

Moreover, the cold anomalies over North America were found to be stronger in the events with the longitudinal peak of downward propagation around 120˚W. Furthermore, we could classify the events in the Eastern Hemisphere into two groups on the basis of the longitude of upward propagation before the event day: The events had the upward propagation in the Western Hemisphere and the Eastern Hemisphere. Composite results of their classified events indicated differences in the wave structures during those events. As in the events in the

Western Hemisphere, the cold anomalies were observed below the DP region in the troposphere, and the events with downward propagation in the Eastern Hemisphere and upward propagation in the Western Hemisphere had stronger cold anomalies. The composite results for the detected events in the Western and Eastern Hemispheres suggested causation mechanisms of the DP events: Negative vertical shear of zonal winds due to deceleration by the upward propagation generates the quasi-barotropic wave structure and the trough enhanced by the downward propagation generate the cyclonic and cold anomalies in the troposphere.

Wave packets propagate downward locally during the DP events; this fact implies the necessity of considering the downward propagation from a viewpoint of WAFz. Thus, LDP events were extracted from WAFz. We designed detection methods of the LDP events on the basis of WAFz averaged over 50˚N through 80˚N at 30 hPa and obtained 194 events in JRA-55. The longitudinal distribution of the LDP events was almost the same as those of the DP events in d4PDF. Moreover, the histogram of longitudinal scale of downward propagation also had two discrete peaks around 150˚ and 75˚. We classified the LDP events on the basis of the histogram of the occurrence longitude and longitudinal scale, making a composite analysis for them. The general characteristics of the LDP events were similar to those of the DP events. However, the LDP events did not necessarily have negative EPFz and the quasi-barotropic wave structure, and the timing of upward and downward propagation was almost always overlapped. For the LDP events with a narrower scale of downward propagation than 112.5˚W, the region of downward propagation was made narrow by the location of upward propagation from the

troposphere. While EPFz was not necessarily negative in the LDP events, cold anomalies were observed in the troposphere as in the DP events.

To show more statistically clear characteristics of the LDP events, we also applied the same analysis to d4PDF. The histogram of the occurrence longitude and longitudinal scale of the LDP events in d4PDF were almost the same as that in JRA-55. We also made classification on the basis of the histogram and composite analysis to these events. The composite results showed differences of upward propagation and wave structure in the stratosphere generate differences in characteristics of the events. On the other hands, causal mechanisms of the LDP events were considered to be almost the same as those in the DP events.

Moreover, for the events in the Western Hemisphere, the events with a downward peak around 120˚W generated stronger cold anomalies over North America. The events with a downward peak around 45˚W or in the Eastern Hemisphere had an influence on European cold weather. In particular, the events in the Eastern Hemisphere with upward propagation in the Western Hemisphere brought about stronger cold weather over Europe.

Thus, in the current study, we investigated the downward propagation of wave packets in detail. We showed the statistical characteristics of the longitudinal distribution and longitudinal scale of the events, the causal mechanisms generating these characteristics, and the impacts on the tropospheric circulation. In particular, we clarified the characteristics of the events that strongly impact tropospheric weather in North America and Europe. This finding would deepen our understanding of the coupling between the stratosphere and the troposphere.

It also contributes to reducing the uncertainties of predicting cold spells. However, further studies are still needed to determine mechanisms bringing about conditions for the appearance of the DP and LDP events.

Acknowledgements

I deeply appreciate to Prof. Toshihiko Hirooka at the Department of Earth and Planetary at Kyushu University for his invaluable advices. I express deep thanks to Prof. Ryuichi Kawamura at the Department of Earth and Planetary at Kyushu University and Associate Prof. Nawo Eguchi at Kyushu University, who are my advisers in Front Researcher Program, for their kind advices. I am grateful to Prof. Hitoshi Mukougawa and Dr. Shunsuke Noguchi at the Department of Earth and Planetary at Kyushu University, who gave me advice and encouragement. I am also indebted to Associate Prof. Yasunobu Miyoshi, Associate Prof. Huixin Liu, and Dr. Kensuke Nakajima for their supports. Finally, I express my deepest gratitude to my family and colleagues for their support and encouragement.

References

Andrews, D. G. (2010). An Introduction to Atmospheric Physics, Second Edition.

Andrews, D. G., Holton, J. R., & Leovy, C. B. (1987). *Middle atmosphere dynamics*. Orlando: Academic Press.

Baldwin, M. P., & Dunkerton, T. J. (2001). Stratospheric Harbingers of Anomalous Weather Regimes. *Science*, *294*(5542), 581–584. https://doi.org/10.1126/science.1063315

Dunn-Sigouin, E., & Shaw, T. A. (2015). Comparing and contrasting extreme stratospheric events, including their coupling to the tropospheric circulation: DUNN-SIGOUIN AND SHAW. *Journal of Geophysical Research: Atmospheres*, *120*(4), 1374–1390. https://doi.org/10.1002/2014JD022116

Harnik, N. (2009). Observed stratospheric downward reflection and its relation to upward pulses of wave activity. *Journal of Geophysical Research*, *114*(D8), D08120. https://doi.org/10.1029/2008JD010493

Harnik, Nili, & Lindzen, R. S. (2001). The Effect of Reflecting Surfaces on the Vertical Structure and Variability of Stratospheric Planetary Waves. *Journal of the Atmospheric Sciences*, *58*(19), 2872–2894. https://doi.org/10.1175/1520-0469(2001)058<2872:TEORSO>2.0.CO;2

Harnik, Nili, Perlwitz, J., & Shaw, T. A. (2011). Observed Decadal Changes in Downward Wave Coupling between the Stratosphere and Troposphere in the Southern Hemisphere. *Journal of Climate*, *24*(17), 4558–4569. https://doi.org/10.1175/2011JCLI4118.1

Hitchcock, P., & Simpson, I. R. (2014). The Downward Influence of Stratospheric Sudden Warmings*. *Journal of the Atmospheric Sciences*, *71*(10), 3856–3876. https://doi.org/10.1175/JAS-D-14-0012.1

Jadin, E. A. (2011). Stratospheric “wave hole” and interannual variations of the stratospheric circulation in late winter. *Natural Science*, *03*(04), 259–267. https://doi.org/10.4236/ns.2011.34033

Kodera, K., & Mukougawa, H. (2017). Eurasian Cold Surges Triggered by the Nonlinear Reflection of Stratospheric Planetary Waves in December 2012. *SOLA*, *13*(0), 140–145. https://doi.org/10.2151/sola.2017-026

Kodera, K., Yamazaki, K., Chiba, M., & Shibata, K. (1990). Downward propagation of upper stratospheric mean zonal wind perturbation to the troposphere. *Geophysical Research Letters*, *17*(9), 1263–1266. https://doi.org/10.1029/GL017i009p01263

Kodera, K., Mukougawa, H., & Itoh, S. (2008). Tropospheric impact of reflected planetary waves from the stratosphere. *Geophysical Research Letters*, *35*(16), L16806. https://doi.org/10.1029/2008GL034575

Kodera, K., Mukougawa, H., Maury, P., Ueda, M., & Claud, C. (2016). Absorbing and reflecting sudden stratospheric warming events and their relationship with tropospheric circulation: Absorbing and Reflecting Sudden Warmings. *Journal of Geophysical Research: Atmospheres*, *121*(1), 80–94. https://doi.org/10.1002/2015JD023359

Kretschmer, M., Coumou, D., Donges, J. F., & Runge, J. (2016). Using Causal Effect Networks to Analyze Different Arctic Drivers of Midlatitude Winter Circulation. *Journal of Climate*, *29*(11), 4069–4081. https://doi.org/10.1175/JCLI-D-15-0654.1

Kretschmer, M., Coumou, D., Agel, L., Barlow, M., Tziperman, E., & Cohen, J. (2018). More-Persistent Weak Stratospheric Polar Vortex States Linked to Cold Extremes. *Bulletin of the American Meteorological Society*, *99*(1), 49–60. https://doi.org/10.1175/BAMS-D-16-0259.1

Kretschmer, M., Cohen, J., Matthias, V., Runge, J., & Coumou, D. (2018). The different stratospheric influence on cold-extremes in Eurasia and North America. *Npj Climate and Atmospheric Science*, *1*(1), 44. https://doi.org/10.1038/s41612-018-0054-4

Lawrence, Z. D., Perlwitz, J., Butler, A. H., Manney, G. L., Newman, P. A., Lee, S. H., & Nash, E. R. (2020). The Remarkably Strong Arctic Stratospheric Polar Vortex of Winter 2020: Links to Record-Breaking Arctic Oscillation and Ozone Loss. *Journal of Geophysical Research: Atmospheres*, *125*(22). https://doi.org/10.1029/2020JD033271

Lubis, S. W., Matthes, K., Omrani, N.-E., Harnik, N., & Wahl, S. (2016). Influence of the Quasi-Biennial Oscillation and Sea Surface Temperature Variability on Downward Wave Coupling in the Northern Hemisphere. *Journal of the*

Atmospheric Sciences, *73*(5), 1943–1965. https://doi.org/10.1175/JAS-D-15-0072.1

Lubis, S. W., Matthes, K., Harnik, N., Omrani, N.-E., & Wahl, S. (2018). Downward Wave Coupling between the Stratosphere and Troposphere under Future Anthropogenic Climate Change. *Journal of Climate*, *31*(10), 4135–4155. https://doi.org/10.1175/JCLI-D-17-0382.1

Lubis, S. W., Huang, C. S. Y., Nakamura, N., Omrani, N.-E., & Jucker, M. (2018). Role of Finite-Amplitude Rossby Waves and Nonconservative Processes in Downward Migration of Extratropical Flow Anomalies. *Journal of the Atmospheric Sciences*, *75*(5), 1385–1401. https://doi.org/10.1175/JAS-D-17-0376.1

Matthias, V., & Kretschmer, M. (2020). The Influence of Stratospheric Wave Reflection on North American Cold Spells. *Monthly Weather Review*, *148*(4), 1675–1690. https://doi.org/10.1175/MWR-D-19-0339.1

Mukougawa, H., Noguchi, S., Kuroda, Y., Mizuta, R., & Kodera, K. (2017). Dynamics and Predictability of Downward-Propagating Stratospheric Planetary Waves Observed in March 2007. *Journal of the Atmospheric Sciences*, *74*(11), 3533–3550. https://doi.org/10.1175/JAS-D-16-0330.1

Nath, D., Chen, W., Wang, L., & Ma, Y. (2014). Planetary wave reflection and its impact on tropospheric cold weather over Asia during January 2008. *Advances in Atmospheric Sciences*, *31*(4), 851–862. https://doi.org/10.1007/s00376-013-3195-8

Nath, D., Chen, W., Zelin, C., Pogoreltsev, A. I., & Wei, K. (2016). Dynamics of 2013 Sudden Stratospheric Warming event and its impact on cold weather over Eurasia: Role of planetary wave reflection. *Scientific Reports*, *6*(1), 24174. https://doi.org/10.1038/srep24174

Perlwitz, J., & Harnik, N. (2003). Observational Evidence of a Stratospheric Influence on the Troposphere by Planetary Wave Reflection. *Journal of Climate*, *16*(18), 3011–3026. https://doi.org/10.1175/1520-0442(2003)016<3011:OEOASI>2.0.CO;2

Perlwitz, J., & Harnik, N. (2004). Downward Coupling between the Stratosphere and Troposphere: The Relative Roles of Wave and Zonal Mean Processes*. *Journal of Climate*, *17*(24), 4902–4909. https://doi.org/10.1175/JCLI-3247.1

Plumb, R. A. (1985). On the Three-Dimensional Propagation of Stationary Waves. *Journal of the Atmospheric Sciences*, *42*(3), 217–229. https://doi.org/10.1175/1520-0469(1985)042<0217:OTTDPO>2.0.CO;2

Shaw, T. A., & Perlwitz, J. (2013). The Life Cycle of Northern Hemisphere Downward Wave Coupling between the Stratosphere and Troposphere. *Journal of Climate*, *26*(5), 1745–1763. https://doi.org/10.1175/JCLI-D-12-00251.1

Shaw, T. A., Perlwitz, J., & Harnik, N. (2010). Downward Wave Coupling between the Stratosphere and Troposphere: The Importance of Meridional Wave Guiding and Comparison with Zonal-Mean Coupling. *Journal of Climate*, *23*(23), 6365–6381. https://doi.org/10.1175/2010JCLI3804.1

Shaw, T. A., Perlwitz, J., Harnik, N., Newman, P. A., & Pawson, S. (2011). The Impact of Stratospheric Ozone Changes on Downward Wave Coupling in the Southern Hemisphere*. *Journal of Climate*, *24*(16), 4210–4229. https://doi.org/10.1175/2011JCLI4170.1

Shaw, T. A., Perlwitz, J., & Weiner, O. (2014). Troposphere-stratosphere coupling: Links to North Atlantic weather and climate, including their representation in CMIP5 models. *Journal of Geophysical Research: Atmospheres*, *119*(10), 5864–5880. https://doi.org/10.1002/2013JD021191